RECOGNIZED IN "Y" CATEGORY BY

ISSN (Print): 3005-5563
ISSN (Online): 3005-5571
Volume: 3 Issue: 1
July - December, 2025

UCP Journal of Science & Technology UCP-JST

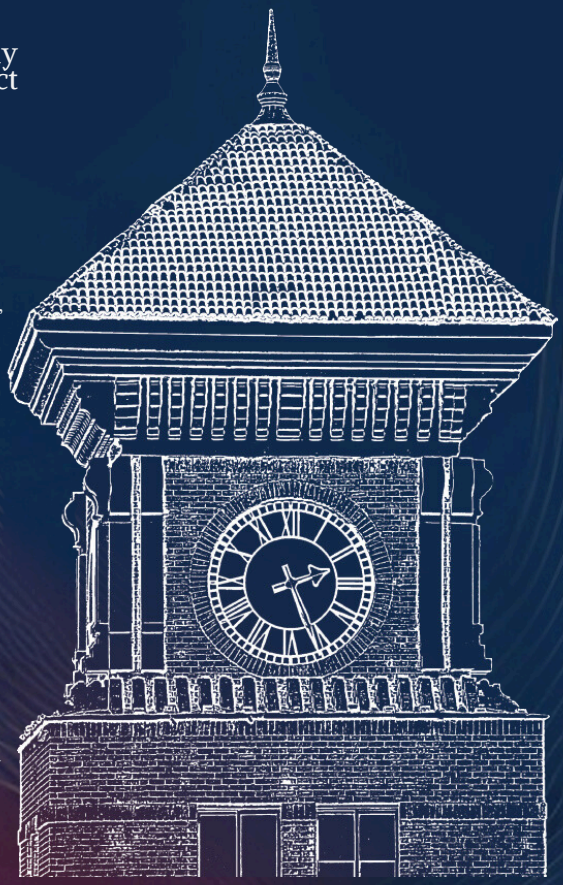

ISSN (Online): 3005-5571
ISSN (Print): 3005-5563
Vol. 3, Issue 1
(July - December 2025)

UCP Journal of Science and Technology(UCP-JST)

HEC Recognized (Y Category)

Volume 3

Issue 1

Faculty of Science and Technology
&
Faculty of Pharmaceutical Sciences

University of Central Punjab,
Lahore, Pakistan

Advisory Board
International Members

National Members

Copyright

Subscription Charges

National: PKR 1000 per issue

International: US$ 200 per issue

Acknowledgment

We are pleased to present Issue 3, Volume 1 of the *UCP Journal of Science & Technology (UCP-JST).* This issue reflects the continued dedication of our editorial team, reviewers, and authors in maintaining the journal's academic quality.

We are proud that UCP-JST has been recognized as a Y Category journal by the Higher Education Commission (HEC) of Pakistan, affirming our commitment to rigorous scholarly standards. Moving forward, we remain focused on enhancing the journal's impact and progressing toward higher levels of recognition.

UCP-JST serves as an open platform for the dissemination of innovative research in science and technology. While published works may be cited with proper acknowledgment, copyright responsibility rests with the respective authors. On behalf of the editorial board, I sincerely thank all contributors for their valuable support and trust..

Sincerely,
Dr. H. Rizwana Kasur
Editor-in-Chief's
UCP -JST

Disclaimer

UCP Journal of Science & Technology (UCP-JST) primarily focuses on providing a platform to promote and contribute to science and technology, however, editors, reviewers and publisher do not accept any legal responsibility for errors, omissions or claims, nor do they provide any warranty, express or implied, with respect to published information. All articles published in the UCP-JST can be cited with due acknowledgement. Author will take the responsibility, if any copyright infringement or any other violation of any law is done by publishing the research work by the author.

Table of Contents

UCP Journal of Science and Technology
Vol. 3, Issue 1 (July - December 2025)
Journal website: http://ojs.ucp.edu.pk/index.php/ucpjst/index

Development and Sensory Evaluation of Calcium- and Vitamin D-Enriched Functional Foods for Bone Health Promotion

Sumaira Saeed[1,2*], Ahmad Mujtaba Noman[1,3], Areej Tariq[4], Saira Qaiser[4], Mehar-un-Nisa Ashiq[4], Noor Amir[4], Fatima Shahid[5]

Abstract

Pakistan faces significant nutritional challenges due to economic instability, limited access to healthy diets, and low nutrition awareness, resulting in widespread calcium and vitamin D deficiencies. These deficiencies contribute to bone-related disorders such as osteopenia and osteoporosis, particularly among vulnerable populations. This study aimed to develop cost-effective, calcium- and vitamin D-enriched functional foods using locally available traditional ingredients (sesame seeds, flaxseed, spinach) and food waste (eggshell powder). Four functional products, Green Crackers, Nutri Snack, Osteomax, and Sementes Wrap, were formulated through appropriate processing techniques. Nutritional analysis revealed Nutri Snack as the richest source of calcium (≈5100 mg/serving), followed by Green Crackers, Osteomax, and Sementes Wrap, with all products providing balanced macronutrient and energy contributions. Consumer acceptability was evaluated using a nine-point Hedonic Scale, and statistical analysis (one-way ANOVA, $p < 0.05$) showed significant differences among formulations. Nutri Snack and 70 g Green Crackers demonstrated the highest overall acceptability scores. The synergistic use of spinach, sesame, flaxseed, and eggshell powder enhanced nutritional density without compromising sensory quality. The findings highlight the potential of utilizing low-cost, locally sourced, and waste-derived ingredients to develop sustainable functional foods that may help alleviate calcium and vitamin D deficiencies. However, further shelf-life studies and clinical trials are recommended prior to commercialization.

Keywords: Functional Food, Calcium, Vitamin D, Egg Shell, Flaxseed, Bone Health, Osteoporosis

1. Introduction

The advancement in food and nutrition sciences has shifted the global trends towards developing novel approaches to managing prevailing health issues. Introducing nutraceuticals and functional foods has mesmerized the healthcare system and pharmaceutics. In

[1]Department of Precision Medicine, University of Campania "Luigi Vanvitelli" 80138 Naples, Italy
[2] Department of Human Nutrition, Faculty of Food Science and Nutrition, Bahauddin Zakariya University, Multan, 60800, Pakistan,
[3] TIMES Institute Multan Pakistan.
[4] Department of nutritional sciences, University of Management and Technology, Sialkot, 51310, Pakistan
[5]University of Central Punjab, Lahore, Pakistan
[*]Corresponding author's E-mail: sumaira.saeed015@gmail.com
Received: 12 January 2025; Received in revised form: 29 October 2025; Accepted: 17 November 2025.
Available online: 23 December 2025.

DOI: https://doi.org/10.24312/ucp-jst.03.01.461

recent decades, their demand has increased immensely due to their natural origin, minimal health hazards, and efficiency in promoting health. The global functional foods and nutraceuticals market was 712.97 billion USD in 2023 and is expected to grow at a compound annual growth rate of 8.4% from 2024 to 2030 (Chopra et al., 2022). Despite this scientific and industrial progress, the disease burden has been increasing every day, affecting millions of people worldwide. Developing and underdeveloped countries face several anomalies due to low income, poor dietary choices, inactive lifestyles, unhygienic foods, environmental hazards, and, most importantly, stress. All these factors contribute significantly to the occurrence of chronic metabolic disorders like diabetes mellitus (DM), hypertension (HTN), cardiovascular disorders (CVDs), hepato-renal syndrome (HRS), gastrointestinal problems, neurovegetative diseases, and pulmonary ailments (Lemieux and Després, 2020). Furthermore, micronutrient deficiency due to low affordability leads to malnutrition and malnutrition-associated complications. Children, older adults, and pregnant females are more prone to micronutrient/micronutrient deficiencies due to vulnerability and high caloric-nutrient demand (Ahmad et al., 2020).

The dynamic duo of Vitamin D and calcium is essential for strengthening bones and teeth and developing and maintaining skeletal health. These two nutrients build and maintain bone mass throughout life, which prevents osteoporosis and fractures in old age. Vitamin D3 (cholecalciferol) is produced in the skin by converting the inactive precursor vitamin D3 (7-dehydrocholesterol) to ultraviolet radiation of the band B kind. The skin can produce vitamin D3 at a rate greater than 90%, whereas only 10% comes from diet. The human body cannot produce calcium independently, so it must be obtained through diet or supplements (Capozzi et al., 2020). There are several ways in which vitamin D is crucial to human health. It plays a vital role in the absorption of dietary calcium in the gastrointestinal tract, the regulation of blood calcium levels, and the deposition of calcium in the bones (Melguizo-Rodríguez et al., 2021). The deficiency of both calcium and Vitamin D can result in various health problems; however, mainly, their deficiency leads to low bone mass and weak bones, eventually to rickets in children and osteoporosis in adults (Shlisky et al., 2022).

Rickets is caused by severe vitamin D deficiency in young people, leading to osteopenia. Osteopenia is a condition in which a loss of bone mineral density (BMD) weakens bones, further leading to osteoporosis. Osteoporosis is a health condition that weakens bones, making them fragile and prone to fractures. Severe cases may lead to osteoarthritis. It can cause joint pain and stiffness (Chanchlani et al., 2020). Osteoporosis is a prevailing global health concern, affecting a substantial number of adults, with ~200 million individuals diagnosed with the condition. Osteopenia and osteoporosis are diagnosed in approximately 22.2% and 59.9% of women, respectively, among women in their 50s. Recent studies suggest that by 2050, approximately 44 million individuals will experience osteopenia, while approximately 5 million will be affected by osteoporosis (Salari et al., 201).

Despite growing global and domestic awareness of micronutrient deficiency, limited studies are available on developing affordable, locally made functional foods fortified with calcium and vitamin D using local materials and food processing waste such as eggshells. Most existing research is centered on supplementation rather than food intervention. The current study, therefore, aimed to formulate and evaluate

Table 1 Nutritional labelling of green crackers per serving

Foods	Fat	Carbohydrates	Protein	Mag-nesium	Calci-um	Potassi-um	Sodium	Zinc	Total calories
Spinach	0.06 g	0.54 g	0.43 g	-	15 mg	84 mg	23.7 mg	-	25kcal
Flour	1.21 g	92.78 g	12.36 g	23.75 g	422.5 mg	155 mg	-	0.78 mg	233kcal
Whole wheat	1.12 g	43 g	8.22 g	82.2 mg	20 mg	21.8 mg	3 mg	2.5 mg	203kcal
Milk	2.62 g	3.64 g	2.59 g		91 mg	115 mg	32 mg	-	48kcal
Butter	23.04 g	0.02 g	0.24 g		7 mg	7 mg	164 mg	-	204kcal
Sesame seed	4.47 g	2.11 g	1.6 g	31.5 g	87 mg	42 mg	0.99 mg	0.7 mg	25 kcal
Total	32.52 g	142.09 g	25.44 g	55.25 g	635.5 mg	424.8	223.69 mg	3.98 mg	927kcal

four novel functional food products fortified with vitamin D and calcium from staple foods (spinach, sesame, flaxseed, and eggshell powder). Specific objectives were to formulate new products from local food ingredients. Evaluate their nutritional and sensory acceptability, and compare product characteristics with control samples for the identification of formulations for future pre-clinical or clinical evaluation

2. Materials and Methodology

Sensory evaluation is critical for evaluating consumer preferences and perceptions of various products. One often-used technique is the Hedonic Scale, which enables participants to score things depending on their level of liking or desire. This article describes the tools and procedures needed for a sensory assessment using the Hedonic Scale. The sensory evaluation Performa is provided in supplementary data.

The sensory panel consisted of 15 semi-trained participants (8 females, 7 males; aged 20–30 years) recruited from the Department of Food and Nutrition. Evaluation was performed using a 9-point hedonic scale ranging from 1 = “dislike extremely” to 9 = “like extremely.”

2.1. Functional Food 1 (Green Crackers)

2.1.1. Ingredients and Procedure:

The ingredients of the green crackers’ recipe include Dried spinach (1/3 cup 70g), Flour (1/2 cup 64 g), Whole wheat (1/2 cup 64 g), Butter (2 tbsp. 28.3 g), Milk (1/3 cup 43 g), Yeast (1 tsp. 4.2 g), Salt (1 tsp. 4.2 g), Baking powder (1/2 tsp. 2.84 g), and Sesame seed (1 tsp. 4.2 g).

First, lukewarm milk (1/3 cup) was added, and 1tsp yeast was mixed well and set aside for 2 to 3 minutes. Take 2 tbsp. of melted butter, pour melted butter into the milk. Add 1 tsp salt to it. Add flour and whole wheat to the milk mixture. Mix them with the help of a spatula. Make dough of it. Add 1/2 cup of spinach and mix the sesame seeds. Now, leave the dough for 30 minutes. Put dough on butter paper and roll out thinly with the help of a rolling pin. Bake at *170 °C* for 18 min until golden brown.

Table 2 Nutritional Labelling of Nutri Snack per serving

Foods	Fat	Carbs	Protein	Calcium	Vit D	Cholesterol	Fiber	Sodium	Total calories
egg	4 g	0.6 g	6 g	30 mg	0.9 mcg	165 mg	0 g	60 mg	60 kcal
butter	81 g	0.1 g	0.9	24 mg	0 mcg	215 mg	0 g	643 mg	717 kcal
white flour	1.25 g	97.68 g	13.2 g	19 mg	0 mcg	0 mg	3.5 g	3 mg	466 kcal
vanilla essence	0 g	0.5 g	0 g	0.5 mg	0 mcg	0 mg	0 g	0.4 mg	12 kcal
brown sugar	0 g	0 g	0 g	64 mg	0 mcg	0 mg	0 g	0 mg	285 kcal
baking powder	0 g	1.1 g	0 g	0 mg	0mcg	0 mg	0 g	363 mg	2.4 kcal
Egg shell powder	0 g	0 g	0.5 g	5.1 g	0 mcg	0 mg	0 g	0 mg	2.1kcal

Nutritional labeling of green crackers is mentioned in detail in Table 1. There are 927 kcal in a cracker.

2.1.2. Possible Interaction:

Regarding spinach cookies and their potential interaction with calcium and vitamin D when consumed with tea, here is what you should consider: Many food products contain oxalate, such as spinach. Foods that contain a high ratio of oxalate affect calcium absorption. The link between soluble and insoluble oxalate in the small intestine affects oxalate bioavailability, and taking calcium together with oxalate-rich food can lower the absorption of both (Akhtar et al., 2011). The interaction of spinach with drugs is minimal. Spinach contains vitamin K in large quantities. The primary function of vitamin K is blood clotting. Warfarin slows the clotting of blood. Spinach slows the effect of warfarin.

2.2. Functional Food 2 (Nutri Snack)

2.2.1. Ingredients and Procedure:

The ingredients of the nutri snack recipe with quantity are eggshell powder (15 grams/1 tbsp.), Vanilla essence (4 drops /half tsp.), Butter (100 grams/2/3 cup), Brown sugar (75 grams/1/2 cup), Egg (1), White flour (128 grams/1 cup), and Baking Powder (4.2 grams/1 tsp.).

The four eggshells were boiled for 20 minutes and then baked for 15 minutes at 150°C. After baking, the samples were ground to a fine powder. Sugar, egg, baking powder, eggshell powder, butter, and white flour were added to another pan and whisked. Mix it well. After that, add vanilla essence. Make the dough and give it the shape of cookies. Then, the oven was preheated and baked at 150°C for 30 to 35 minutes until light brown. After that, cookies are ready and served.

2.2.2. Nutritional value per serving per cookie (large)

In Table 2, the nutritional value of the nutri snack per serving is mentioned. Cookies contain 403 mg of calcium, 7.6 g of carbohydrates, 6.7 g of fat, 1.58 g of proteins, 9.2 mg of cholesterol, 82.2 mg of sodium, 0.26 g of fiber, and 118.80 calories total.

2.2.3. Possible Interaction

Calcium absorption can be influenced by many factors, including the presence of certain compounds in food. For example, oxalates are found in some foods, such as spinach, which can bind to calcium and inhibit its absorption. However, no specific compounds in milk or tea can interfere with calcium absorption. In contrast, tea, especially black tea, contains tannins that

Table 3 Nutritional labelling of Osteomax per serving

Ingredients	Fat	Carbs	Protein	Calcium	Cholesterol	Fiber	Sodium	Total kcal
lotus seeds	1.2 g	41.2 g	9.8 g	3.2 mg	0 mg	16 g	3.2 mg	212 kcal
sesame seeds	9 g	4.2 g	3.2 g	2 mg	0 mg	3.3 g	2 mg	104 kcal
2 tbsp. poppy seeds	7.4 g	5 g	3.2 g	3.2 mg	0 mg	3.7 g	3 mg	94 kcal
flax seeds	9.9 g	9.9 g	5.7 g	35.8 mg	0 mg	7.8 g	4.2 mg	142 kcal
seedless dry dates	0 g	31 g	1 g	34 mg	0 mg	2.6 g	1 mg	110 kcal
almonds	24 g	9.08 g	9.98 g	264 mg	01 mg	12 g	0 mg	579 kcal
Dry ginger	0.5 g	1.07 g	0.11 g	2 mg	0 mg	0 mg	0 mg	4.8 kcal
crystal sugar	0 g	0 g	0 g	0 mg	0 mg	0 g	1 mg	9.0 kcal

can inhibit calcium absorption, and its effect is considered moderate. On the other hand, studies have shown that the impact of tea consumption on calcium absorption is minimal, mainly when calcium intake is adequate. Milk is a good source of calcium, and it contains lactose, which aids in calcium absorption. Moreover, milk is fortified with vitamin D, which helps facilitate calcium absorption (Waheed et al., 2019). Vitamin D is a fat-soluble vitamin that is better absorbed when consumed with dietary fat. Since milk contains fat, consuming egg-shell cookies with milk may enhance vitamin D absorption in the milk. In summary, consuming eggshell cookies with tea or milk is unlikely to impact calcium or vitamin D absorption significantly (Fleet, 2022).

2.3. Functional Food 3 (OSTEOMAX)

2.3.1. Ingredients and Procedure:

Ingredients of the osteomax recipe with quantity are Lotus seeds (2 cups/280 grams), Sesame seeds (2 tbsp. /20 grams), Poppy seeds (2 tbsp/18 grams), Flax seeds 2 tbsp./20 grams, Seedless dry dates 4/40 grams, Almonds 1 cup/100-gram, Dry ginger (1 inch/5 gram).

Take a bowl and roast 2 cups of lotus seeds and 1 cup of almonds until adequately roasted. Allow them to cool completely. Next, roast the four seedless dry dates. In a separate pan, add the 2 tbsp. of sesame seeds, 2 tbsp. flax seeds, 2 tbsp. of poppy seeds and dry ginger (cut into 1-inch pieces). Roast them properly, then let them cool completely. All the roasted ingredients were combined in a grinder, along with the two pieces of crystal sugar. They were ground into fine powder. Transfer the powder to an airtight container. Your calcium booster powder is now ready. Roast ingredients at 120 °C for 10 min; grind to fine powder

2.3.2. Serving per tablespoon:

A nutritional serving of Osteomax is given in Table 3. Fat 1.3 g, Carbohydrate 2.6 g, Protein 0.86 g, Calcium 9.05 mg, Fiber 1.19 g, Sodium 0.37 mg, Total kcal 33 kcal.

2.3.3. Versatile uses of Osteomax:

Add this powder to milk for a nutritious drink, sprinkle it over yogurt for an added crunch and flavor, blend the powder into smoothies for a healthy boost, or use it as a topping for salads or roasted vegetables. The seed powder was mixed with honey or nut butter to make a delicious spread.

Table 4 Nutritional composition Sementes wrap

Food	Fat	Carbs	Protein	Cholesterol	Calcium	Potassium	Vit D	Fiber	Calories
Wholegrain flour	1 g	76 g	10 g	0	18.8 g	230 mg	0.01 ug	13 g	366 kcal
White flour	1 g	100 g	13.64 g	0	18.8 g	107 mg	0	3.4 g	233kcal
Sesame seed	14.4 g	5 g	6 g	0	49 g	173.2 mg	_	5.1 g	297 kcal
Flax seed	11 g	10 g	18 g	0	92 g	300.8 mg	17 µg	10 g	450 kcal
Total	27.4 g	191	170.64	0	178.6 g	811 mg	11.01 ug	31.5 g	1,420kcal

2.3.4. Possible Interaction:

When considering the interaction between food and nutrient absorption, almonds and sesame seeds stand out with notable interactions. Almonds are good calcium sources and contain phytic acid, which may slightly inhibit calcium absorption. Sesame seeds, also rich in calcium, contain oxalates that could hinder calcium absorption to a minor extent. However, the overall impact of these interactions is considered minimal. Additionally, when you consume the prepared calcium booster powder with milk, you benefit from the synergistic effect of calcium and vitamin D absorption. Milk is a good source of calcium and naturally contains small amounts of vitamin D, which enhances calcium absorption. Therefore, combining osteomax powder with milk can further support the absorption and utilization of calcium and vitamin D. The remaining ingredients in your recipe, including lotus seeds, poppy seeds, seedless dry dates, dry ginger, flaxseeds, and crystal sugar, do not exhibit significant interactions with any specific nutrients or drugs. Their consumption alongside milk does not pose any notable interference with nutrient absorption.

2.4. Functional Food 4 (SEMENTES WRAP)

2.4.1. Ingredients and Procedure:

Ingredients of the segments recipe with quantities are listed: Whole wheat flour (1 cup/128 grams), White flour (2 cups/256 grams), Sesame seed (3 tbsp. /37 grams), and Flax seed. (3 tbsp. /37gram), Salt 1 Pinch, Oil (2 tablespoons/28grams).

First, 37 g of flaxseed and 37 g of sesame seeds were ground well to make powder. Take 2 cups of white flour and 1 cup of whole-grain flour. Add a pinch of salt. And two tablespoons of oil. The solution is gradually mixed with water to make dough. In addition, leave it for half an hour. Flaxseed and sesame seed powder were added and mixed well. Roll a small portion of the dough with a rolling pin. Make a 6-inch wrap of it. The wrap was added to a hot pan until it was cooked. Cook each side on a pre-heated pan at 180 °C for 1–2 min. Filling of wrap includes Chicken, Yogurt, Cucumbers, Lettuce, and Cheese

2.4.2. Serving per wrap:

The nutrients available in the Sementes wrap are Calcium 22.35 mg, Carbs 38.2 g, Fat 5.8 g, Protein 9.5 g, and Fiber 6.3 g. The total calories are 1174 kcal, and the Calories from each wrap are 234 kcal. The nutritional serving of the Sementes wrap is listed in Table 4.

2.4.3. Possible Interaction:

Flax seeds contain phytic acid, an anti-nutrient, ranging from 23 to 33 g/kg of flaxseed meal. Phytic acid interferes with calcium, zinc, magnesium, copper, and iron absorption. It is a potent chelator, forming protein and mineral-phytic acid complexes and thus reducing their

Table 5 Processing conditions for the developed calcium- and vitamin D-enriched functional foods

Functional Food	Main Ingredients	Processing Steps	Processing Temperature (°C)	Processing Time (minutes)	Remarks
Green Crackers	Spinach, wheat flour, sesame seeds, butter, milk	Kneading dough → resting → rolling → baking in oven	170 ± 2 °C	15–20	Baked until crisp and light golden brown
Nutri-Snack Cookies	Eggshell powder, white flour, butter, brown sugar, egg	Eggshells boiled → baked → ground → dough preparation → baking	150 ± 2 °C	30–35	Baked until light brown and firm
Osteomax Powder	Lotus seeds, almonds, sesame, flax, poppy seeds, dry ginger	Dry roasting of ingredients → cooling → grinding → mixing with sugar → packaging	120 ± 2 °C (roasting)	10–15	Roasted to a light golden color; no moisture left
Sementes Wrap	Whole wheat flour, white flour, sesame, flaxseed	Dough kneading → resting → rolling → pan cooking	180 ± 5 °C (pan surface)	1–2 per side	Cooked until brown spots appear and the surface is dry

bioavailability. The consumption of flaxseed may decrease the absorption of medication, vitamins, and minerals. Therefore, oral drugs should be taken 1 hour before or 2 hours after flaxseed to prevent reduced absorption of anticoagulants, antiplatelet drugs, NSAIDs, and antihypertensive drugs (Chen and Xu, 2023).

3. Statistical Analysis:

Compile the sensory evaluation form data into a format that will be useful for analysis. Determine the overall preference or liking based on the Hedonic Scale ratings by calculating the average rating for each product. If needed, use statistical analysis to find significant differences between goods using t-tests or analysis of variance (ANOVA)

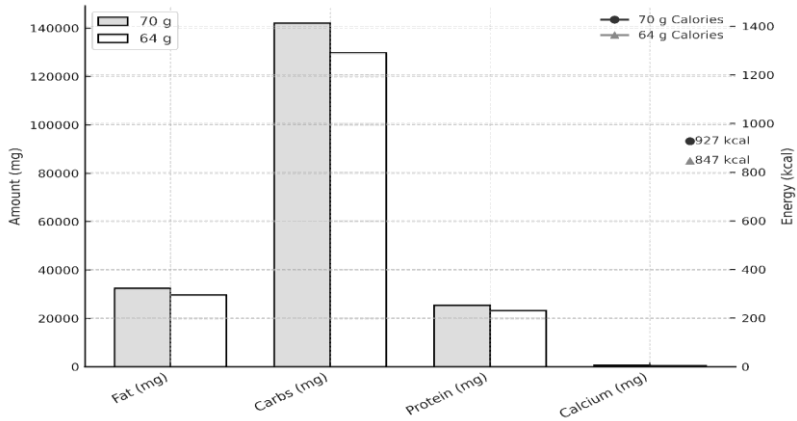

Figure 1 Nutritional comparison of 70g and 64g spinach-based crackers

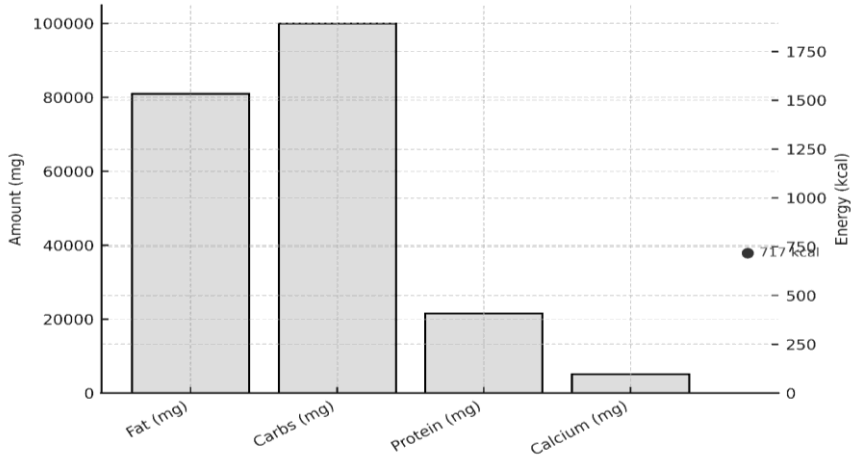

Figure 2 Nutritional Composition of Nutri Snack

Sensory data were analyzed using one-way analysis of variance (ANOVA) to compare mean scores among formulations, followed by Tukey's post-hoc test at $p < 0.05$ using SPSS v.26. Results are expressed as mean ± standard deviation (SD).

4. Results and Discussion:

These Functional foods were developed to enhance individuals' calcium and vitamin D levels. A hedonic scale was used for sensory evaluation, with the main aim of checking the acceptability of products.

4.1 Green Crackers (Spinach-Based)

Figure 1 illustrates the comparative nutritional and sensory evaluation of 70 g and 64 g spinach-based green crackers. The 70 g formulation demonstrated superior overall acceptability compared to the 64 g version. Sensory attributes, including texture, flavor, aroma, and appearance, were consistently rated higher for the 70 g crackers. The improved acceptability was primarily associated with better crispness and a less dense structure, whereas the 64 g crackers were comparatively harder and less palatable.

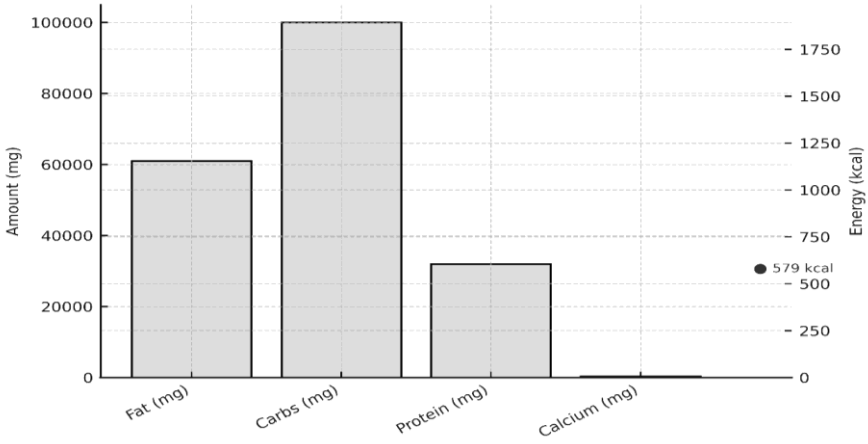

Figure 3 Nutritional composition of Osteomax

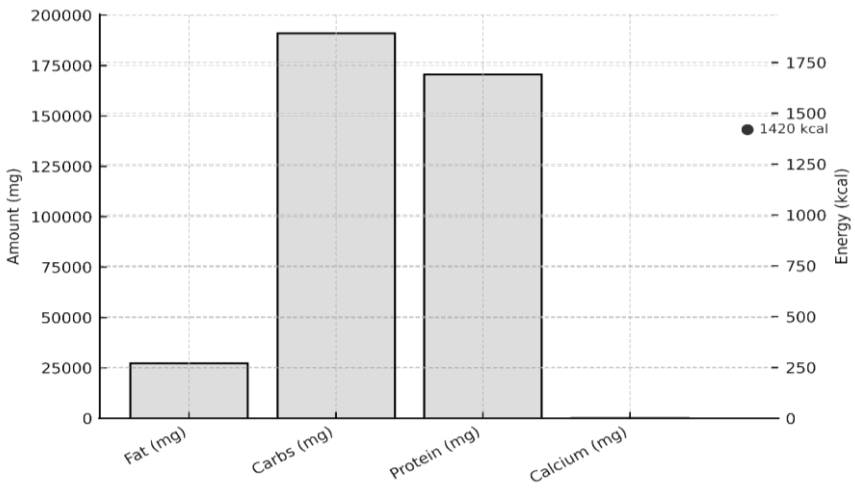

Figure 4 Nutritional Composition of Sementes Wrap

From a nutritional perspective, spinach contributes significantly to the mineral enrichment of the product, particularly calcium. It is well documented that one cup of raw spinach provides approximately 29.7 mg of calcium (Waseem et al., 2021). Calcium plays a vital role in bone mineralization, neuromuscular signaling, and muscle contraction. Previous studies have also shown that consuming spinach with vitamin C-rich foods enhances calcium absorption. Czarnowska-Kujawska et al. (2022) reported that fortifying bakery products with spinach (40 %) and kale (20 %) increased calcium, iron, and folate contents by up to twofold. In the present formulation, the incorporation of spinach powder substantially improved the calcium profile of the crackers while maintaining a desirable sensory texture. Consequently, the 70 g spinach-based green cracker can be considered the optimized formulation balancing nutritional value and consumer acceptability.

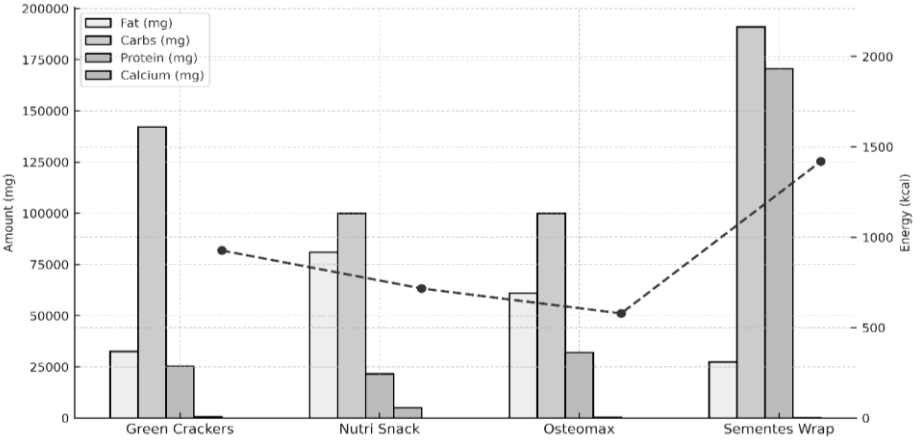

Figure 5 Comparative nutritional composition of functional foods

4.2 Nutri-Snack Cookies (Eggshell-Based)

Figure 2 presents the nutritional and sensory evaluation of Nutri-Snack cookies formulated using eggshell powder as a calcium fortification. The results revealed that Nutri-Snack cookies exhibited higher scores for appearance, aroma, sweetness, and overall acceptability compared with the control formulation. The enhanced sensory quality may be attributed to the optimized balance between texture and sweetness, contributing to consumer preference.

Eggshell powder (ESP), the principal ingredient in this formulation, represents a sustainable approach to valorizing food industry by-products. Eggshells are composed primarily of calcium carbonate (approximately 94%) and trace minerals such as magnesium and phosphorus, which are highly bioavailable. Aditya et al. (2021) demonstrated that eggshell-derived calcium is efficiently absorbed by the human body. Additionally, proper thermal or microbiological processing ensures safety by eliminating potential pathogens (Kulshreshtha et al., 2022).

Clinical investigations further confirm the functional value of ESP in improving bone mineral density, promoting tooth enamel re-mineralization, and supporting urinary stone clearance (Opris et al., 2020). Compared to other natural calcium sources, such as oyster shells, eggshell powder contains beneficial micro-minerals, offering a superior nutritional profile. Incorporating ESP into bakery and dairy products is thus an effective strategy to improve dietary calcium intake. Previous studies have validated eggshells as a low-cost, bioavailable, and safe calcium source suitable for functional food development (Arif et al., 2022). Consequently, the Nutri-Snack cookies developed in this study demonstrate both nutritional enhancement and consumer acceptance, supporting their potential as a fortified functional food.

4.3 Osteomax Powder (Seed Blend)

Figure 3 presents the sensory evaluation of Osteomax, a functional seed-based powder formulated from a blend of nutrient-rich seeds. The product achieved an exceptional overall acceptability score of 144 on the hedonic scale, reflecting high consumer preference for its appealing flavor, aroma, and smooth texture. Although all sensory attributes performed well, sweetness received slightly lower ratings, likely due to the inclusion of flaxseeds, which are naturally low in carbohydrates and high in dietary fiber.

Table 6 Mean Sensory Scores of Functional Food Formulations (9-Point Hedonic Scale*)

Product	Appearance	Aroma	Flavour	Texture	Overall Acceptability
Green Crackers (64 g spinach)	7.4 ± 0.3[b]	7.5 ± 0.2[b]	7.2 ± 0.4[b]	7.6 ± 0.3[b]	7.5 ± 0.3[b]
Green Crackers (70 g spinach)	8.2 ± 0.3[a]	8.0 ± 0.3[a]	8.1 ± 0.2[a]	8.4 ± 0.2[a]	8.1 ± 0.4[a]
Nutri Snack (eggshell fortified)	8.5 ± 0.2[a]	8.3 ± 0.3[a]	8.4 ± 0.3[a]	8.2 ± 0.3[a]	8.3 ± 0.2[a]
Osteomax (seed-based powder)	8.1 ± 0.3[a]	8.0 ± 0.2[a]	7.8 ± 0.2[b]	8.3 ± 0.3[a]	8.2 ± 0.3[a]
Sementes Wrap (sesame + flax)	7.8 ± 0.3[b]	8.0 ± 0.3[a]	7.2 ± 0.3[b]	7.9 ± 0.3[b]	7.6 ± 0.3[b]

Values represent mean ± SD (n = 25). Means within a column followed by different superscripts (a, b) differ significantly ($p < 0.05$).

This compositional characteristic contributes to glycemic regulation and supports the development of functional foods targeted at individuals with metabolic concerns (Rehman et al., 2021).

Nutritionally, flaxseeds are recognized for their rich profile of essential minerals, particularly calcium and potassium, and bioactive compounds that influence hormone regulation related to calcium deposition and bone health (Batool et al., 2024). Additionally, flaxseeds provide omega-3 fatty acids and lignans, which play significant roles in vitamin D and calcium metabolism. Chen et al. (2019) demonstrated that dietary supplementation with 10% flaxseed oil over 22 weeks improved bone formation biomarkers (ALP, P1NP, β-catenin, and osterix) while reducing bone resorption marker CTX-1 in experimental models.

Collectively, these findings support the nutritional potential of Osteomax powder as a plant-based functional supplement for promoting bone health and enhancing mineral absorption. The synergistic combination of seeds and flaxseed-derived bioactives establishes Osteomax as a valuable nutritional intervention for supporting skeletal integrity and overall wellness.

4.4 Sementes Wrap (Flaxseeds and Sesame)

Figure 4 illustrates the sensory evaluation of the Sementes Wrap, a functional formulation enriched with flaxseeds and sesame seeds. Interestingly, the control (simple wrap) exhibited higher scores in overall acceptability, flavor, and

sweetness compared to the Sementes Wrap. However, the Sementes Wrap achieved superior results for aroma and appearance, indicating that while its visual and aromatic appeal was enhanced by the inclusion of seeds, its taste profile was influenced by the inherent bitterness of sesame. The slightly lower sweetness and flavor perception can thus be attributed to the characteristic taste of sesame seeds.

Despite the minor sensory differences, sesame and flaxseeds provide substantial nutritional advantages, particularly in relation to bone health. Sesame seeds are rich in calcium (975 mg/100 g) and potassium (468 mg/100 g), both essential for maintaining bone mineral density (Arooj et al., 2023). Experimental studies have demonstrated that supplementation with sesame seed oil (0.25–0.5 mL/kg/day) or its extracts can enhance bone strength and mineral density in animal models. These effects are linked to the antioxidant and anti-inflammatory properties of sesame bioactives, which help mitigate bone loss and support skeletal health (Hsu et al., 2024).

Moreover, sesamolin, a natural lignan isolated from sesame oil, has been reported to protect against bone degradation by modulating NF-κB and MAPK signaling pathways (Yang et al., 2021). Therefore, while the Sementes Wrap exhibited moderate sensory acceptance, it possesses considerable nutritional value due to the synergistic effects of flaxseed and sesame-derived bioactives that contribute to bone health and overall well-being.

4.5 Nutritional Composition of Functional Foods

The developed calcium- and vitamin D-enriched products Green Crackers, Nutri Snack, Osteomax, and Sementes Wrap showed considerable variation in macronutrient and mineral profiles (Figure 5). Among them, Nutri Snack exhibited the highest calcium concentration (≈5100 mg per serving) due to the inclusion of eggshell powder, followed by Green Crackers (≈635 mg), Osteomax (≈344 mg), and Sementes Wrap (≈179 mg). The elevated calcium in Nutri Snack underscores the potential of eggshell waste as a bioavailable, low-cost calcium source. Energy values ranged from 579 kcal (Osteomax) to 1420 kcal (Sementes Wrap), primarily reflecting fat and carbohydrate content. Green Crackers provided a balanced nutritional profile (32.5 g fat, 25.4 g protein, 142 g carbohydrates), offering a moderate-energy, high-fiber alternative suitable for elderly populations at risk of osteopenia.

The high-energy Sementes Wrap, rich in flax and sesame seeds, contributed substantial unsaturated fats and lignans known to modulate bone metabolism. These compositional results confirm that the formulated foods collectively deliver synergistic sources of calcium, vitamin D, and essential fatty acids, key for maintaining bone mineralization and endocrine regulation of calcium homeostasis.

4.6 Sensory Evaluation and Product Acceptability

The sensory response pattern assessed through a nine-point Hedonic Scale revealed statistically significant ($p < 0.05$) differences among formulations (Table 6). Green Crackers containing 70 g spinach powder achieved the highest mean score (8.1 ± 0.4) for texture, crispness, and overall acceptability, outperforming the 64 g variant. Nutri Snack cookies were highly rated for appearance, aroma, and sweetness, consistent with their butter-rich matrix and eggshell calcium content. Osteomax, a powdered seed blend, achieved high acceptability due to its nutty aroma and smooth texture, while Sementes Wrap displayed moderate acceptability, largely limited by a bitter aftertaste from sesame oxalates.

The overall sensory pattern demonstrates that fortification with natural calcium sources can enhance nutritional

quality without compromising consumer appeal when ingredient ratios are optimized.

4.7 Sensory Evaluation and Product Acceptability

Sensory evaluation of the developed calcium- and vitamin D-enriched functional foods was conducted using a nine-point Hedonic Scale by a panel of 25 semi-trained assessors. Attributes including appearance, aroma, flavor, texture, and overall acceptability were recorded, and data were analyzed by one-way ANOVA followed by Tukey's post-hoc test ($p < 0.05$).

The sensory profiles (Table 5) revealed significant ($p < 0.05$) differences among formulations. **Green Crackers** fortified with 70 g spinach powder achieved the highest scores for texture (8.4 ± 0.2) and overall acceptability (8.1 ± 0.4), outperforming the 64 g variant, which scored lower for color and mouthfeel. The moderate green hue and crisp texture of the 70 g formulation improved visual and textural perception without introducing bitterness.

Nutri Snack cookies obtained the highest overall sensory scores (8.3 ± 0.2) for appearance, aroma, and flavor. Butter and eggshell-derived calcium contributed to a desirable creamy flavor and cohesive structure, enhancing palatability. **Osteomax**, a seed-based powder blend, received high texture and aroma scores (8.3 ± 0.3 and 8.0 ± 0.2, respectively) but a slightly lower flavor rating (7.8 ± 0.2), possibly due to mild flaxseed bitterness. Nevertheless, its balanced sensory performance supports its suitability as a functional supplement.

The **Sementes Wrap** achieved moderate acceptance (7.6 ± 0.3) because of a slight bitter aftertaste associated with sesame oxalates, though its aroma and appearance were rated favorably. Flavor masking strategies, such as the incorporation of herbs, yogurt-based dressings, or low-sodium condiments, may further enhance consumer perception.

Mean sensory scores are summarized in Table 6. Overall, Nutri Snack and Green Crackers (70 g spinach) exhibited the most balanced and desirable sensory profiles. The results confirm that fortification with natural calcium and vitamin D sources did not negatively influence consumer acceptance. On the contrary, the optimized ingredient ratios improved both texture and aroma, reinforcing the feasibility of producing nutritionally enhanced foods with high market appeal.

4.8 Functional and Mechanistic Insights

The integration of spinach, flaxseed, sesame, and eggshells yielded foods combining micronutrient density with functional bioactives. Spinach provides oxalate-bound calcium and magnesium, whose bioavailability can increase in the presence of vitamin C and lipid matrices. Eggshell powder contributed to highly soluble calcium carbonate and trace elements (Sr, Mg, F) that enhance bone remodeling. Seeds such as flax and sesame provide α-linolenic acid and lignans, which influence osteoblast differentiation via the Wnt/β-catenin pathway. Together, these interactions underline the multi-mechanistic potential of the developed foods: (i) direct calcium and vitamin D supply, (ii) enhanced intestinal absorption through lipid and phytochemical synergy, and (iii) modulation of bone-formation signaling.

4.9 Overall Evaluation

From both nutritional and sensory perspectives, all four formulations exhibited promising potential as cost-effective functional foods for calcium and vitamin D supplementation. Among them, the 70 g spinach Green Crackers and the Nutri Snack cookies emerged as the most acceptable and nutrient-dense prototypes. Minor formulation adjustments, such as flavor masking of sesame bitterness or partial fat substitution, could further

enhance consumer perception and commercial feasibility.

5. Conclusion

These cost-effective functional foods are rich in calcium and other bioactive compounds, and they can improve bone health and overall well-being in the elderly. However, caution is needed with calcium-rich foods for those on blood-thinning medications. The overall sensory evaluation showed that all products were good in taste, aroma, flavor, and other parameters, but concerning green crackers, the 70g spinach product showed better results.

5.1 Antioxidant Potential of Functional Ingredients

Although antioxidant assays were not performed in the present work, the ingredients used, spinach, flaxseed, and sesame seeds, are rich in phenolic compounds, lignans, and tocopherols that possess significant antioxidant activity (Arooj et al., 2023; Batool et al., 2024). These bioactives may indirectly contribute to bone protection by reducing oxidative stress induced bone resorption. Future studies should quantify the antioxidant capacity (e.g., DPPH, ABTS, FRAP) of the developed products to substantiate their therapeutic potential

5.2 Future Research

Future research must evaluate the stability and shelf-life of these fortified foods under a range of temperature and humidity conditions to ensure product safety and nutrient retention during storage. Future studies should determine the storage stability and shelf-life of such fortified foods under different temperatures and humidities to ensure product safety and nutrient retention upon storage. Furthermore, pilot-scale human trials assessing the bioavailability of calcium and vitamin D and their effect on bone markers are suggested to validate pre-clinical findings. Because nutrient quality and sensory response are not adequate to determine the bioavailability or physiological action of calcium and vitamin D, pilot human studies are needed to determine the absorption and bone metabolism activity of these functional foods in real consumers.

The present study focused on developing and evaluating calcium- and vitamin D-enriched functional foods using locally available ingredients and by-products. Although sensory evaluation and nutrient profiling confirmed their acceptability and nutritional potential, human bioavailability and physiological efficacy cannot be determined through compositional analysis alone. The absorption and utilization of calcium and vitamin D are influenced by several factors, including individual metabolic status, gut health, and interactions with other dietary components (Capozzi et al., 2020; Fleet, 2022).

Therefore, conducting pilot-scale human trials is essential to assess how effectively these nutrients are absorbed and contribute to bone health biomarkers such as serum calcium, 25(OH)D, alkaline phosphatase, and bone mineral density. Such translational research bridges the gap between food formulation and clinical application, validating the functional efficacy of developed products before large-scale commercialization or public health implementation.

Funding

N/A

Conflict of interest

All authors declare that there is no conflict of interest.

Consent of publication

All authors gave their consent for publication.

References

Aditya, S., Stephen, J., & Radhakrishnan, M. (2021). Utilization of eggshell waste in calcium-fortified foods and other industrial applications: A review. *Trends*

in Food Science & Technology, *115*, 422-432.

Ahmad, D., Afzal, M., & Imtiaz, A. (2020). Effect of socioeconomic factors on malnutrition among children in Pakistan. *Future Business Journal*, *6*, 1-11.

Akhtar, M. S., Israr, B., Bhatty, N., & Ali, A. (2011). Effect of cooking on soluble and insoluble oxalate contents in selected Pakistani vegetables and beans. *International Journal of Food Properties*, *14*(1), 241-249.

Arif, S., Pasha, I., Iftikhar, H., Mehak, F., & Sultana, R. (2022). Effects of eggshell powder supplementation on nutritional and sensory attributes of biscuits. *Czech Journal of Food Sciences*, *40*(1).

Arooj, A., Rabail, R., Naeem, M., Goksen, G., Xu, B., & Aadil, R. M. (2023). A comprehensive review of the bioactive components of sesame seeds and their impact on bone health issues in postmenopausal women. *Food & Function*, *14*(11), 4966-4980.

Batool, I., Altemimi, A. B., Munir, S., Imran, S., Khalid, N., Khan, M. A., ... & Aadil, R. M. (2024). Exploring Flaxseed's potential in enhancing bone health: Unveiling osteo-protective properties. *Journal of Agriculture and Food Research*, 101018.

Capozzi, A., Scambia, G., & Lello, S. (2020). Calcium, vitamin D, vitamin K2, and magnesium supplementation and skeletal health. *Maturitas*, *140*, 55-63.

Chanchlani, R., Nemer, P., Sinha, R., Nemer, L., Krishnappa, V., Sochett, E., ... & Raina, R. (2020). An overview of rickets in children. *Kidney international reports*, *5*(7), 980-990.

Chen, F., Wang, Y., Wang, H., Dong, Z., Wang, Y., Zhang, M., ... & Xu, J. (2019). Flaxseed oil ameliorated high-fat-diet-induced bone loss in rats by promoting osteoblastic function in rat primary osteoblasts. *Nutrition & Metabolism*, *16*, 1-13.

Chen, W., & Xu, D. (2023). Phytic acid and its interactions in food components, health benefits, and applications: A comprehensive review. *Trends in Food Science & Technology*, 104201.

Chopra, A. S., Lordan, R., Horbańczuk, O. K., Atanasov, A. G., Chopra, I., Horbańczuk, J. O., ... & Arkells, N. (2022). The current use and evolving landscape of nutraceuticals. *Pharmacological Research*, *175*, 106001.

Czarnowska-Kujawska, M., Starowicz, M., Barišić, V., & Kujawski, W. (2022). Health-promoting nutrients and potential bioaccessibility of breads enriched with fresh kale and spinach. *Foods*, *11*(21), 3414.

Fleet, J. C. (2022). Vitamin D-mediated regulation of intestinal calcium absorption. *Nutrients*, *14*(16), 3351.

Hsu, C. C., Ko, P. Y., Kwan, T. H., Liu, M. Y., Jou, I. M., Lin, C. W., & Wu, P. T. (2024). Daily supplement of sesame oil prevents postmenopausal osteoporosis via maintaining serum estrogen and aromatase levels in rats. *Scientific reports*, *14*(1), 321.

Kulshreshtha, G., Diep, T., Hudson, H. A., & Hincke, M. T. (2022). High value applications and current commercial market for eggshell membranes and derived bioactives. *Food Chemistry*, *382*, 132270.

Lemieux, I., & Després, J. P. (2020). Metabolic syndrome: past, present and future. *Nutrients*, *12*(11), 3501.

Melguizo-Rodríguez, L., Costela-Ruiz, V. J., García-Recio, E., De Luna-Bertos, E., Ruiz, C., & Illescas-Montes, R. (2021). Role of vitamin D in the metabolic syndrome. *Nutrients*, *13*(3), 830.

Opris, H., Dinu, C., Baciut, M., Baciut, G., Mitre, I., Crisan, B., ... & Bran, S. (2020). The influence of eggshell on bone regeneration in preclinical in vivo studies. *Biology*, *9*(12), 476.

Rehman, A., Saeed, A., Kanwal, R., Ahmad, S., & Changazi, S. H. (2021). Therapeutic effect of sunflower seeds and flax seeds on diabetes. *Cureus*, *13*(8).

Salari, N., Ghasemi, H., Mohammadi, L., Behzadi, M. H., Rabieenia, E., Shohaimi, S., & Mohammadi, M. (2021). The global prevalence of osteoporosis in the world: a comprehensive systematic review and meta-analysis. *Journal of orthopaedic surgery and research*, *16*, 1-20.

Shlisky, J., Mandlik, R., Askari, S., Abrams, S., Belizan, J. M., Bourassa, M. W., ... & Weaver, C. (2022). *Calcium deficiency worldwide: prevalence of inadequate intakes and associated health outcomes* (Vol. 1512, No. 1, pp. 10-28).

Waheed, M., Butt, M. S., Shehzad, A., Adzahan, N. M., Shabbir, M. A., Suleria, H. A. R., & Aadil, R. M. (2019). Eggshell calcium: A cheap alternative to expensive supplements. *Trends in Food Science & Technology*, *91*, 219-230.

Waseem, M., Akhtar, S., Manzoor, M. F., Mirani, A. A., Ali, Z., Ismail, T., ... & Karrar, E. (2021). Nutritional characterization and food value addition properties of dehydrated spinach powder. *Food Science & Nutrition*, *9*(2), 1213-1221.

Yang, X., Liang, J., Wang, Z., Su, Y., Zhan, Y., Wu, Z., ... & Zhou, B. (2021). Sesamolin protects mice from ovariectomized bone loss by inhibiting osteoclastogenesis and RANKL-mediated NF-κB and MAPK signaling pathways. *Frontiers in Pharmacology*, *12*, 664697.

UCP Journal of Science and Technology
Vol. 3, Issue 1 (July - December 2025)
Journal website: http://ojs.ucp.edu.pk/index.php/ucpjst/index

Power Line Communication Feasibility Study for Advanced Metering Infrastructure Project of an Electric Utility in Pakistan

Sabir Hussain[1*], Ghulam Jaffer[2], Saddam Hussain[3]

Abstract

Power Line Communication (PLC) leverages existing power lines for communication purposes, offering an economically viable alternative to other communication methods that entail the additional expense of establishing new infrastructure. This paper presents a comprehensive analysis of tests conducted on PLCs within the context of the Advanced Metering Infrastructure (AMI) Project, focusing on grid modernization. Addressing the unique challenges posed by power lines requires meticulous planning, particularly in the strategic placement of filters. The study specifically targets two urban areas, subjecting them to thorough examination using a Noise toolkit consisting of a Coupler and a Spectrum Analyzer. The research incorporates three distinct load types—domestic, commercial, and industrial—to conduct a comparative analysis of the results obtained. While PLC has been deployed internationally, there is limited large-scale field data available in the Pakistani context. This study contributes important baseline measurements and technical benchmarks, demonstrating that G3-PLC, operating in the FCC band, is a reliable and scalable solution for smart metering communication in urban distribution networks.

Keywords: Advanced Metering Infrastructure (AMI), Smart Meter (SM), Power Line Communication (PLC), Low-Tension Distribution Network (LTDN), Narrowband (NB), Broadband (BB).

1. Introduction

Islamabad Electric Supply Company (IESCO) is a public electric distribution company that supplies, distributes, and sells electricity from Attock to Jhelum; an area spanning six districts of Punjab, Pakistan and a consumer base of approx. 3.5 million. As part of grid modernization, the Advanced Metering Infrastructure (AMI) project was undertaken with funding from Asian Development Bank (ADB). The project is aimed at improving the meter-to-cash facility on the LT distribution network. The AMI project consists of several technological advancements to the legacy system, including a Smart Meter (SM) at the customer's premises, Communication Infrastructure between SM and a Head End System (HES) and between HES and the Meter Data Management System (MDMS). The MDMS is a centralized module that contains analytical tools required to communicate with other modules. It is also aimed at monitoring, management, control, and integration of smart metering data with other systems such as Billing System, Consumer

[1] Islamabad Electric Supply Company (IESCO), Islamabad, Pakistan
[2] EDGJ® Consultancy, Luxembourg, Luxembourg
[3] School of Science, Harbin Institute of Technology, Shenzhen 518055, China
[*]Corresponding author's E-mail: engineersabirhussain14@gmail.com
Received: 25 October 2025; Received in revised form: 10 December 2025; Accepted: 16 December 2025.
Available online: 23 December 2025.

DOI: https://doi.org/10.24312/ucp-jst.03.01.718

Information System (CIS), Geographic Information System (GIS), Outage Management System (OMS), etc (Ramyar et al., 2014).

The communication infrastructure for the AMI Project at IESCO consists of Power Line Communication (PLC) and a cellular network. The PLC is used as a means of communication between SM and Data Concentrator Unit (DCU), whereas cellular technology is the preferred mode of communication between HES and MDMS, and in the case of independent transformers, between SM and HES (direct link). The choice of communication infrastructure depends on the cost and flexibility of deployment. PLC is a natural choice of communication due to the already laid infrastructure of power lines, large coverage, and low cost. The cellular WAN provides a wireless link, and therefore, it is desirable for areas where PLC is not feasible.

1.1 Literature Review

The PLC carries data on the same conductor line that is used for AC/DC Power transmission (50 Hz or 60 Hz) at frequencies below 500kHz. Applications of PLC range from Automatic Meter Reading (AMR) to Remote Monitoring, and Home/Industrial Automation (Ramyar et al., 2014; Galli et al., 2011).

The PLC is broadly categorized into Narrowband (NB) PLC, Mid-Band PLC, and Broadband (BB) PLC (Stefano et al., 2011; ITU-T G.9903, 2012). Examples of NB-PLC include G-3 and PRIME, Mid-Band PLC includes High-speed Power Line Communication (HPLC), and Broadband PLC includes High-Definition Power Line Communication (HD-PLC), HomePlug AV (HomePlug), and Gigabit Home Networking (G.hn) standards. PLC standards are specifications that define how communication signals can be transmitted over the power lines. These standards ensure interoperability and compatibility among devices and systems that use PLC technology (IEEE Std 1901.2-2013; G3-PLC Alliance, 2023). Some of the notable standards include:

ITU-T G.hn (G.9960/G.9961/G.9962/G.9963): This set of standards, developed by the International Telecommunication Union (ITU), defines a high-speed, low-complexity networking standard for multimedia networking over power lines, phone lines, and coaxial cables. It aims to provide a unified standard for various wired communication media (Enel Group, 2022).

IEEE 1901: The Institute of Electrical and Electronics Engineers (IEEE) 1901 standard specifies the use of broadband communication over power lines. It includes provisions for coexistence with other power line communication technologies and outlines the Physical (PHY) and Medium Access Control (MAC) layers (G3-PLC Alliance, 2023).

HomePlug AV (IEEE 1901.1): This is a specific implementation of the IEEE 1901 standard for power line communication in home networking environments. HomePlug AV focuses on delivering high-speed data over existing home electrical wiring (G3-PLC Alliance, 2023).

ITU-T G.9903 (PRIME): The ITU-T G.9903 standard, also known as PRIME (Powerline Intelligent Metering Evolution), is designed for narrowband power line communication systems. It is often used in smart grid applications, particularly for advanced metering infrastructure (IEEE Std 1901.2-2013).

IEC 61334 (CENELEC EN 50065): The International Electrotechnical Commission (IEC) and the European Committee for Electrotechnical Standardization (CENELEC) have developed standards such as IEC 61334, which specifies the data communication protocols for power line communication in electricity metering.

G3-PLC (ITU-T G.9903, IEEE 1901.2): G3-PLC is a power line communication standard that builds upon the ITU-T G.9903 standard. It is designed for smart grid applications, offering robust and reliable communication for utility companies (G3-PLC Alliance, 2023, and Enel Group, 2022).

PLC suffers from interference, which can severely impair its performance. The types of interference include colored noise, white noise, narrowband noise, crosstalk, impulse noise, and asynchronous impulse noise. Furthermore, PLC has further drawbacks, including security issues (eavesdropping and jammers) (Yan et al., 2012, and Ahmed et al., 2021), power cable degradation, and the cost of installation of filters and repeaters. Filters are typically used for SMs in situations where communication signals are affected by unwanted signals. Strategic placement of filters is of utmost importance and needs careful planning. To pre-emptively address potential communication issues, a proactive approach involves analyzing the noise beforehand. To achieve this, a comprehensive survey was conducted to assess and confirm that the performance of the PLC falls within an acceptable range.

Power Line Communication (PLC) has gained traction globally as a reliable communication technology for Advanced Metering Infrastructure (AMI). It uses existing electrical power lines to transmit data, thereby eliminating the need for new communication infrastructure. This makes PLC a cost-effective solution, especially in urban environments where low-voltage distribution networks are already established. (Galli et al., 2011) emphasized the role of PLC in smart grids, highlighting the technology's adaptability to noisy environments and its suitability for applications like AMR, demand-side management, and distribution automation. (Mohassel et al., 2014) emphasized the cost-efficiency and scalability of PLC, particularly narrowband versions such as G3-PLC and PRIME. G3-PLC, based on the ITU-T G.9903 standard, supports IPv6, robust modulation schemes (OFDM), and offers strong performance under electromagnetic interference (IEEE Std 1901.2-2013 and G3-PLC Alliance, 2023). IEEE 1901.2 and PRIME (ITU-T G.9904) are also widely adopted in utility environments.

Large-scale PLC deployments have been successful in Europe and Asia. Utilities such as EDF (France) and Enel (Italy) adopted G3-PLC and PRIME, while Chinese and Japanese utilities use PLC for suburban and rural networks (Enel Group, 2022; Yan et al., 2012; and Ahmed et al., 2021). Recent reviews by (Ahmed et al., 2021) and Sajid et al. 2023) highlight that PLC's performance is highly dependent on load profiles, topology, and environmental noise. This is especially relevant for Pakistan, where consumer-side interference (e.g., motors, UPS systems) is common.

The Pakistan Smart Grid Roadmap (NTDC, 2019) recognized PLC as a viable solution for distribution-level automation. ADB-supported pilot projects such as IESCO's AMI rollout are among the first to test PLC feasibility at this scale in the country (NTDC, 2019, and Asian Development Bank, 2020). This paper adds value by contributing real-world, large-sample analysis of G3-PLC under Pakistan's urban grid conditions, helping define local SNR, noise, and profile delivery benchmarks.

2. Methodology

A. Site Identification

A diverse range of sites was systematically tested, encompassing residential, commercial, and industrial areas. The testing occurred at different times, including normal conditions and peak hours, to capture variations in noise with different loads at different times.

Three subdivisions in densely populated areas of Rawalpindi were selected for this task.

B. Noise Measurement Equipment

The test setup included the following:

1) Coupler: for coupling the PLC signal with the Power signal

2) Spectrum Analyzer: The Spectrum Analyzer was used to analyze the frequency range and signal strength within the PLC communication band. It was configured with a frequency span from 100 kHz to 500 kHz, a resolution bandwidth (RBW) of 9.1 kHz, and a video bandwidth (VBW) of 30 kHz. The sweep time was set to 10 milliseconds, with a reference level of 100 dBµV and an attenuation of 10 dB. The vertical scale was in dBµV, and two detector modes were used: Max Hold to capture the peak PLC signal (displayed as a yellow line), and Average to measure background noise levels (shown as a green line). These settings allowed for clear identification and comparison of the PLC signal versus noise in different site conditions.

3) Smart Meter: for sending a continuous signal

4) Laptop: to initiate the signal

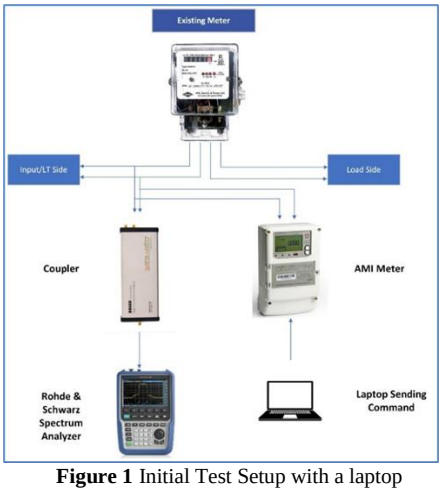

Figure 1 Initial Test Setup with a laptop

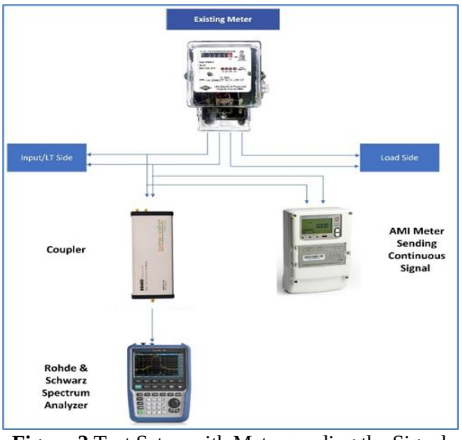

Figure 2 Test Setup with Meter sending the Signal

C. Test Setup

Initially, the experimental setup featured a prototype incorporating a laptop running specialized software that triggered a signal transmission to the DCU, initiating a PLC signal, which was subsequently visualized on the Spectrum Analyzer, as illustrated in Figure 1.

Later, the AMI meter was programmed in such a way that it was continuously/periodically giving a PLC signal so that the noise and Signal-to-Noise ratio (SNR) can be measured, as shown in Fig. 2. Residential, Commercial, and Industrial loads were tested using the prototype described during different times of the day, i.e, normal and peak hours.

D. Spectrum Analysis

To understand the output of the spectrum analyzer, it is essential to examine the graph generated by the Spectrum Analyzer, as illustrated in Fig. 3. The graph's horizontal axis denotes the frequency range, approximately set between 100 and 500kHz (~FCC Band), while the vertical axis signifies signal strength in dBµV. Various lines on the graph convey distinct information. The Yellow Line corresponds to the latched maxima and generally depicts the PLC Signal in the 100k-500k band. The Green Line represents the instantaneous state,

Figure 3 Spectrum Analyzer Output

which is mostly Noise. The lines labelled M1, M2, M3, and M4 indicate markers placed to capture readings at specific points. The vertical variance between the yellow line and the green line, marked at four distinct points, reflects the SNR. The "robust" mode of G3-ALLIANCE improves communication under noisy channel conditions, operating at -1 dB SNR. However, the baseline for this survey is SNR 10 dBµV, above the minimum required in harsh conditions.

E. Defined Benchmarks for Evaluation

To ensure reliable PLC communication and assess feasibility for AMI deployment, the following technical benchmarks were used in this study:

Minimum Signal-to-Noise Ratio (SNR): 10 dBµV (As per G3-PLC specifications for robust mode; values below may impair communication). Acceptable Noise Level: Below 80 dBµV (Higher noise levels, especially below 200 kHz, can interfere with signal stability). Maximum Transmission Distance: 421 meters (Based on the longest tested distribution line in this study with successful profile delivery). Head-End System (HES) Data Retrieval KPI: ≥97% of daily profiles delivered within 24 hours - 100% of profiles within 48 hours (as per SoR requirements). These benchmarks guided field data interpretation and performance classification of G3-PLC under residential, commercial, and industrial load conditions.

3. Results

The analysis was conducted in Rawalpindi city in the areas where smart meters are to be installed in the scope of the project. A large sample size was obtained from over 100 locations. Three typical surveys' data are presented below for reference: one each from residential, commercial, and industrial areas, respectively.

Also, the metering point loading conditions were very diverse, which was also a factor in understanding the noise profile. The effect of load was not directly proportional to the noise profile on the sampling point, but the nature of loads connected in the vicinity of the same distribution line seems to have a greater effect on the noise profile.

Figure 4 Output of the Spectrum Analyzer for the Residential Area

A. Residential Area – PLC Signal and Noise Performance

The minimum SNR observed was 39 dBµV @ 155KHz, and the maximum was 56 dBµV @ 250KHz. For stable communication, a minimum SNR of 10 dBµV is required. In this case, the average SNR 39.5 dBµV exceeds the minimum SNR by 29.5 dBµV (Figure 4 and Table 1).

B. Commercial Area – PLC Signal and Noise Performance

The following is data from a survey in a commercial area (Tubewell setup, Service Road West, Rawalpindi). The minimum SNR observed was 25 dBµV @ 155KHz, and the maximum was 52 dBµV @ 250KHz. For stable communication, a minimum SNR of 10 dBµV is required. In this case, the average SNR 42.25 dBµV exceeds the minimum SNR by 32.25 dBµV (Figure 5 and Table 2).

C. Industrial Area – PLC Signal and Noise Performance

The following is data from a survey in an industrial area. The minimum SNR observed was 19 dBµV @ 155KHz and the maximum was 43 dBµV @ 250KHz. For stable communication, a minimum SNR of 10 dBµV is required. In this case, the average SNR 32.5 dBµV exceeds the minimum SNR by 22.5 dBµV. The performance of the G3 PLC communication may also be analysed through the Head-End System. The HES allows for the collection of communication statistics of the AMI nodes, including the G3 PLC-enabled nodes. Typically, one DCU is installed at the source of each distribution line at the transformer, which acts as the focal point for all the downstream G3 smart meters. The DCUs are GSM-enabled and use 2G/4G data to connect with the Headend Server to relay data. The HES collects energy profiles, amongst other data from the smart meters, on a periodic basis. The rate at which the energy profiles are successfully fetched by the Headend system is an indicator of the health of G3 PLC smart meters' communication (Figure 8). The following indicators are used to determine the health of G3 PLC smart meters' communication:

Table 1 Residential Area Noise Markers' Data

Meter Type / Phase	Spectrum Frequency KHz		PLC Signal Peak Value (dBµV)		Noise Signal Peak Value (dBµV)		SNR
1Ø Domestic	M1	155	M1	81	M1	39	42
	M2	250	M2	95	M2	56	39
	M3	350	M3	87	M3	45	42
	M4	450	M4	85	M4	50	35
			Av.	87	Av.	47.5	39.5

Table 2 Commercial Area Noise Markers' Data

Meter Type / Phase	Spectrum Frequency KHz		PLC Signal Peak Value (dBµV)		Noise Signal Peak Value (dBµV)		SNR
1Ø Commercial	M1	155	M1	86	M1	61	25
	M2	250	M2	99	M2	47	52
	M3	350	M3	97	M3	53	44
	M4	450	M4	95	M4	47	48
			Av.	94.25	Av.	52	42.25

Figure 5 Output of the Spectrum Analyzer for the Commercial Area

1) Daily Energy Profile Data Collection Rate

The G3 PLC smart meters are configured to record energy profiles on 24-hour intervals. These energy registers are pushed to the HES daily once the profile period elapses, which in this case is 0000 hours. The success rate is categorized in the delay in arrival of the profiles at the HES. The criteria are divided into arrival times corresponding to the colour indicated in the following legend in hours / Days (Exclude Collect indicates meters which were excluded from collection by HES).

Two distribution transformers covered entirely with G3 PLC downstream smart meters are presented below as the case study. The bar chart represents the percentage of daily energy profiles received from the G3 PLC smart meters for the corresponding day (Figure 7 & 9).

Case I: 200kVA Transformer @ Al Noor Colony, Street 7, Rawalpindi

The 200kVA transformer feeds 245 metering units, all of which are G3 PLC-based. The distribution line spans 421m in length. The daily profile reads are retrieved with a 100% rate within the first 24 hours, and over 97% of them are within the first 3 hours of profile generation. This is consistently achieved every day of the week. It is an indicator of PLC communication health and robustness, as evident from the 100% profile reading made by the HES through PLC.

Case II: 200kVA Transformer @ KRL Road (Near Faisal Bank), Rawalpindi

The 200kVA transformer feeds 156 metering units, all of which are G3 PLC-based. The distribution line spans 225m in length. The daily profile reads are retrieved with a 100% rate within the first 24 hours of profile generation. Also, a minimum of 70% of the profiles are retrieved within the

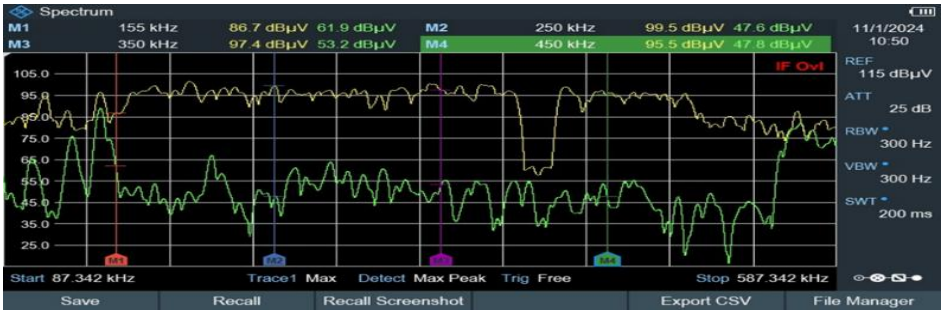

Figure 6 Output of the Spectrum Analyzer for the Industrial Area

Figure 7 G3 PLC Smart Meters Daily Profile Data (07 days)

first 3 hours of profile generation, while 80% availability is observed within the first 12 hours. It is again observed that PLC communication health is allowing for 100% profile readings within the same day.

Figure 8 G3 PLC Connectivity to the Head End System (HES)

2) Hourly Energy Profile Data Collection Rate

The G3 PLC smart meters are also configured to record energy profiles on hourly intervals. These energy registers are pushed to the HES once the profile period elapses, which in this case is every one hour. The success rate is categorized in the delay in arrival of the profiles at the HES. The criteria are divided into arrival times corresponding to the colour indicated in the following legend in hours / Days (Exclude Collect indicates meters which were excluded from collection by HES).

Two distribution transformers covered entirely with G3 PLC downstream smart meters are presented below as the case study. The bar chart represents the percentage of hourly energy profiles received from the G3 PLC smart meters for the corresponding hour of the day (Figure 10 & 11).

Case I: 200kVA Transformer @ Al Noor Colony, Street 7, Rawalpindi

The 200kVA transformer feeds 245 metering units, all of which are G3 PLC-based. The distribution line spans 421m in length. All hourly energy profiles are being retrieved by the Headend within the first 24 hours of profile generation at the smart meter. Over 95% profiles are available in the HES within the first 6-12 hours of profile generation. The success rate of 100% profile arrival at HES within the first 24 hours of the profiling period is indicative of good PLC health.

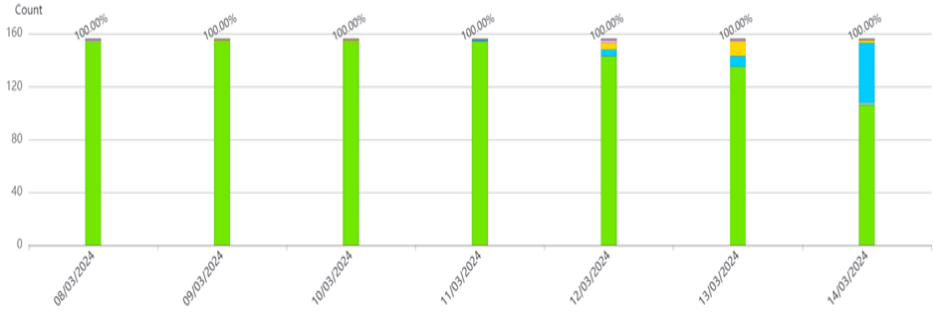

Figure 9 G3 PLC Smart Meters Daily Profile Data (07 days)

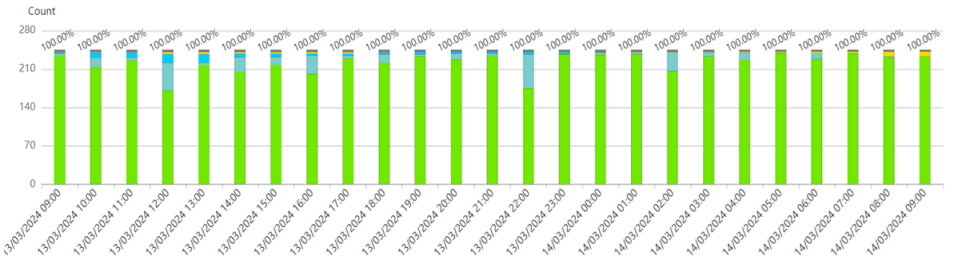

Figure 10 G3 PLC Smart-Meters Hourly Profile data [Last 24 Hours] - Al Noor

Case II: 200kVA Transformer @ KRL Road (Near Faisal Bank), Rawalpindi

The 200kVA transformer feeds 156 metering units, all of which are G3 PLC-based. The distribution line spans 225m in length. 98% of the hourly profiles in this case are being retrieved by the Headend within the first 12 hours, except for intervals occurring from 12 pm to 18 pm, where retrieval is within 24 hours. The intervals for which 98-99% data is retrieved after 24 hours shall be considered in the missing data retrieval cycle (data was extracted from HES before the 48-hour window). This may be caused by low GSM network QoS or related to the nature of the load affecting the noise profile during daylight hours, due to which profile delivery is delayed. Based on hourly data collection statistics, the G3 PLC delivers hourly profiles with a minimum 98% success rate within a 24-hour window and/or with system optimization or through missing data cycles, 100% data can be ensured within the subsequent 24 hours of profile generation. Also, this is initial installation data before the full AMI system is commissioned, and any system optimizations yet to be made. The G3 PLC devices operate within the FCC band (154.687 - 487.5 kHz), as no noticeable activity was identified outside the band.

To ensure effective communication, findings against the three main criteria are as follows:

- The Signal to Noise Ratio should exceed 10dBµV: All survey points were found to satisfy the criteria for average SNR in the FCC band, as shown in Fig. 12.
- Ideally, the noise level should be maintained below 80dBµV: Less than 10% of the cases were found to have higher noise below 200kHz. However, above 200kHz, the noise is acceptably low to allow communication as shown in Fig. 13.
- Length of the transmission paths: PLC signal transmission was successful up to 421m (sample from the longest

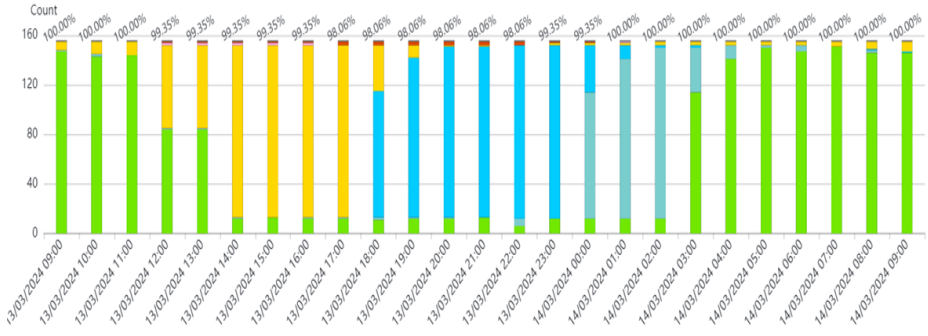

Figure 11 G3 PLC Smart-Meters Hourly Profile data [Last 24 Hours] – KRL Road

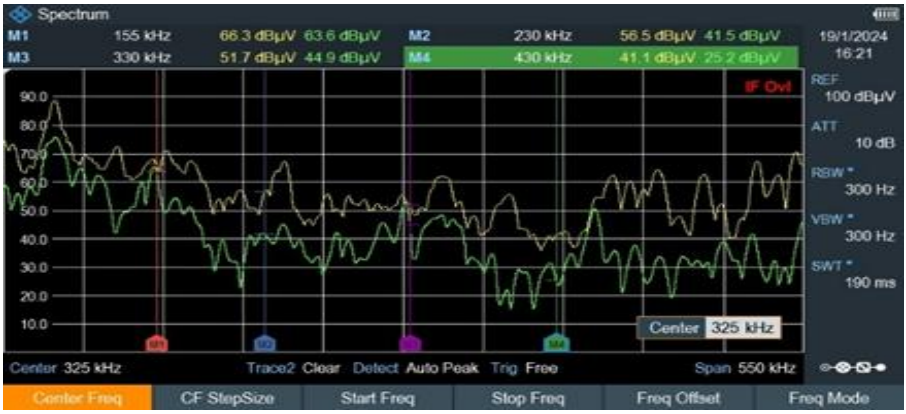

Figure 12 Sample Noise Report

distribution line commissioned in roll-out).

There was some correlation found between the noise profile and time of day as shown in Figure 12. In some case, noise was higher in the evening compared to samples obtained during the daytime as shown in Figure 13.

4. Conclusion

The PLC noise profiles gathered through this survey exercise are reflective of a typical distribution line noise profile in the FCC band. In the case of the two transformers analyzed, the transformer with more PLC meters tends to be better in communication health. The noise levels are observed to be under the acceptable limits for successful communication as demonstrated in the results, and fulfill the criteria set for the survey baseline. This is with due consideration of the time of day as well as the momentary prohibitive level of noise. The results are further supported by data availability statistics on the Head End server. Daily Energy Profiles are being retrieved by the HES at a 100% success rate within the next 24 hours. This exceeds the Statements of Requirement (SoR) KPI of 97% HES data availability within 24 hours and 100% within 48 hours from the PLC nodes.

It is observed that the need for PLC noise removal filters (to reduce noise to acceptable levels) may not be necessary in most cases. This is due to a naturally high PLC success rate as established by analysing data availability of G3 PLC

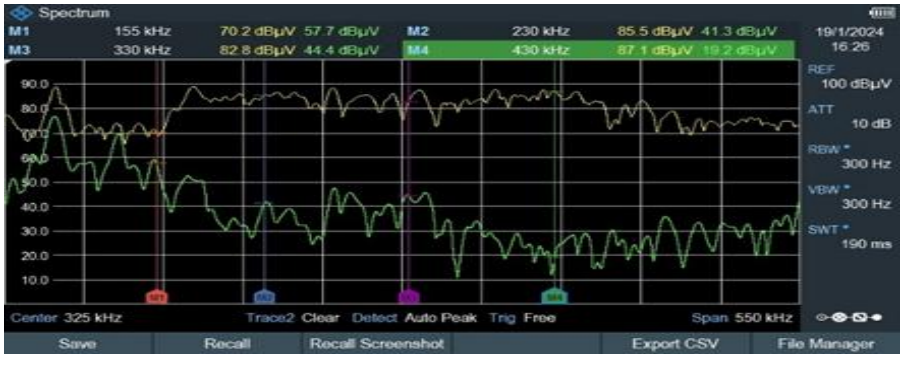

Figure 13 Sample SNR Report

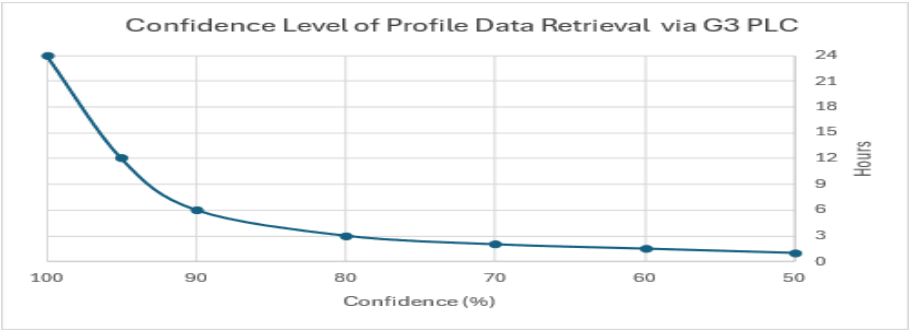

Figure 14 Confidence Level of Profile Data Retrieval

devices at the HES server. It is expected that most of the rare anomalies can be resolved by replacing the PLC with a GSM module while retaining the metering unit. However, there could be some cases where a noise filter may be required. It is also noteworthy that IESCO uses the FCC Band for NB G3 PLC, which operates outside the range of typical GT PV inverters, further helping PLC against unclean consumer power injection to the distribution network.

Acknowledgment

The authors extend their deepest gratitude to the Islamabad Electric Supply Company (IESCO) for its invaluable support in conducting this study. The provision of field access, PLC communication data, and technical insights from IESCO's AMI Telecom Team significantly contributed to the quality and accuracy of the findings. The collaboration and dedication of the engineers and staff involved in the AMI project are sincerely appreciated.

Statements & Declaration

Funding

The authors declare that no funds, grants, or other financial support were received during the preparation of this manuscript.

Conflict of Interest

The authors have declared there is no conflict of interest.

Ethical Approval

Not applicable.

References

Ahmed, M. S., Hussain, S., & Nadeem, A. (2021). Noise and SNR impact on PLC-based AMI in South Asia. *Renewable Energy Journal, 75*, 231–238.

Asian Development Bank. (2020). *Advanced metering infrastructure (AMI) project for IESCO: Implementation report*. ADB South Asia Energy Division.

Enel Group. (2022). *Smart metering and PLC deployment*. Enel Corporate Publications. https://www.enel.com/

G3-PLC Alliance. (2023). *G3-PLC global deployment report 2023*. https://www.g3-plc.com/

Galli, S., Scaglione, A., & Wang, Z. (2011). For the grid and through the grid: The role of power line communications in the smart grid. *Proceedings of the IEEE, 99*, 998–1027.

IEC. (1995). *IEC 61334: Distribution automation using low-speed narrowband power line communications*. International Electrotechnical Commission.

IEEE Standards Association. (2013). *IEEE Std 1901.2-2013: Standard for low-frequency (less than 500 kHz) narrowband power line communications for smart grid applications*.

ITU-T. (2012). *ITU-T G.9903: Narrowband orthogonal frequency division multiplexing power line communication transceivers for G3-PLC networks*. International Telecommunication Union.

NTDC. (2019). *Pakistan smart grid roadmap 2020–2030*. National Transmission & Despatch Company, Government of Pakistan.

Ramyar, R. M., Alan, F., Faarah, M., & Kaamran, R. (2014). A survey on advanced metering infrastructure. *International Journal of Electrical Power & Energy Systems, 63*, 473–484.

Sajid, A., Khan, H. U., & Khan, S. (2023). Performance analysis of narrowband PLC for AMI in Pakistan. *International Journal of Smart Grid and Clean Energy, 12*, 105–112.

Yan, Y., Qian, Y., Sharif, H., & Tipper, D. (2012). A survey on cyber security for smart grid communications. *IEEE Communications Surveys & Tutorials, 14*, 998–1010.

UCP Journal of Science and Technology
Vol. 3, Issue 1 (July - December 2025)
Journal website: http://ojs.ucp.edu.pk/index.php/ucpjst/index

Ligand-Based Drug Design Studies of Different Flavonoids as Potential Inhibitors of BCR-ABL

Hafiz Asad Ur Rahman Sheikh[1], Muhammad Faisal Maqbool[1*], Muhammad Khan[1], Hafiz Abdullah Shakir[1], Alishaba Khan[1], Syed Shahid Imran Bukhari[2], Muhammad Abrar Yousaf[3],

Abstract

BCR-ABL is a gene formed by the breakdown and fusion of pieces of two different chromosomes. It causes the production of abnormal blood cells to produce a protein called tyrosine kinase that promotes cancer by allowing uncontrollable cell growth. The BCR-ABL fusion gene is found in most patients with chronic myelogenous leukemia (CML), which is an uncommon type of bone marrow cancer. Several clinical inhibitors have been discovered to lower the BRC-associated CML. But all these clinically practiced inhibitors are potentially harmful to normal cells. Therefore, there is a dire need to identify such novel inhibitors that must be cost-effective, easily available, multitargeted, and less toxic to normal cells. In our study, we have identified some polyphenols, such as Baicalein and Erysubin A, as potential inhibitors of BRC. Dasatinib and Bosutinib are used as controls in our current study. In this context, we investigate thirteen flavonoids as potential ligands through structure-based virtual screening sourced from the PubChem database, with the aim of identifying inhibitors targeting BCR-ABL. Further studied for extra precision, molecular docking was performed using AutoDock Vina, which shows binding affinity of compounds between -6.9 to -10.5 kcal/mol. Erysubin A and Baicalein were the most suitable flavonoids with binding affinities of -10.5 and -10.0 kcal/mol, respectively, compared to clinical inhibitors, i.e., Bosutinib and Dasatinib, having affinities of -7.9 and -8.7 kcal/mol, respectively. Further studies have occupied that Erysubin A and Baicalein have significant interactions with various residues of most sustainable amino acids. The molecular dynamics simulation study indicates the stability and compactness of the protein complex with top drugs, especially Baicalein and Erysubin A. Hence, these results supported the idea that these polyphenols are potential compounds with the ability to inhibit cancer by disrupting the fusion gene activity; hence, further in vitro and in vivo studies are recommended for their development as a novel target to lower the burden of CML.

Keywords: Molecular docking, Flavonoids, BCR-ABL Inhibitor, Drug Discovery, Cancer Treatment

[1] Institute of Zoology, University of the Punjab, Lahore
[2] Department of Zoology, Science College, Wahdat Road, Lahore.
[3] Section of Biology and Genetics, Department of Neurosciences, Biomedicine and Movement Sciences, University of Verona, 37134 Verona, Italy
[*]Corresponding author's E-mail: faisal.ms.zool@pu.edu.pk
Received: 09 October 2025; Received in revised form: 04 December 2025; Accepted: 15 December 2025.
Available online: 23 December 2025.

DOI: https://doi.org/10.24312/ucp-jst.03.01.704

1. Introduction

CML is a form of myeloproliferative cancer characterized by the massive production of immature WBCs and comprises 15% of all leukemia cases among adults (El-Damasy et al., 2023). A hybrid Philadelphia chromosome (HPC) is formed in patients with leukemia by the transfer of the Abelson (ABL) gene from chromosome 9 to the Breakpoint Cluster Region (BCR) of chromosome number 22. As a result of this transfer, HPC carries a chimeric gene BCR-ABL (Rowley, 1973). The BCR-ABL carries the genetic code for tyrosine kinase (TK) oncoprotein, increasing cell division in CML (Kumar et al., 2016). The C-terminal of the ABL comprises the actin as well as binding sites (Sherbenou et al., 2010). The N-terminal of the ABL comprises two different domains, like SH2 and SH3 (homologous to SRC protein) that maintain the activity of TK (Colicelli, 2010). Any mutation occurring in the gene of the SH2 region may hamper the process of phosphorylation, whereas a mutation in the SH3 region may lead to the process of cell transformation (Blume-Jensen & Hunter, 2001). The N-terminal of the BCR upregulates the reactivity of TK as well as the binding potential of ABL. Serine-TK region of BCR regulates the signaling cascades managed by the ABL (Ren, 2005). A plethora of studies revealed that ABL TK potentially assists in cellular growth and signal transduction (Wang, 1993). BCR-ABL may upregulate the process of cell proliferation and multiple other abnormalities in bone marrow, which consequently affects the production of leukocytes (Baccarani et al., 2006).

Till date, different drugs have been discovered as inhibitors of BCR-ABL. Among them, imatinib is the first-generation FDA-approved inhibitor of BCR-ABL to treat patients with CML (Capdeville et al., 2002). Despite imatinib's initial effectiveness in most CML patients, resistance and drug intolerance hinder its efficacy in about 40% of patients (Pandrala et al., 2022). Imatinib resistance mostly occurs due to mutations within the region of BCR-ABL kinase (Hughes et al., 2006), which affects its appropriate binding with the target (O'Hare et al., 2007). Second-generation inhibitors of BCR-ABL, including dasatinib, nilotinib, and bosutinib, have been used to treat adult patients of CML with resistance to imatinib (El-Damasy et al., 2023). However, second-generation inhibitors failed to overcome the effects of various imatinib-resistant mutations (Vener et al., 2020). In 2012, the 3rd generation inhibitor of BCR-ABL, ponatinib was finally get some success and was approved by the FDA for clinical use. It proved to be an excellent inhibitor of imatinib-resistant mutations; however, some serious concerns arose against the use of ponatinib because it was associated with severe vascular/cardiotoxic effects. Ponatinib is a multi-kinase inhibitor, and it is thought that its cardiotoxic effect is due to its multi-kinase activity and synchronous inhibition of some important kinases that play a key role in cardiovascular function (El-Damasy et al., 2023). Therefore, there is a dire need to design novel inhibitors for BCR-ABL kinase that offer an appropriate approach for the treatment of ALL and CML.

Polyphenolic compounds are heterogeneous groups of plant secondary metabolites. They are further divided into 6 groups (flavonoids, flavanols, isoflavonoids, flavones, flavanones, and anthocyanidins). Interestingly, most flavonoids are derived from natural resources like fruits, vegetables, and different plants, so these compounds can be less toxic, frequently available, cost-effective, and multitargeted (Ashaq et al., 2021). Flavonoids are well known due to their wide range of anticancer activities; they influence the concentration of reactive oxygen species (ROS), arrest the cell cycle at various phases, cause apoptosis and autophagy, and reduce cancer cell proliferation and invasion (Kopustinskiene et al., 2020). By viewing

Table 1: Molecular Formula and Molecular weight of ligands used in this study.

Sr No	Ligands	Nature	Molecular Formula	Molecular Weight (g/mol)
Ct- 1	**Dasatinib-(BMS354825)**	Clinical compounds used as a control	$C_{22}H_{26}ClN_7O_2S$	488.0
Ct-2	**Bosutinib**		$C_{26}H_{29}Cl_2N_5O_3$	530.4
F-1	**Baicalein**	Flavonoids used as potential anti-cancer agent	$C_{15}H_{10}O_5$	270.24
F-2	**Bavachin**		$C_{20}H_{20}O_4$	324.4
F-3	**Erysubin A**		$C_{20}H_{16}O_6$	352.3
F-4	**Isobavachin**		$C_{20}H_{20}O_4$	324.4
F-5	**Nobiletin**		$C_{21}H_{22}O_8$	402.4
F-6	**Tricin**		$C_{17}H_{14}O_7$	330.29
F-7	**Apigenin**		$C_{15}H_{10}O_5$	270.24
F-8	**Acacetin**		$C_{16}H_{12}O_5$	284.26
F-9	**Chyrsin**		$C_{15}H_{10}O_4$	254.24
F-10	**Naringenin**		$C_{15}H_{12}O_5$	272.25
F-11	**Quercetin**		$C_{15}H_{10}O_7$	302.23
F-12	**Galangin**		$C_{15}H_{10}O_5$	270.24
F-13	**Kaempferol**		$C_{15}H_{10}O_6$	286.24

Ct* for Control **F*** Flavonoids

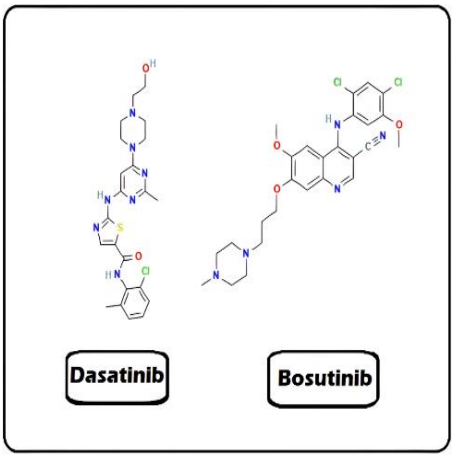

Figure 1 Clinical compounds Dasatinib and Bosutinib used as controls in the current study.

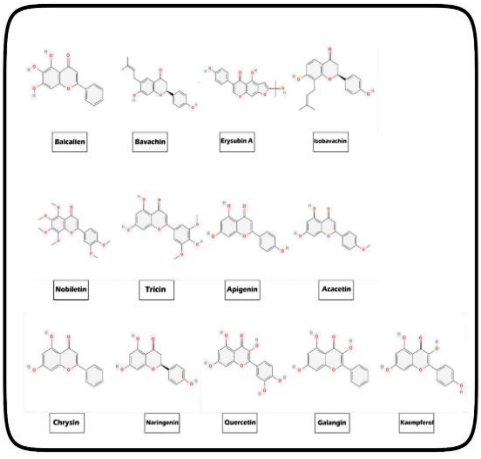

Figure 2 Structural formulas of different flavonoids used as inhibitors of BCR-ABL.

The bioactive potential of flavonoids here in this study, we screened more than 100 flavonoids and identified thirteen of them as potential inhibitors of BCR-ABL by using different bioinformatic tools, as it's the fastest and most cost-effective way to propose any effective molecule as a candidate for a potential novel drug.

2. Materials and Methods

2.1 Ligand Preparation:

Three-dimensional (3D) flavonoids and clinical compounds used as controls were downloaded from the PubChem database (https://www.pubchem.ncbi.nlm.nih.gov/) (Kim et al., 2019). Pymol software was used to make a PDB format of retrieved ligands (DeLano et al., 2002) and then to PDBQT format using AutoDock MGL Tools 1.5.7. (Berman et al., 2000). Figure 1 shows that both clinical compounds, Dasatinib and Bosutinib, are used as controls. 13 best docked flavonoids, Baicalein, Bavachin, Erysubin A, Isobavachin, Nobiletin, Tricin, Apigenin,

Acacetin, Chrysin, Naringenin, Quercetin, and Galangin are shown in Figure 2. The molecular weight and molecular formula of all the ligands is given in Table 1.

2.2 Protein Preparation

Crystal structure (3D) of BCR-ABL oncoprotein oligomerization domain (PDB Id: 1K1F) (Figure 3) was downloaded from Protein Data Bank (https://www.rcsb.org/) (Berman et al., 2000). For further preparation, the protein structure was opened in AutoDock MGL Tools 1.5.7 (Morris et al., 2009). Using AutoDock MGL Tools 1.5.7, molecules of water were deleted, polar hydrogens and Kollman charges were added. After Preparation, the receptor protein was saved in the PDBQT format. The locality of active sites for ligand docking was determined by generating the 3D map of the grid box on the receptor region of the macromolecule using AutoDock MGL Tools 1.5.7 (Morris et al., 2009). The grid size was determined at 40×40×40 xyz points with 0.375 Å spacing, and the grid center was designed as x = 37.000, y = 46.026, z = -14.901.

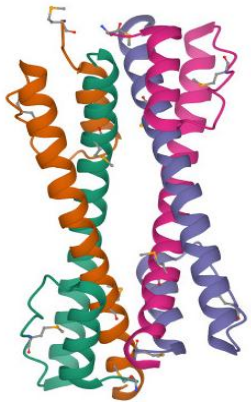

Figure 3 Crystal structure of the BCR-ABL oncoprotein oligomerization domain.

2.3 Molecular Docking and Visualization

AutoDock vina (Trott et al., 2010) program was utilized for molecular docking using the PDBQT form of BCR-ABL and selected ligands. Visualization of the BCR-ABL oncoprotein oligomerization domain with interacting ligands was performed using BIOVIA Discovery Studio 2021 (Biovia et al., 2016).

2.4 Drug Likelihood and Toxicity Prediction

The potential inhibitors or best docked ligands are determined by the results, expressing their binding energies. However, ADMET (Absorption, Distribution, Metabolism, Excretion, and Toxicity) properties provide significant methodologies being processed in drug discovery and development (Jia et al., 2022). The Lipinski rule of five determined efficiency, metabolism, and safety by calculating different parameters. Toxicology predictions highlight the quantity of small molecules that could be tolerated by human and animal models (Pires et al., 2015). ADMET properties, Lipinski rule of five, and toxicity prediction for decided ligands were calculated as reported by Yousaf et al. (2024).

Table 2: Results of molecular docking showing binding energies and different interactions of ligands with BCR-ABL.

Ligands	Binding Energies (**kcal/mol**)	Hydrogen Bonding	Hydrophobic Interactions	Electrostatic Interactions
Dasatinib-(BMS354825)	-8.7	ARG43, GLN47 ASN50, GLN14 ASN50, GLN47	ARG43, ILE42 LYS39, ALA40	ARG43
Bosutinib	-7.9	ARG43, GLN14 ASN50	ARG43, LYS39 ILE42	ARG43
Baicalein	-10.0	ARG43, ASN50 ASN50, GLN14 GLU46	ARG43, LYS39	ARG43
Bavachin	-8.7	ARG43, LYS39 ALA13	ARG43, LYS39 ILE42	ARG43, GLU36
Erysubin A	-10.5	ARG43, ASN50 GLU46, LYS39	LYS39	GLU36, GLU36
Isobavachin	-7.7	ARG43, GLN14	ARG43	GLU46
Nobiletin	-6.9	ARG43, GLN14 GLU46, GLN47	ARG43	GLU46
Tricin	-8.0	GLN47, ASN50 ALA13, LYS39 ASN50, ARG43	LYS39, ARG43	
Apigenin	-7.7	ARG43, LYS39 GLU46, GLU36 ALA13	ALA40, LYS39 ARG43	ARG43, GLU36
Chrysin	-7.7	GLU36, LYS39	LYS39, ARG43	ARG43, GLU36
Naringenin	-8.1	LYS39, ARG43 GLN14, GLU46	ARG43, LYS39	ARG43
Galangin	-7.6	ARG43, ASN50	ARG43, LYS39	GLU46
Quercetin	-8.0	ARG43, GLN14	ARG43, LYS39	ARG43
Acacetin	-8.0	ARG43, ASN50 GLN14, GLU46 GLU36	LYS39, ARG43	ARG43
Kaempferol	-7.9	ARG43, LYS39	LYS39, ARG43 ALA40, ILE42	ARG43, GLU36

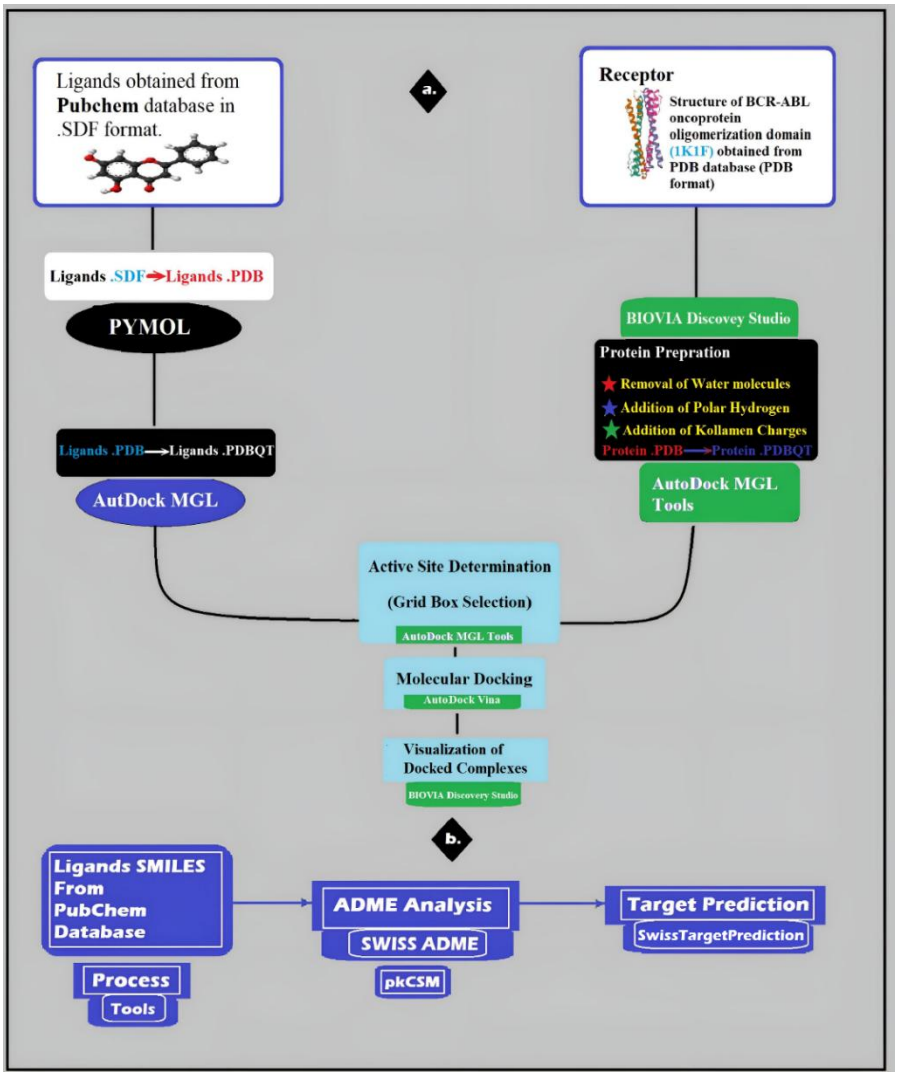

Figure 4 The overall flowchart of the current study.

2.5 Target Prediction

Target prediction is a significant tool to assess the phenotypical side effects or potential cross-reactivity due to small biomolecule action (Gfeller et al., 2014; Keiser et al., 2007). Swiss Target Prediction (https://www.swisstargetprediction.ch) (Vener et al., 2020) was used to predict the possible targets with *Homo sapiens* by using PubChem SMILES of ligands as input. The overall flowchart for the current study is shown in Figure 4.

2.6 Molecular dynamics simulation

The stability of the protein-ligand complex was further checked by using the analysis of molecular dynamics (MD) simulations. These simulations were conducted over a 50 ns period using the GROMOS96 43a1 force field within the GROMACS 2019.2 software package, facilitated by WebGRO for molecular

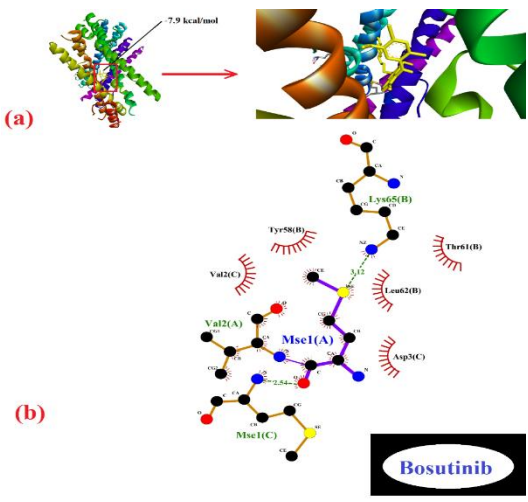

Figure 5 Bosutinib with its binding sites, bindin energies, and interactions with amino acid residu through docking with BCR-ABL.

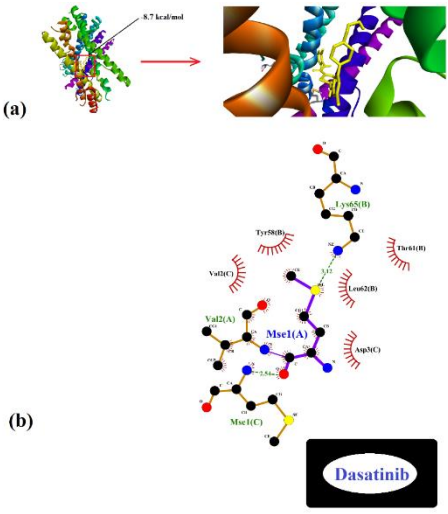

Figure 6: Dasatinib with their binding sites, binding energies and interactions with amino acid residues through docking with BCR-ABL.

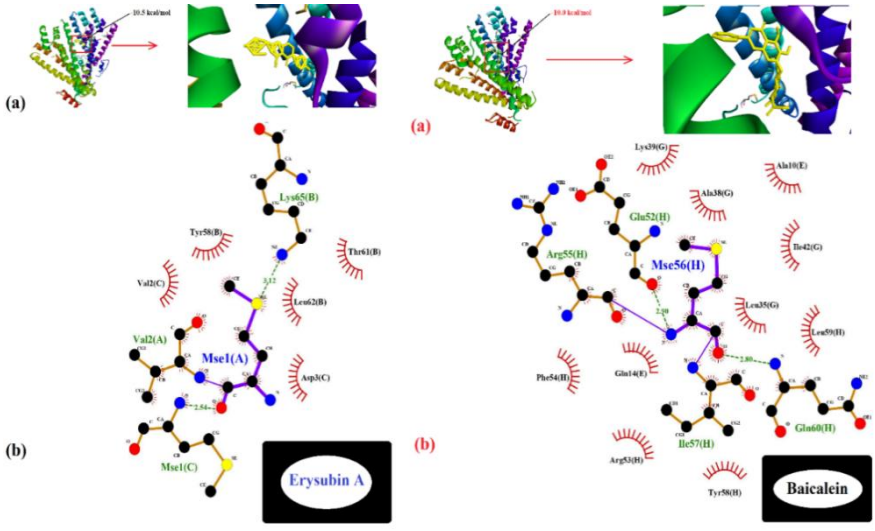

Figure 7: Erysubin A and Baicalein with their binding sites, binding energies and interactions with amino acid residues through docking with BCR-ABL.

simulations, as described by Yousaf et al. (2024).

3. Results

The binding energies and interactions of all ligands with BCR-ABL are given in Table 2. In the current study, we found Erysubin A and Baicalin as potent lead inhibitors of BCR-ABL, as they show better binding affinities as compared to control drugs.

For the ligand displacement at the binding site of protein, the hydrogen bonds are the most important, and their presence in the docked complex indicates the good interaction between selected ligands and

Table 3: Shows different parameters of Lipinski's rule for selected flavonoids against BCR-ABL.

LIGANDS	HBR (Hydrogen Bond acceptor)	HBD (Hydrogen Bond donor)	Log P	Lipinski Rule	
				Drug likeliness	Violation
Dasatinib-(BMS354825)	6	3	2.80	Yes	Zero
Bosutinib	7	1	4.28	Yes	One; MW>500
Baicalein	5	3	2.24	Yes	Zero
Bavachin	4	2	3.53	Yes	Zero
Erysubin A	6	3	2.85	Yes	Zero
Isobavachin	4	2	3.53	Yes	Zero
Nobiletin	8	0	3.02	Yes	Zero
Tricin	7	3	2.15	Yes	Zero
Apigenin	5	3	2.11	Yes	Zero
Acacetin	5	2	2.52	Yes	Zero
Chrysin	4	2	2.55	Yes	Zero
Naringenin	5	3	1.84	Yes	Zero
Quercetin	7	5	1.23	Yes	Zero
Galangin	5	3	1.99	Yes	Zero
Kaempferol	6	4	1.58	Yes	Zero

protein, leading to the inhibition of the targeted protein (Aanouz et al., 2020; Aarjane et al., 2020). All studied flavonoids contain H-bonding with amino acids, a maximum of six hydrogen bonds present in multiple polyphenols, while a minimum of hydrogen bonding is present in chrysin, which has only two H-bonds with amino acids. Table 2 has shown that, the binding affinity of Bosutinib was -7.9 kcal/mol and it formed three hydrogen bonds with amino acids residues by ARG43, GLN14, ASN50 and three hydrophobic and one electrostatic interaction, while Dasatinib has binding affinity -8.7 kcal/mol and it formed six hydrogen bonds with amino acid residues by ARG43, GLN47, ASN50, GLN14, ASN50, GLN47 and three hydrophobic and one electrostatic interaction. Figure 5 and 6 depicted the binding energies and amino acid residues in 3D and 2D diagram of docked ligands act as a control i.e., Dasatinib and Bosutinib.

All studied compounds demonstrated strong interactions with the binding site residues of BCR-ABL; their binding affinity ranges between -6.9 kcal/mol to -10.5 kcal/mol. Erysubin A shows the

highest affinity as -10.5 kcal/mol, while Baicalein shows next, his a binding affinity was -10.0 kcal/mol. Erysubin A formed four hydrogen bonds, one hydrophobic and three electrostatic interactions with amino acid. While Baicalein has formed five hydrogen bonds, two hydrophobic and one electrostatic interaction with the amino acid, as shown

Table 4: Toxicity properties for controls and selected flavonoids used as BCR-ABL inhibitors.

Ligand	ADMET Toxicity	Max. tolerated dose (human)(log mg/kg/day)	hERG I inhibitor	hERG II inhibitor	Oral Rat Acute Toxicity(mol/kg)	Oral Rat Chronic Toxicity (log mg/kg_bw/day)	Liver Toxicity	Skin Sensitisation	*T. pyriformis* toxicity (log ug/L)	Minnow toxicity (log mM)
Dasatinib	No	No	No	No	No	No	No	No	No	No
Bosutinib	No	0.066	No	Yes	2.736	0.421	Yes	No	0.323	1.3
Baicalein	No	0.498	No	No	2.325	2.645	No	No	0.42	1.25
Bavachin	No	-0.445	No	No	2.27	1.227	No	No	0.909	0.76
Erysubin A	Yes	0.596	No	Yes	2.507	1.444	No	No	0.296	1.195
Isobavachin	No	-0.157	No	No	2.394	1.435	No	No	0.853	1.389
Nobiletin	No	0.443	No	No	2.459	0.82	No	No	0.315	0.686
Tricin	No	0.351	No	No	2.229	1.82	No	No	0.329	1.754
Apigenin	No	0.328	No	No	2.45	2.298	No	No	0.38	2.432
Chrysin	No	0.016	No	No	2.289	0.955	No	No	0.535	1.746
Naringenin	No	-0.176	No	No	1.791	1.944	No	No	0.369	2.136
Galangin	No	0.333	No	No	2.45	2.323	No	No	0.382	2.385
Quercetin	No	0.499	No	No	2.471	2.612	No	No	0.288	3.721
Acacetin	No	0.09	No	No	2.22	1.259	No	No	0.422	1.00

in Figure 7.

3.1 Drug-likeliness

The incompatible interaction between inhibitors and protein or enzyme may not guarantee the inhibitor stability as a drug; therefore, ADME analysis plays a critical role during the drug formation process. ADME analysis depends on Lipinski's rule of five, which is a thumb rule for the evaluation of drug likeness (Lipinski, 2004). This rule provides a vital parameter for the evaluation of pharmacokinetic parameters of drugs such as absorption, distribution, metabolism, and excretion

(ADME) for designing and developing of drug (Ertl et al., 2000). According to the rule, any molecule can be studied for drug development if it has a Molecular weight ≤ 500 Da, a Number of H-Bond donors (HBD) ≤ 5, a Number of H-Bond acceptors (HBR) ≤ 10, LogP (lipophilicity) ≤ 5 (Veber et al., 2002). Compounds having fewer than three of these conditions are unlikely to be assigned as an orally bioavailable drug and will cause trouble on ingestion (Mendis et al., 2011).

The molecular characters of all ligands were weighed by SwissADME (Talele et al., 2010). The results of physicochemical

properties in Table 3 revealed that the molecular weight of selected flavonoids ranged from 254.24 Da (chrysin) to 402.4

Da (Nobiletin) (≤ 500), number of HBD from 2 (Bavachin, Isobavachin, Chrysin and Acacetin) to 5 (Quercetin) (≤ 5), number of HBR from 4 (Bavachin, Chrysin and Isobavachin) to 7 (Tricin and Quercetin) (≤ 10) and the value of LogP varied from 1.23 (quercetin) to 3.53 (Bavachin and Isobavachin) (≤ 5), results differs for the controls i.e., Dasatinib and Bosutinib. Dasatinib has a molecular weight of 488 (g/mol) (≤ 500), number of HBD 3 (≤ 5), number of HBR 6 (≤ 10), and value of LogP 2.80 (≤ 5), and obeys all Lipinski rules with zero violation. Our other control, i.e., Bosutinib, has the molecular weight of 530 (g/mol) (> 500), number of HBD 1 (≤ 5), number of HBR 7 (≤ 10), and value of LogP 4.28 (≤ 5), and obeys Lipinski rule with one violation, i.e., (M.W > 500). The overall data showed that all selected flavonoids were observed to obey Lipinski's rule. Table 3 shows the values of HBR, HBD, Log P, and Lipinski violation, while the molecular weight of each compound is mentioned in Table 1.

3.2 Toxicity Prediction

Summary of pkCSM predictions (Pires et al., 2015) has been displayed in Table 4. The results suggested that all investigated compounds do not possess any ADMET toxicity. Positive prediction of ADMET represents the carcinogenicity of a compound (Pires et al., 2015; Xu et al., 2012). The highest tolerated dose (HTD) for humans is estimated to be the toxic range of any drug, which is mentioned as a starting dose during phase 1 clinical trials (Pires et al., 2015). Values of HTD for all compounds were lower except Quercetin and Erysubin A (0.499 and 0.596 mg/kg/day, respectively), which have slightly higher values than the threshold level of 0.477 log mg/kg/day. Inhibition of human ether-a-go-go gene (hERG) was not observed by all of the compounds, but for hERG II, Inhibition was predicted for only Erysubin A. hERG lowers the activity of potassium channels, which leads to the development of long QT syndrome (Vandenberg et al., 2001; Chiesa et al., 1997). hERG potassium channels permanently banned the use of several drugs (Pires et al., 2015). Oral rat chronic toxicity was evaluated from 0.955 log mg/kg_bw/day (chrysin) to the highest value of 2.645 log mg/kg_bw/day for Baicalein. None of the compounds was found to be positive for skin and liver toxicity. In this study, no compound showed skin sensitization. For toxicity against *T. pyriformis* (a protozoan), a compound having a predicted value of pIGC50 (negative algorithm of concentration which is needed to inhibit 50% of growth in log μg/L) < −0.5 log μg/L is regarded as toxic. No compound showed the value in the described range of T. pyriformis toxicity. For Fathead Minnows fish, the lethal concentration (LC50) causing 50% mortality in the Minnows test group, LC50 < 0.5 mM (log LC50 < −0.3) is considered to show acute toxicity (Pires et al., 2015; Cheng et al., 2011). No compound was found to exhibit Minnow toxicity as a result of toxicity analysis.

3.3 Target Prediction

The target prediction analysis for the compounds used as controls in our current study, i.e., Dasatinib and Bosutinib, and

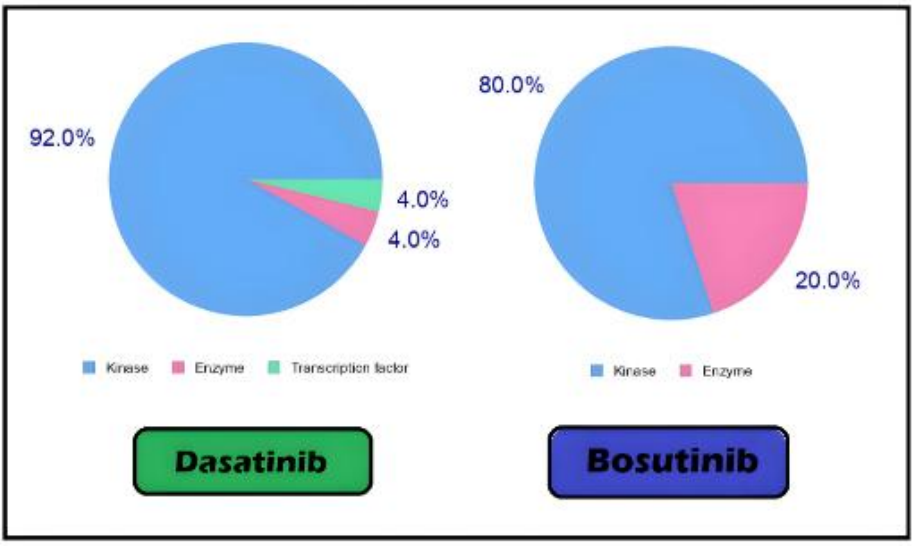

Figure 8: Top twenty-five (25) targets predicted by the SwissTargetPrediction database for Dasatinib and Bosutinib used as a control in our current study

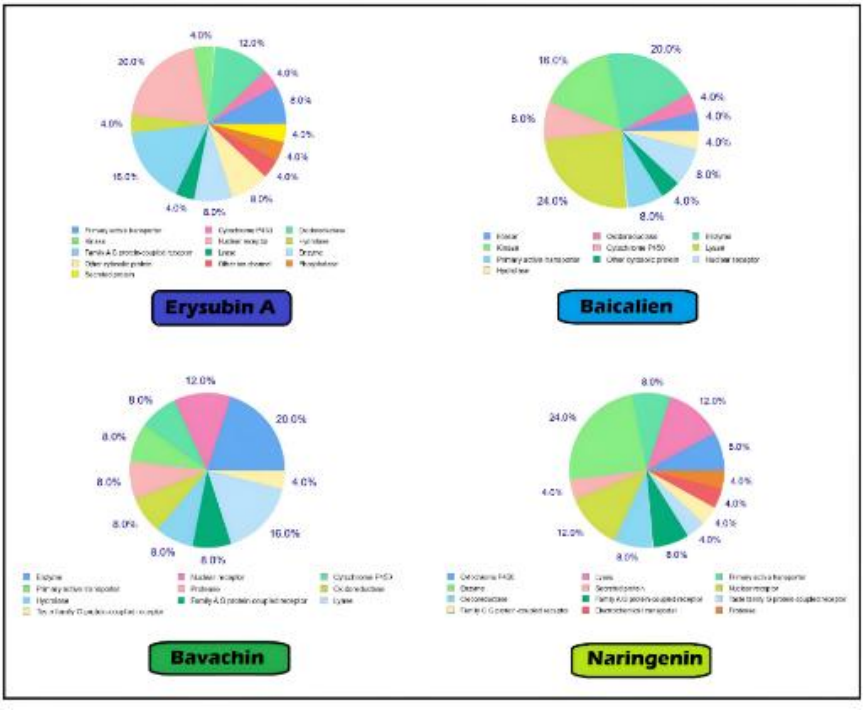

Figure 9: Top twenty-five (25) targets predicted by the SwissTargetPrediction database for top top-ranked flavonoids used in our current study

our selected flavonoids used as ligands to inhibit BCR-ABL activity, was performed by Swiss Target Prediction software, and the top twenty-five observations were

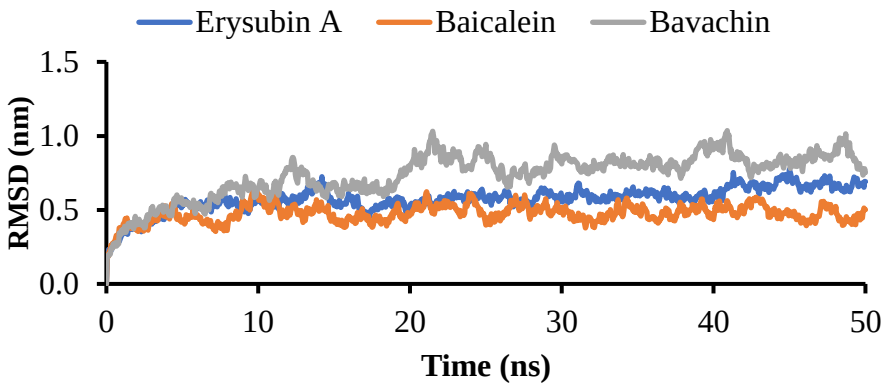

Figure 10: RMSD values for Erysubin A, Baicalein, and Bavachin in complex with BCR-ABL over a 50 ns molecular dynamics (MD) simulation. The RMSD values indicate the structural stability of each compound-protein complex.

displayed as pie-charts in Figure 8. For Dasatinib, the pie-chart predicted 4% enzyme, 92.0% of kinase, and 4.0% of Transcription factor as target. Analysis predicted that Bosutinib targeted the 80% kinase and 20% enzyme. The figure shows the pie charts of top twenty-five observations of compounds used as a control.

For Erysubin A, SwissTargetPrediction software predicted the top twenty-five observations, that are displayed as pie-chart, predicted 20% of nuclear receptor, 16% family A-G protein-coupled receptor, 12% of oxidoreductase, 8% of primary active transporter, 8% of enzyme, 8% of other cytosolic protein, 4% of each lyase, other secreted protein, phosphatase, cytochrome P450, other ion channel, nuclear receptor and hydrolase as a target as shown in figure 9. The pie chart of Baicalein for the top twenty-five observations predicted 4% eraser, 16% kinase, 8% primary active transporter, 4% hydrolase, 4% oxidoreductase, 8% cytochrome P450, 4% other cytosolic protein, 20% enzyme, 8% nuclear receptor, and 24% lyase as a target. Bavachin for the top twenty-five observations in the pie-chart targeted 20% enzyme, 16% lyase, 8% hydrolase, 8% primary active transporter, 4% Taste family G protein-coupled receptor, 12% protein receptor, 8% protease, 8% Family A G protein-coupled receptor, 8% cytochrome P450, and 8% oxidoreductase as by pie-chart. From top four, our last ligand i.e., Naringenin got the target prediction from Swiss Target Prediction software for the top twenty-five observations that displayed 24% of enzyme, 8% of cytochrome P450, 12% of nuclear receptor, 12% of lyase, 8% oxidoreductase, 4% family C G protein-coupled receptor, 4% secreted protein, 8% A G protein-coupled receptor, 4% electrochemical Transporter, 4% protease and % taste family G protein-coupled receptor.

The average probability scores for our selected flavonoids were around zero. Previous studies have shown that a probability value greater than zero was considered to depict a reasonable drug-ligand interaction (Gfeller et al., 2014; Thomas et al., 2020). The probability score of the analyzed ligands indicated that they have better attraction towards the target of the specific binding site.

3.4 MD simulation

Root mean square deviation (RMSD) values indicate the stability of each

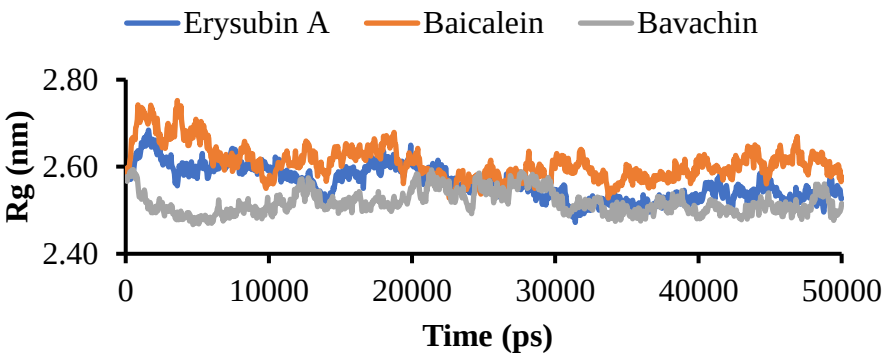

Figure 11: Rg values for Erysubin A, Baicalein, and Bavachin in complex with BCR-ABL over a 50 ns MD simulation. The Rg values reflect the compactness of each complex.

compound within the protein complex. Erysubin A has a mean RMSD of 0.573 nm, ranging from 0. 0000005 nm to 0.772 nm. Baicalein exhibits a lower mean RMSD of 0.474 nm, with a maximum of 0.640 nm. In contrast, Bavachin shows the highest mean RMSD at 0.736 nm with a range of 0.0000004-1.0357153 (Figure 10).

The radius of gyration (Rg) assesses the compactness of each compound-protein complex. Erysubin A maintains a mean Rg of 2.562 nm, with values ranging from 2.472 nm to 2.684 nm. Baicalein shows slightly higher compactness, with a mean Rg of 2.609 nm. Bavachin has a mean Rg of 2.518 nm, which may indicate a somewhat less compact interaction (Figure 11).

4. Discussion

ABL and BCR genes are found on chromosomes number 9 and 22, respectively. In BCR-ABL induced leukemia, the translocation of BCR and ABL genes occurs between chromosomes 22 and 9, thus resulting in the generation of the BCR-ABL oncogene, which is the leading cause of CML (Amarante-Mendes et al., 2022). Multiple therapeutic agents are available to minimize the burden of CML, but their safety and reliability is a major challenge. The idea of using natural products for the treatment of cancer has been remarkably proven (Yousaf et al., 2024). This study will mainly focus on identifying new inhibitors of BCR-ABL from a wider variety of flavonoids by using different computational methods. In this study, different flavonoids have been used as anti-cancer agents against the activity of TK, which leads to the production of uncontrolled cells and leads to bone marrow cancer mostly. 90% of CML patients have the BCR-ABL oncogene in them. 13 flavonoids: Baicalein, Bavachin, Erysubin A, Isobavachin, Nobiletin, Tricin, Apigenin, Acacetin, Chrysin, Naringenin, Quercetin, Galangin, Kaempferol were used as potential anti-cancer agents to inhibit tyrosine kinase activity. Molecular docking was performed to calculate the binding affinity of flavonoids used as a ligand in this study. Clinical compounds, i.e., Dasatinib and Bosutinib, score binding affinity -8.7 and -7.9 kcal/mol, respectively. Results of molecular docking ranked flavonoids based on binding affinity as: Erysubin A (-10.5 kcal/mol > Baicalein (-10.0 kcal/mol) > Bavachin (-8.7 kcal/mo) > Naringenin (-8.1 kcal/mol) > Quercetin, Acacetin, Tricin (-8.0 kcal/mol), Kaempferol (-7.9 kcal/mol) >

Isobavachin, Apigenin, Chrysin (-7.7 kcal/mol) > Galangin (-7.6 kcal/mol) > Nobiletin (-6.9 kcal/mol). Erysubin A and Baicalein were front-line compounds with the top binding affinity among all. Therefore, supported as a potential anti-cancer agent. Moreover, results of drug likeness and toxicity analysis further supported the idea to propose flavonoids as a potent inhibitor of BCR-ABL.

Finally, the MD simulation data on RMSD and Rg values for Erysubin A, Baicalein, and Bavachin in complex with BCR-ABL provide insights into the stability and structural behavior of these compounds. The RMSD values reveal stability within the BCR-ABL binding site, with lower values indicating a stable interaction and higher values suggesting increased fluctuation. Following equilibration after the initial rise, the complexes displayed consistent stability with only minor fluctuations, which serve as strong indicators of system stability (Kuzmanic & Zagrovic, 2010). Baicalein shows the lowest average RMSD, implying a relatively stable binding configuration, while Erysubin A, with a slightly higher RMSD, also demonstrates stable interaction. In contrast, Bavachin's higher RMSD suggests a more flexible or less stable binding interaction, as evidenced by its greater structural deviations. The Rg values reflect the compactness of the complex structures, where a lower Rg generally suggests a more compact and potentially tighter binding interaction. Baicalein has the highest Rg, followed closely by Erysubin A, indicating both form relatively compact complexes with BCR-ABL. Bavachin exhibits slightly lower compactness, consistent with a more flexible interaction with the protein. In summary, these RMSD and Rg data suggest that Baicalein and Erysubin A establish relatively stable and compact interactions with BCR-ABL, while Bavachin shows more flexibility and reduced stability. These differences in stability and compactness may be significant for understanding the varying binding efficiencies or potential effectiveness of these compounds when targeting BCR-ABL.

5. Conclusion

The ABL gene from chromosome 9 joins to the BCR gene on chromosome 22, to form the BCR-ABL. It causes the production of abnormal cells that upregulate the TK activity, which consequently causes uncontrolled cell growth. 90% of patients having CML have the BCR-ABL oncogene. Several antioncogenic therapeutics have been approved for the treatment of CML, but their success is limited due to their toxic nature. Flavonoids have been well known due to their lot of bio-medicinal properties. 13 flavonoids: Baicalein, Bavachin, Erysubin A, Isobavachin, Nobiletin, Tricin, Apigenin, Acacetin, Chrysin, Naringenin, Quercetin, Galangin, Kaempferol were used as potential anti-cancer agents to inhibit tyrosine kinase activity. Erysubin A and Baicalein were front-line polyphenols with the top binding affinity among others. Therefore, both were supported as potential anti-cancer agents and pointed towards further in vitro and in vivo studies to confirm their mechanism of action and ensure their development as a novel anticancer agent. We recommend the several in vitro analyses, like biochemical kinase inhibition assays (to measure IC_{50}), cellular phosphorylation assays such as pCRKL or pSTAT5 (to confirm target engagement), and cell-viability assays in BCR-ABL positive cell lines like K562 to validate our in silico BCR-ABL inhibition results, several standard in vitro assays can be used, Additional apoptosis or colony-formation assays may further support the inhibitory activity.

References

Aanouz, I., Belhassan, A., El-Khatabi, K., Lakhlifi, T., El-Ldrissi, M., & Bouachrine, M. (2020). Moroccan Medicinal plants as inhibitors against SARS-CoV-2 main protease: Computational investigations. Journal of Biomolecular Structure and Dynamics, 1-9.

Aarjane, M., Aouidate, A., Slassi, S., & Amine, A. (2020). Synthesis, antibacterial evaluation, in silico ADMET and molecular docking studies of new N-acylhydrazone derivatives from acridone. Arabian Journal of Chemistry, 13(7), 6236-6245.

Yousaf MA, Anwer SA, Basheera S, Sivanandan S. Computational investigation of Moringa oleifera phytochemicals targeting EGFR: molecular docking, molecular dynamics simulation and density functional theory studies. Journal of Biomolecular Structure and Dynamics. 2024 Mar 3;42(4):1901-23.999999

Amarante-Mendes GP, Rana A, Datoguia TS, Hamerschlak N, Brumatti G. BCR-ABL1 Tyrosine Kinase Complex Signaling Transduction: Challenges to Overcome Resistance in Chronic Myeloid Leukemia. Pharmaceutics. 2022 Jan 17;14(1):215. doi: 10.3390/pharmaceutics14010215. PMID: 35057108; PMCID: PMC8780254.

Ashaq A, Maqbool MF, Maryam A, Khan M, Shakir HA, Irfan M, Qazi JI, Li Y, Ma T. Hispidulin: A novel natural compound with therapeutic potential against human cancers. Phytother Res. 2021 Feb;35(2):771-789. doi: 10.1002/ptr.6862. Epub 2020 Sep 18. PMID: 32945582.

Baccarani, M., Saglio, G., Goldman, J., Hochhaus, A., Simonsson, B., Appelbaum, F., & Hehlmann, R. (2006). Evolving concepts in the management of chronic myeloid leukemia: Recommendations from an expert panel on behalf of the European LeukemiaNet. *Blood*, 108, 1809–1820. doi:10.1182/blood-2006-02-005686

Berman, H. M., Westbrook, J., Feng, Z., Gilliland, G., Bhat, T. N., Weissig, H., Shindyalov, I. N., & Bourne, P. E. (2000). The protein data bank. Nucleic acids research, 28(1), 235-242.

Blume-Jensen, P., & Hunter, T. (2001). Oncogenic kinase signalling. *Nature*, 411, 355–365. doi:10.1038/35077225

Capdeville R, Buchdunger E, Zimmermann J, Matter A. Glivec (STI571, imatinib), a rationally developed, targeted anticancer drug. Nat Rev Drug Discov. 2002;1(7):493–502. [Crossref] [PubMed] [Web of Science ®], [Google Scholar]

Cheng, F., Shen, J., Yu, Y., Li, W., Liu, G., Lee, P. W., & Tang, Y. (2011). In silico prediction of Tetrahymena pyriformis toxicity for diverse industrial chemicals with substructure pattern recognition and machine learning methods. Chemosphere, 82(11), 1636-1643.

Chiesa, N., Rosati, B., Arcangeli, A., Olivotto, M., & Wanke, E. (1997). A novel role for HERG K+ channels: spike-frequency adaptation. The Journal of Physiology, 501(2), 313-318.

Colicelli J. ABL tyrosine kinases: evolution of function, regulation, and specificity. Sci Signal. 2010 Sep 14;3(139):re6. doi: 10.1126/scisignal.3139re6. Erratum in: Sci Signal. 2011 Aug 30;4(188):er4. PMID: 20841568; PMCID: PMC2954126.

D. Biovia, H. Berman, J. Westbrook, Z. Feng, G. Gilliland, T. Bhat, T.J.T.J.o.C.P. Richmond, Dassault Systèmes BIOVIA, Discovery Studio Visualizer, v. 17.2, San Diego: Dassault Systèmes, 2016, 10 (2000) 0021-9991.

DeLano, W. L. (2002). Pymol: An open-source molecular graphics tool. CCP4 Newsletter on protein crystallography, 40(1), 82-92.

El-Damasy, A.K., Jin, H., Park, J.W., Kim, H.J., Khojah, H., Seo, S.H., Lee, J.H., Bang, E.K. and Keum, G., 2023. Overcoming the imatinib-resistant BCR-ABL mutants with new ureidobenzothiazole chemotypes endowed with potent and broad-spectrum anticancer activity. *Journal of Enzyme Inhibition and Medicinal Chemistry*, *38*(1), p.2189097.

Ertl, P., Rohde, B., & Selzer, P. (2000). Fast calculation of molecular polar surface area as a sum of fragment-based contributions and its application to the prediction of drug transport properties. Journal of medicinal chemistry, 43(20), 3714-3717

Gfeller, D., Grosdidier, A., Wirth, M., Daina, A., Michielin, O., & Zoete, V. (2014). SwissTargetPrediction: a web server for target prediction of bioactive small molecules. Nucleic acids research, 42(W1), W32-W38.

Hughes T, Deininger M, Hochhaus A, Branford S, Radich J, Kaecla J, et al. Monitoring CML patients responding to treatment with tyrosine kinase inhibitors: review and recommendations for harmonizing current methodology for detecting BCR-ABL transcripts and kinase domain mutations and for expressing results. Blood. 2006;108(1):28–37.

Jia L, Gao H. Machine Learning for In Silico ADMET Prediction. Methods Mol Biol. 2022;2390:447-460. doi: 10.1007/978-1-0716-1787-8_20. PMID: 34731482.

Keiser, M. J., Roth, B. L., Armbruster, B. N., Ernsberger, P., Irwin, J. J., & Shoichet, B. K. (2007). Relating protein pharmacology by ligand chemistry. Nature biotechnology, 25(2), 197-206.

Kim, S., Chen, J., Cheng, T., Gindulyte, A., He, J., He, S., Li, Q., Shoemaker, B. A., Thiessen, P. A., & Yu, B. (2019). PubChem 2019 update: improved access to chemical data. Nucleic acids research, 47(D1), D1102-D1109.

Kopustinskiene DM, Jakstas V, Savickas A, Bernatoniene J. Flavonoids as Anticancer Agents. Nutrients. 2020 Feb 12;12(2):457. doi: 10.3390/nu12020457. PMID: 32059369; PMCID: PMC7071196.

Kumar, H., Raj, U., Gupta, S., & Varadwaj, P. K. (2016). *In-silico* identification of inhibitors against mutated BCR-ABL protein of chronic myeloid leukemia: a virtual screening and molecular dynamics simulation study. *Journal of Biomolecular Structure and Dynamics*, *34*(10), 2171–2183. https://doi.org/10.1080/07391102.2015.1110046

Kuzmanic, A., & Zagrovic, B. (2010). Determination of ensemble-average pairwise root mean-square deviation from experimental B-factors. *Biophysical journal*, *98*(5), 861-871.

Lipinski, C. A. (2004). Lead-and drug-like compounds: the rule-of-five revolution. Drug Discovery Today: Technologies, 1(4), 337-341.

Mendis, S., Puska, P., Norrving, B., & Organization, W. H. (2011). Global atlas on cardiovascular disease prevention and control. World Health Organization.

Morris, G. M., Huey, R., Lindstrom, W., Sanner, M. F., Belew, R. K., Goodsell, D. S., & Olson, A. J. (2009). AutoDock4 and AutoDockTools4: Automated docking with selective receptor flexibility. Journal of computational chemistry, 30(16), 2785-2791.

O'Hare T, Eide CA, Deininger MWN. Bcr-Abl kinase domain mutations, drug resistance, and the road to a cure for chronic myeloid leukemia. Blood. 2007;110(7):2242–2249.

Pandrala M, Bruyneel AAN, Hnatiuk AP, Mercola M, Malhotra SV. Designing Novel BCR-ABL Inhibitors for Chronic Myeloid Leukemia with Improved Cardiac Safety. J Med Chem. 2022;65(16):10898–

Pires, D. E., Blundell, T. L., & Ascher, D. B. (2015). pkCSM: predicting small-molecule pharmacokinetic and toxicity properties using graph-based signatures. Journal of medicinal chemistry, 58(9), 4066-4072.

Ren, R. (2005). Mechanisms of BCR–ABL in the pathogenesis of chronic myelogenous leukaemia. *Nature Reviews Cancer*, 5, 172–183. doi:10.1038/nrc1567

Rowley, J. D. (1973). A new consistent chromosomal abnormality in chronic myelogenous leukaemia identified by quinacrine fluorescence and giemsa staining. *Nature*, 243, 290–293. doi:10.1007/978-3-7643-8117-2_6

Sherbenou, D. W., Hantschel, O., Kaupe, I., Willis, S., Bumm, T., Turaga, L. P., Lange, T., … Deininger, M. W. (2010). BCR-ABL SH3-SH2 domain mutations in chronic myeloid leukemia patients on imatinib. *Blood, 116*, 3278–3285.

Talele, T. T., Khedkar, S. A., & Rigby, A. C. (2010). Successful applications of computer aided drug discovery: moving drugs from concept to the clinic. Current topics in medicinal chemistry, 10(1), 127-141.

Thomas, L., Mathew, S., & Johnson, S. (2020). In-silico prediction of role of chitosan, chondroitin sulphate and agar in process of wound healing towards scaffold development. Informatics in Medicine Unlocked, 20, 100406.

Trott, O., & Olson, A. J. (2010). AutoDock Vina: improving the speed and accuracy of docking with a new scoring function, efficient optimization, and multithreading. Journal of computational chemistry, 31(2), 455-461.

Vandenberg, J. I., Walker, B. D., & Campbell, T. J. (2001). HERG K+ channels: friend and foe. Trends in Pharmacological Sciences, 22(5), 240-246.

Veber, D. F., Johnson, S. R., Cheng, H.-Y., Smith, B. R., Ward, K. W., & Kopple, K. D. (2002). Molecular properties that influence the oral bioavailability of drug candidates. Journal of medicinal chemistry, 45(12), 2615-2623.

Vener C, Banzi R, Ambrogi F, Ferrero A, Saglio G, Pravettoni G, et al. First-line imatinib vs second-and third-generation TKIs for chronic-phase CML: a systematic review and meta-analysis. Blood Adv . 2020;4(12):2723–2735.

Wang, J. Y. J. (1993). Abl tyrosine kinase in signal transduction and cell-cycle regulation. *Current Opinion in Genetics & Development*, 3, 35–43. doi:10.1016/j.tibs.2007.10.006

Xu, C., Cheng, F., Chen, L., Du, Z., Li, W., Liu, G., Lee, P. W., & Tang, Y. (2012). In silico prediction of chemical Ames mutagenicity. Journal of chemical information and modeling, 52(11), 2840-2847.

UCP Journal of Science and Technology
Vol. 3, Issue 1 (July - December 2025)
Journal website: http://ojs.ucp.edu.pk/index.php/ucpjst/index

Kobus (Bovidae, Artiodactyla) from Late Miocene of Mohal Pati and Hasnot, Jhelum, Punjab, Pakistan

Mariam Zaheer[1*], Muhammad Akbar Khan[1]

Abstract

Kobus represents an extant genus of the family Bovidae that is also found in fossilized form. The genus is also known from the Siwaliks, and its remains are relatively rare compared to other bovid taxa, especially in the Late Miocene. This study is focused on the collection of fossils of the genus *Kobus* from the Mohal Pati and Hasnot area of the district Jhelum, Punjab, Pakistan. The remains include a mandibular fragment, and isolated upper and lower dentition, and a morphometric study of these remains indicates that they belong to the extinct species, *Kobus porrecticornis*, found from the Siwaliks, particularly from the Late Miocene. The description of these remains adds more knowledge to the morphological features of this species, which will be helpful to a better understanding of the Siwalik bovids in general and the relationship of this species with extant species in particular.

Keywords: Bovidae*, Kobus,* Mohal Pati, Hasnot, Siwaliks

1. Introduction

The Siwalik Group, which is known for its preservation of remains of mammals from 18 Ma to 0.6 Ma, has its best exposure in the Potwar Plateau of Pakistan (Flynn et al., 2024; Pilbeam, 2025) and has attracted researchers from around the globe who were interested in the study of fossils of these mammalian taxa (Pilbeam, 2025). One of the mammalian orders, Artiodactyla, attained the highest diversity among the other large mammals (Khan et al., 2010, 2013), and at least seven families (Bovidae, Giraffidae, Tragulidae, Cervidae, Suidae, Hippopotamidae, Anthracotheriidae) are known from the Siwaliks of Pakistan. The four families (Bovidae, Giraffidae, Tragulidae, Cervidae) constitute the suborder Ruminantia, which is the most diverse suborder (Khan et al., 2010). The family Bovidae is best known among the other ruminants, but some of the taxa of this family are poorly represented in terms of the number of fossils (Pilgrim, 1939; Akhtar, 1992). The least well-represented taxa include the genus *Elachistoceras*, *Kobus*, *Palaeohypsodontus*, *Nisidorcas*, and *Protragelaphus* (Gentry et al., 2014, 2025). The genus *Kobus* first appeared in the upper Miocene deposits representing the Dhok Pathan Formation belonging to the Middle Siwalik Subgroup of the Siwalik Group (Pilgrim, 1939; Khan et al., 2010; Gentry et al., 2014, 2025) and is still living in Africa, hence an extant genus of the bovids. Among fossils, the genus is monospecific with *Kobus porrecticornis* (8.1-7.7 Ma), although Gentry *et al*. (2025) have reported the presence of two more species in the form of *Kobus* sp. 1 and *Kobus* sp. 2 from the same deposits but with a different time

[1] Fossil Display & Research Centre, Institute of Zoology, University of the Punjab, Quaid-e-Azam Campus, Lahore, Pakistan
*Corresponding author's E-mail: mariamzaheer2009@gmail.com
Received: 26 July 2025; Received in revised form: 20 November 2025; Accepted: 24 November 2025.
Available online: 23 December 2025.

DOI: https://doi.org/10.24312/ucp-jst.03.01.641

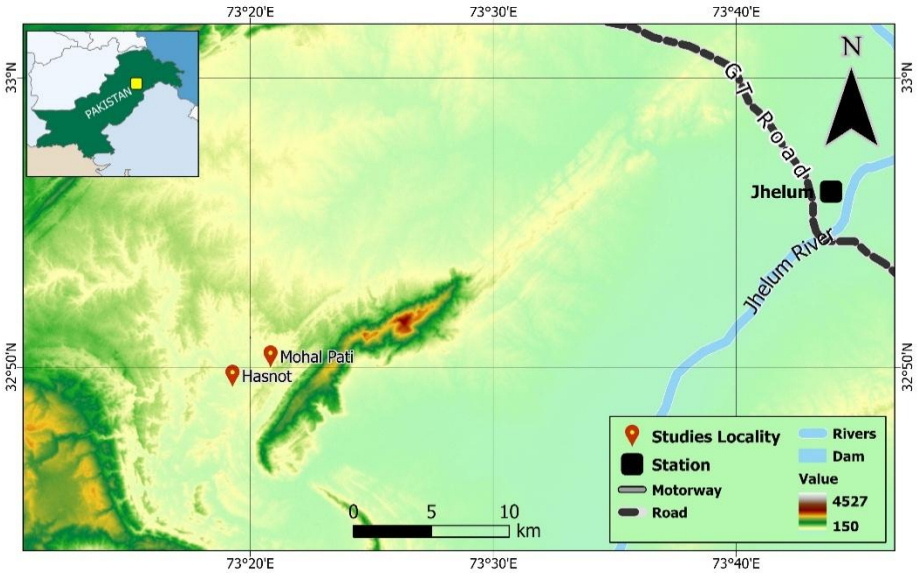

Figure 1. The geographic position of the Mohal Pati and Hasnot in the district Jhelum, Punjab, Pakistan.

frame. However, the morphology of the other two species is yet unknown, and most of the specimens are predominantly known for *Kobus porrecticornis*.

In this study, we describe the remains of the extinct species of the genus *Kobus* known predominantly from the Siwaliks of the Indian subcontinent. The specimens are valuable as they show the morphological variations present in the dental element of the Siwalik species, particularly p4s. The specimens have been collected from some localities, Mohal Pati and Hasnot villages, and the geographic and geological settings of these areas are given below.

Geographic & geological settings

The villages Mohal Pati and Hasnot are in the district Jhelum of the Punjab province of Pakistan. The village Hasnot, which lies about 70 km west of Jhelum city, is famous for its palaeontological collections made from the mid-1800s by various foreign researchers and has been reported in many pre-independence and post-independence palaeontological works (e.g., Pilgrim, 1913, 1937, 1939; Colbert, 1935; Sarwar, 1977; Akhtar, 1992; Khan et al., 2009; Khan & Flynn, 2017; Khan et al., 2020). The village Mohal Pati is located 3 km northeast of Hasnot. Both these villages have well-exposed Dhok Pathan outcrops in their vicinity. The outcrops/deposits present around these villages show dark to light colored sandstone and pale-yellow clay/siltstone that alternate with each other in cyclic deposition with a minute quantity of conglomerates that alternate (Barry et al., 2002; Zaheer & Khan, 2024). The age of these deposits ranges from 8 to 6.4 Ma (Fig. 1).

2. Materials and Methods

The material includes six specimens comprising upper and lower teeth. The material was collected through the surface collection, i.e., the collection areas or outcrops were surveyed/explored, and the material exposed on the surface was collected. The material was brought to the lab for preparation while completely wrapped in cotton. The material was prepared using fine needles. Each specimen was cataloged after preparation. The dental terminology follows Gentry *et*

Table 1 The nature of the material described in this study is within the collection area.

Catalog No.	Nature/Position	Locality
PUPC 23/355	A partially broken right upper third molar (rM3)	Mohal Pati
PUPC 23/361	An isolated right lower fourth premolar (rp4)	Hasnot
PUPC 24/158	An isolated left lower fourth premolar (lp4)	Mohal Pati
PUPC 24/157	A small left mandibular fragment having a fourth premolar (p4) and roots of the first molar (m1)	Mohal Pati
PUPC 24/159	Partially broken conjoined right lower fourth premolar and first molar (rp4-m1)	Mohal Pati
PUPC 24/183	An isolated left upper third molar (lM3)	Mohal Pati

al. (1999). The measurements were occlusal length and width, and were taken in millimeters with the use of digital Vernier calipers. Canon 6D was used for photography, and plates were prepared in Adobe Photoshop CC. The material

described is kept in the Palaeontology Laboratory, which is under the ownership of the University of the Punjab, Lahore, Pakistan. *Abbreviation:* est., estimated; L, Langebaanweg collection; PUPC, Punjab University Palaeontological Collection.

3. Systematic Palaeontology

Order Artiodactyla Owen, 1848
Family Bovidae Gray, 1821
Subfamily Antilopinae Gray, 1821
Tribe Reduncini Blaine, 1914 *sensu* Simpson, 1945
Genus *Kobus* Smith, 1840

***Kobus porrecticornis* Pilgrim, 1939**

Type specimen: GSI-B 229, frontlet with the horn cores (Pilgrim, 1939).
Type locality: Tatrot, Jhelum district, Punjab, Pakistan (Pilgrim, 1939).
Diagnosis: As given in Pilgrim (1939).
Stratigraphic range: Upper Miocene deposits of the Dhok Pathan (Gentry et al., 2014, 2025) and from the lower Pliocene deposits of the Tatrot Formations representing the Middle and Upper Siwalik Subgroup (Khan & Akhtar, 2014; Iqbal et al., 2015; Zaheer & Khan, 2024).

Studied material: Table 1 represents the nature of the material described in this study, with the collection area. PUPC 24/183, an isolated left upper third molar (lM3) (Mohal Pati); PUPC 23/355, partially broken right upper third molar (rM3) (Mohal Pati); PUPC 23/361, an isolated right lower fourth premolar (rp4) (Hasnot); PUPC 24/158, an isolated left lower fourth premolar (lp4) (Mohal Pati); PUPC 24/157, A small left mandibular fragment having fourth premolar (p4) and roots of the first molar (m1) (Mohal Pati); PUPC 24/159, partially broken conjoined right lower fourth premolar and first molar (rp4-m1) (Mohal Pati).

4. Results

PUPC 24/183 represents an isolated third left upper molar (LM3). The molar shows an early stage of wear (Fig. 2.1). The tooth is mesodont. The enamel is preserved only on the base of the protocone and hypocone; the rest is lost

due to weathering. The preprotocrista is longer than the postprotocrista, which is slightly anteriorly directed at its apex. The prehypocrista is slanting and also longer than the posthypocrista. Both the anterior and posterior fossettes are large and prominent, where the anterior one is C-like in appearance, is wider than the posterior, and possesses a small spur anteriorly. The posterior fossette is narrow anteriorly and wider posteriorly. The parastyle is almost broken, half of its length, though it is well developed and thick. The mesostyle is the thickest and lingually flared. The metastyle is prominent but weakly developed. The paraconous rib is prominent and larger than the metaconous rib, which is weak and more prominent at its base. The median valley is deep but narrow.

PUPC 23/355 is an upper third molar that shows signs of early wear and most of the protocone and apical part of the paracone are lost due to partial breakage (rM3) (Fig. 2.2). Due to this breakage, only a small part of the postprotocrista is preserved while some part of the pre- and postparacrista are lost from the apical portion. The hypocone and the metacone are fully preserved. The prehypocrista is longer than the posthypocrista, and overall, the lingual side of the hypocone is crescentic shaped, i.e., round. Metacone is also well preserved and slightly lingually oriented. Most of the anterior fossette is lost because of breakage. On the other hand, the completely preserved posterior fossette shows moderate broadness with a small spur almost in the center. Both the styles and ribs are large, prominent, flanked, and broad.

PUPC 23/361 is a lower fourth premolar (p4) that shows early wear (Fig. 2.3). The tooth is without any breakage and exceptionally preserved. It is pentacuspidate, trilobed, with three prominent valleys and a large groove. The anterior lobe has a large paraconid with its prominent parastylid. The postparacristid is in contact with the protoconid, which is the largest and highest cusp and has prominent pre- and postcristids. The metaconid is long, lingually projected, its cristid is bent anteriorly, and it is in contact with the paraconid. The contact between the metaconid and paraconid results in the closure of the anterior valley, which is the largest and broadest, and gives this premolar a semi-molarized appearance. The hypoconid and entoconid form the third lobe. The hypoconid is a small but

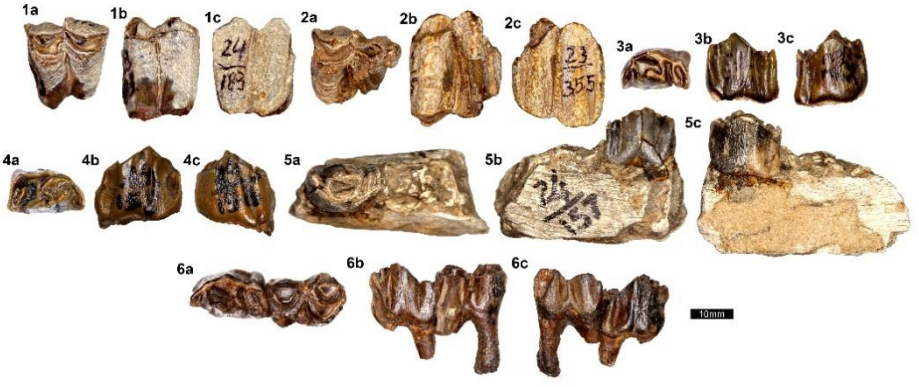

Figure 2. *Kobus porrecticornis*. **1.** PUPC 24/183, an isolated left upper third molar (lM3); **2.** PUPC 23/355, partially broken right upper third molar (rM3); **3.** PUPC 23/361, an isolated right lower fourth premolar (rp4); **4.** PUPC 24/158, an isolated left lower fourth premolar (lp4); **5.** PUPC 24/157, A small left mandibular fragment having a fourth premolar (p4) and roots of the first molar (m1); **6.** PUPC 24/159, partially broken conjoined right lower fourth premolar and first molar (rp4-m1). Views: a) occlusal, b) lingual, c) labial. The scale bar is equal to 10 mm.

Table 2. Measurements of the described teeth of *Kobus porrecticornis* in comparison with previously reported material.

Taxa	Catalog No.	Position	Length	Width	References
Kobus porrecticornis	PUPC 24/183*	Left M3	18.90	19.00	This study
	PUPC 23/355*	Right M3	20.20	17.20**	
	PUPC 23/361*	Right p4	16.70	10.30	
	PUPC 24/157*	Left p4	15.70	10.80	
	PUPC 24/158*	Left p4	17.50	10.30	
	PUPC 24/159*	Right p4	16.80	10.30	
		Right m1	16.30	10.70	
	PUPC 14/186	Left p4	13.50	8.00	Iqbal et al., 2015
		Left m1	18.20	11.00	
	PUPC 83/837	Left m1	16.50	10.80	Khan et al., 2014
Kobus subdolus	L15605	Left p4	12.00	8.00 est.	Gentry, 1980
		Left m1	15.00 est.	10.00 est.	
	L32850	Right p4	10.40	-	
	L46067	Right p4	11.40	-	
Reduncini gen. et sp. indet.	PUPC 68/60	Left p4	15.20	10.20	Siddiq et al., 2020

*Studied material. ** preserved measurements.

prominent cusp, while the entoconid is long and oriented lingually, and the entostylid is long, present perpendicular to the entoconid and also oriented lingually. The median valley is present between the metaconid and entoconid and is moderately broad and fully open lingually. The posterior valley is present between the entoconid and the entostylid.It is narrow and partially open apically. A large and deep groove is present between the protoconid and hypoconid. Enamel shows moderate rugosity.

PUPC 24/158 represents the second isolated lower fourth premolar (p4) in this study. The premolar shows the signs of the middle stage and slight breaking that resulted in the missing of a small part of the paraconid, parastylid, metaconid,

entoconid, and entostylid (Fig. 2.4). Both the paraconid and metaconid are oriented towards each other, and contact between them results in complete closure of the anterior valley. The metaconid is prominent and directed towards the entoconid but does not contact it. Hence, the median fossette is open. Due to the presence of a contact between the entoconid and entostylid, the posterior fossette has become completely closed. The morphology of other characteristics is like the PUPC 23/361.

A single mandibular fragment (PUPC 24/157) has a lower fourth premolar (p4) which is completely preserved, while only the roots of the m1 are preserved (Fig. 2.5). The mandibular body (corpus) shows the pattern of extreme weathering, presence of siltstone in which it was preserved, and woody texture. Despite the weathering, the corpus remains robust and thick, and its depth and width increase from anterior to posterior. The preserved mandibular length is 46.3 mm. The lower fourth premolar shows moderate wear. The parastylid, paraconid, protoconid, and entostylid are cracked and have been fixed using glue. The anterior valley is fully closed due to the fusion of the paraconid and the metaconid, and both the protoconid and the fused paraconid and metaconid make a globular or round appearance of this part of the tooth. Except for the above-mentioned and narrow and slim entoconid and entostylid, the other features of the tooth are morphologically like PUPC 23/361. The preserved roots of m1 show that the molar was bilobed, and the roots of the posterior lobe are visible at the point of breakage of the mandible.

PUPC 24/159 represents two teeth that are conjoined and sequentially representing a lower fourth premolar (p4) and lower first molar (m1), (Fig. 2.6). Except for the partial breakage of parastylid and metaconid, reduced paraconid, narrowing of the anterior valley, and the preservation of posterior roots, the p4 is like PUPC 23/361 in its morphology. The first lower molar (m1) shows extreme wear and partial breakage of the protoconid and the entoconid. Due to the extreme wear, both fossettes have become extremely narrow and crescentic in shape. A large and thick ectostylid is present in the median valley. The metastylid is prominent but moderately thick, while the mesostylid is extremely thick and large and round in appearance. The ribs are weakly developed. The anterior roots are partial, while the posterior roots are almost completely preserved.

4.1 Comparison

The described material includes three lower fourth premolars, and these are helpful in the identification of the studied specimens as reduncine (Table 2). The p4s of the reduncine have a partially or completely closed anterior valley, which results from the contact or fusion of the paraconid and metaconid (Gentry, 1980). In reduncine p4s, there is a tendency of the paraconid and metaconid to grow towards each other resulting either in contact or fusion of both these cusps and this situation is already known in the p4s of African extinct species *Kobus subdolus* from early Pliocene deposits of Langebaanweg, South Africa particularly in the mandible (L15605) described and illustrated by Gentry (1980, fig. 24); in one of the specimen (PUPC 14/186), from Pliocene deposits, of the Siwalik species, *Kobus porrecticornis* which was described and illustrated by Iqbal *et al*. (2015, fig. 2.1) and in one specimen (PUPC 68/60) from the Pleistocene deposits of the Siwaliks which was described as Reduncini gen. et sp. indet. by Siddiq *et al*. (2020, fig. 2F). Further, confirmation of reduncine affinity of the p4 specimens came from the work of Gentry (1980) who reported the occurrence of such closure of the anterior valley in 15 out of 31 p4s of *Redunca*

arundinum and also found in ontogenetically older *Kobus ellipsiprymnus*.

Other than above mentioned character, the fossil specimens show multiple dental traits common with primitive reduncines. The p4 has a strongly projected hypoconid and the presence of a groove between the hypoconid and protoconid, which is narrow and deep. in addition, as shown by the described material, teeth are mesodont or moderately hypsodont, with the presence of small but strong goat folds in the molars as well as a strong and developed median basal pillar in the median/transverse valleys. According to Gentry (1978, 1980), these features are noted in the taxa *Kobus subdolus*, *Kobus porrecticornis*, and *Kobus* aff. *porrecticornis*. The studied lower molar, PUPC 24/159, also shows the reduncine features, which include and are crowned by well-developed ribs, pinched labial cusps, a weak goat fold, and a small ectostylid (Fig. 2.6). These are reduncine features differentiating them from the Alcephalini, which possess rounded ribs and cusps, a prominent goat fold, and an enlarged ectostylid. Since *Kobus* constituted the majority of reduncine fauna in the Late Miocene (Gentry et al., 2014), we use *Kobus* for our attribution and identification as the species, *K. porrecticornis*.

5. Discussion

The subfamily Antilopinae is known from the Middle Miocene deposits of the Siwalik Group, and its first representatives come from the Kamlial Formation (Lower Siwalik Subgroup) in the form of Antilopinae unnamed genus and sp. (Gentry et al., 2025). The subfamily is today represented by many genera. However, the tribe Reduncini is known by a single genus, *Kobus,* which is also an extant genus that is now found in Africa with six species of antilopes of varying body size. The fossils of this genus are also known from the Late Miocene of Asia and Africa (Gentry, 1970; Gentry, 1997). It belongs to the tribe Reduncini of the family Bovidae (Pilgrim, 1939; Gentry, 1998; Gentry et al., 2025) and its fossils have been recovered from the Siwalik Group of Pakistan and India (Pilgrim, 1939; Khan et al., 2014; Iqbal et al., 2015; Zaheer & Khan, 2024; Gentry et al., 2025). The Siwalik species of genus *Kobus* is *K. porrecticornis,* which was originally described by Lydekker (1878) under the name of *Antilop porrecticornis* and again by the same author (Lydekker, 1886) under the name of *Gazella porrecticornis*. Pilgrim (1939) included the species under a new genus, *Dorcadoxa*. Later, Gentry (1970) placed the species in the genus *Kobus,* and Thomas (1980) and Gentry (1978, 1980) followed this suggestion, and this suggestion is still in use. According to the study of Thomas (1980), *K. porrecticornis* first appeared in the Dhok Pathan Formation in the type zone of this formation at the base of the Kundvali unit between sandstones 6 and 7, i.e., from the loc. 97. It is reported from the Baard's Quarry lower assemblage at Langebaanweg, Lukeino, and Mpesida in Africa as a reduncine species, which is the same or a similar species to the Siwaliks. The age of the Baard's Quarry lower assemblage, as reported by Hendey (1978), is about 2.0 Ma, i.e., the Pliocene, indicating that the Langebaanweg 'E' Quarry assemblage, despite the occurrence of the ancient *Kobus*, is older than Baard's Quarry lower assemblage as noted by Gentry (1980). According to Gentry (1997), it was previously observed by him (1980) that the horn cores collected from Baard's Quarry have smaller supraorbital pits as compared to the other localities, and in the Lukeino specimens, Thomas (1980) noted the presence of internal sinuses near the supraorbital pit. While discussing the relationship of *Kobus porrecticornis*,

Pilgrim (1913) followed the suggestions of Lydekker (1886) and placed it in the tribe Antilopini and suggested a close relationship of the *Aepyceros* based on the characters of the horn core and the maxilla. However, the reduncine affinity of *Kobus porrecticornis* was suggested much later by Gentry (1970).

Among the described material, the lower fourth premolars, i.e., p4s, are considered diagnostic in the family Bovidae. The described p4s are diagnostic enough in our case as shown in the study of Gentry (1980), which reported the closure of the anterior valley in the reduncine p4, and its occurrence ratio is nearly 50 percent in one species and more than 50 percent in other species. Other material described in this study also shows morphological features that are typical for the genus *Kobus,* which is known from the upper Miocene to lower Pliocene deposits, as shown in the comparison section of the described material. For about a hundred years, only one species of the genus was known the Siwalik, *Kobus porrecticornis*. But in recent studies by Gentry *et al*. (2014, 2025) have reported the presence of two more species from the Siwaliks without any description and illustration and these include: *Kobus* sp. 1 which is a slightly older species whose range is 9.3-7.9 Ma and a younger species of the genus, *Kobus* sp. 2 which is also known from Late Miocene with an age of 7.3-5.9 Ma. They further suggested that *K. porrecticornis* is restricted to the Miocene and its range is 8.1-7.7 Ma. Such an age limitation of *K. porrecticornis* in the upper Miocene deposits Siwaliks, does not correspond to the previous works done by Khan *et al*. (2008, 2014), and Iqbal *et al*. (2015) reporting *K. porrecticornis* from the much younger deposits in the Tatrot Formation (3.5-3.3 Ma).

6. Conclusions

In this study, we described the remains of the Siwalik reduncine species, *Kobus porrecticornis,* from the Late Miocene localities present in the surroundings of Mohal Pati and Hasnot villages. The material described includes the upper and lower dentition, which also includes the lower fourth premolars (p4s). The p4 is considered diagnostic in the ruminants, and in our case study, it we well applied. The description of this material shows the morphological variation in the M3s and p4s and hence adds further knowledge to the morphology of this species, which will result in a better understanding of this species.

References

Akhtar, M. (1992). Taxonomy and Distribution of the Siwalik Bovids (Doctoral Dissertation). University of the Punjab, Lahore, Pakistan.

Barry, J. C., Morgan, M. E., Flynn, L. J., Pilbeam, D., Behrensmeyer, A. K., Raza S. M., & Kelley, J. (2002). Faunal and environmental change in the late Miocene of the Siwaliks of northern Pakistan. *Paleobiology, 28,* 1-71. DOI:10.1666/0094-8373(2002)28[1:FAECIT]2.0.CO;2

Colbert, E. H. (1935). Siwalik mammals in the American Museum of Natural History. *Transactions of the American Philosophical Society New Series, 26,* 1-401. DOI:10.2307/1005467

Flynn, L. J., Raza, S. M., Morgan, M. E., Barry, J. C., & Pilbeam, D. (2024). The Potwar Siwaliks: an impressive Neogene record of terrestrial rocks and fossils. In R.M. Clary, E. J. Pyle & W. M. Andrews (Eds.), *Geology's Significant Sites and their Contributions to Geoheritage* (pp.331–342). Geological Society, London, Special Publications, 543. DOI:10.1144/SP543-2022-251

Gray, J. E. (1821). On the Natural Arrangements of Vertebrose Animals.

Monthly Journal and Review, *15*, 296-310.

Gentry, A. W. (1970). The Bovidae (Mammalia) of the Fort Ternan fossil fauna In L. S. B. Leakey & R J. G. Savage (Eds.), *Fossil Vertebrates of Africa,* Vol. 2 (pp. 243-324) Academic Press, London.

Gentry, A. W. (1978). Bovidae, In H. B. S. Cooke & V. J. Maglio (Eds.), *Evolution of African Mammals* (pp. 540-572). Cambridge, MA: Harvard University Press, Cambridge.

Gentry, A. W. (1980). Fossil Bovidae (Mammalia) from Langebaanweg, South Africa. *Annals of South Africa Museum*, *79*(8), 213-337.

Gentry, A. W. (1997). Fossil ruminants (mammalia) from the Manonga valley, Tanzania. In *Neogene Paleontology of the Manonga Valley, Tanzania: A Window into the Evolutionary History of East Africa* (pp. 107-135). Boston, MA: Springer US.

Gentry, A. W., Solounias, N., & Barry, J. C. (2014). Stability in higher level taxonomy of Miocene bovid faunas of the Siwaliks. *Annales Zoolgici Fennici*, *51*, 49-56.

Gentry, A. W., Solounias, N., & Barry, J. C. (2025). Siwalik Bovidae. In C. Badgley, M. E. Morgan & D. Pilbeam (Eds.), *At the Foot of the Himalayas: Paleontology and Ecosystem Dynamics of the Siwalik Record* (369-388). Johns Hopkins University Press.

Gentry, A. W., Rössner, G. E., & Heizmann, E. P. S. (1999). Suborder Ruminantia. In G. E. Rössner & K. Heissig (Eds.), *The Miocene land mammals of Europe* (pp. 225-258). Verlag Dr. Friedrich Pfeil, München.

Hendey, Q. B. (1978). Late tertiary mustelidae (mammalia, Carnivora) from langebaanweg, South Africa. *Annals of the South African Museum, 76*(10), 329-357.

Iqbal, A., Khan, A. M., & Akhtar, M. (2015). *Kobus porrecticornis* (Reduncini) from the Upper Siwaliks of Tatrot, Pakistan. *Journal of Animal and Plant Sciences*, *25*(3), 466-471.

Khan, M. A., & Akhtar, M. (2014). Antelopes (Mammalia, Ruminantia, Bovidae) from the Upper Siwaliks of Tatrot, Pakistan, with description of a new species. *Paleontological Journal*, *48*(1), 79-89.

Khan, M. A., & Flynn, L. J. (2017). New small mammals from the Hasnot–Tatrot area of the Potwar Plateau, northern Pakistan. *Paläontologische Zeitschrift*, *91*(4), 589-599.

Khan, M. A., Khan, A. M., Iqbal, M., Akhtar, M., & Mahboob, S. (2008). Reduncine fossils from the Upper Siwaliks of Tatrot. *The Journal of Animal and Plant Sciences*, 18, 50-52.

Khan, M. A., Iliopoulos, G., & Akhtar, M. (2009). Boselaphines (Artiodactyla, Ruminantia, Bovidae) from the Middle Siwaliks of Hasnot. Pakistan. *Geobios, 42,* 739-753.
DOI: 10.1016/j.geobios.2009.04.003

Khan, M. A., Akhtar, M., & Iqbal, M. (2010). The late Miocene artiodactyls in the Dhok Pathan type locality of the Dhok Pathan formation, the Middle Siwaliks, Pakistan. *Pakistan Journal of Zoology Supplement Series*, *10*, 1-90.

Khan, M. A., Akhtar, M., Babar, M. A., Abbas, S. G., Siddiq, M. K., Nawaz, M. K., Mubashar, M., Yaqoob, H., Nazir, S., Farheen, S., Draz, O., Shahbaz, S., Sultana, N., Zahra, N., & Noreen, S. (2013). Some new remains of middle Miocene mammals from the Chinji Formation, northern Pakistan. *Pakistan Journal of Zoology Supplementary Series*, *13*, 1-55.

Khan, M.A., Iqbal, J., Ali, S., & Akhtar, M., (2014). New remains of Tragoportax (Boselaphini, Bovidae, Mammalia) from the Middle Siwaliks of Dhok Pathan, Northern Pakistan. *Pakistan Journal of Zoology, 46*(2), 463-470.

Khan, M. A., Kelley, J., Flynn, L. J., Babar, M. A., & Jablonski, N. G. (2020). New fossils of *Mesopithecus* from Hasnot, Pakistan. *Journal of Human Evolution*, *145*, 102818. DOI:10.1016/j.jhevol.2020.102818

Lydekker, R. (1878). Indian Tertiary and Post-Tertiary vertebrate. 3. Crania of Ruminants. *Palaeontologia Indica, 10*, 88-181.

Lydekker, R. (1886). Catalogue of the fossil mammalian in the British Museum. Part II. Containing the order Ungulata, Suborders Perissodactyla, Toxodontia, Condylartha, and Amblypoda. London, pp. 186.

Pilbeam, D. (2025). A long story. In C. Badgley, M. E., Morgan & D. Pilbeam (Eds.), *At the Foot of the Himalayas: Paleontology and Ecosystem Dynamics of the Siwalik Record* (3-11). John Hopkins University Press.

Pilgrim, G. E. (1913). Correlation of the Siwaliks with mammal horizons of Europe. *Records of Geological Survey of India, 43*(4), 264-326.

Pilgrim, G. E. (1937). Siwalik antelopes and oxen in the American Museum of Natural History. *Bulletin of American Museum of Natural History*, *72*, 729-874.

Pilgrim, G. E. (1939). The fossil bovidae of India. *Paleontogia Indica New Series*, 26(1), 1-356.

Simpson, G. G., (1945). The principles of classification and a classification of mammals. *Bulletin of American Museum of Natural History*, *85*, 1-350.

Sarwar, M. (1977). Taxonomy and distribution of the Siwalik Proboscidea. *Bulletin of Department of Zoology, University of the Punjab*, 1-72.

Siddiq, M. K., Dar, F. Y., Khan, M. A., Babar, M. A., Abbas, S. G., Ghaus, A., Iqbal. M., & Akhtar, M. (2020). Antelopes (Mammalia) from Pabbi Hills of Sardhok, Pakistan. *Pakistan Journal of Zoology*, *52*(1), 263-271. DOI:10.17582/journal.pjz/2020.52.1.263.271

Thomas, H. (1980.) Les bovides du Miocene superieur des couches de Mpesida et de la formation de Lukeino (district de Baringo, Kenya), In R.E. F. Leakey and B. A. Ogot, (Eds.), *Proceedings of the 8th Pan-African Congress of Prehistory; Nairobi, 1977* (pp. 82-91).

Zaheer, M. & Khan, M. A. (2024). The Late Miocene Bovids of Mohal Pati, Jhelum, Punjab, Pakistan. *Journal of Animal and Plant Science*, *34*(4), 962-976. DOI:10.36899/JAPS.2024.4.0780

UCP Journal of Science and Technology
Vol. 3, Issue 1 (July - December 2025)
Journal website: http://ojs.ucp.edu.pk/index.php/ucpjst/index

Nutritional and Sensory Evaluation of Weaning Food Formulated with Mixed Fruits (Banana and Beetroot)

Laiba Younas[1]*, Malaika Riaz[1], Abdul Mueez Ahmad[1*], Fatima Javed[1], Rimsha Amjad[1], Fatima Liaqat[1]

Abstract

Malnutrition has a serious impact on the health of infants over the weaning period. Complementary foods that are nutritionally balanced should be given to ensure perfect growth and development. This study was meant to come up with both nutrient-enriched and taste-acceptable weaning foods using banana and beetroot due to their high nutritional content. Banana and beetroot were dried through a hybrid oven (60 °C) and a hot air oven (607 ^{0}C), respectively, and turned into powder. Six weaning food formulations were prepared using different proportions of whole wheat flour, banana powder, and beetroot powder (T-T6). They were researched on sensory properties, phytochemicals composition, and proximate composition. It has been noted that T6 contained the highest amounts of ash and fiber, and T1 contained the most amounts of fat, protein, and hydration. While T5 was the most sensory acceptable with a score of 8.3 due to its balanced banana content. Based on these findings, the nutritional value and attractiveness of weaning foods may be boosted by the incorporation of powdered banana and beetroot into the foods.

Keywords: Weaning Food, Nutrition, Banana, Beetroot, Infant

1. Introduction

Weaning is an important phase of infant development, as well as growth, the process that typically begins at the age of six months. The milk of the mother contains all the needed nutrients during the first half of the first year; however, over time, as a child grows, the milk ceases to satisfy their growing nutritional requirements (Morison et al., 2016). Therefore, in order to prevent malnutrition, encourage healthy growth, and develop appropriate feeding practices, complementary foods must be introduced on time (Shitemi et al., 2018).

Complementary foods should be soft, rich in nutrients, and easy to digest at this phase so that babies can progressively become accustomed to a range of flavors and textures. The World Health Organization states that in order to meet the changing nutritional demands of newborns, these foods must be safe, hygienic, and sufficient in calories, protein, as well as micronutrients (D'Auria et al., 2018). Stunting, developmental delays, and nutrient shortages have all been closely linked to inadequate or poorly designed weaning meals (Bhutta et al., 2013). For this reason, special care should be taken to create complementary foods that are simultaneously nutrient-dense as well as baby-friendly.

The best options for improving the nutritional value of weaning diets are fruits and vegetables. Their inherent abundance

[1]National Institute of Food Science and Technology, University of Agriculture, Faisalabad, 38000, Pakistan
*Corresponding author's E-mail: laibayounas.ly@gmail.com , mueez183@gmail.com
Received: 11 April 2025; Received in revised form: 07 July 2025; Accepted: 17 November 2025.
Available online: 23 December 2025.

DOI: https://doi.org/10.24312/ucp-jst.03.01.505

of vital minerals, vitamins, fiber, anti-oxidants, as well as phytochemicals, promotes metabolic health, immunity, and cognitive function (Slavin & Lloyd, 2012; Liu, 2013). Although these benefits exist, studies reveal that a considerable part of children who are 7 to 24 months old fail to consume proper quantities of vegetables and fruits (Grimm et al., 2014). Therefore, increasing their inclusion in supplemental foods may help address vitamin deficiencies and lower the chance of developing chronic illnesses in later life.

A popular food throughout infancy, bananas (*Musa paradisiaca*) are known for their favorable digestion, desirable flavor, as well as smooth texture. They are abundant in B-complex vitamins, calcium, phosphorus, and potassium, all of which are crucial for neurological and musculoskeletal development (Kabeer et al., 2023). Bananas have also shown promise for usage in processed foods, including flour, puree, alongside snacks, that can be added to a range of weaning food items.

Beetroot is an important for nutrition for babies (*Beta vulgaris L.*), a root vegetable in the Chenopodiaceae family. It contains high amounts of iron, vitamin C, flavonoids, carotenoids, and polyphenols that facilitate hemoglobin synthesis, enhance immunity, and have anti-inflammatory and antioxidant properties (Chhikara et al., 2019). Although taste preferences have limited its use in newborn feeds, beetroot's growing popularity in functional food items shows that it may be incorporated into weaning diets.

Considering how vital it is to address the deficiency of micro nutrients through broadened diets, the development of complementary foods employing ingredients that are accessible locally, like banana, beetroot, as well as flour made from whole wheat, can offer a practical solution. Therefore, the purpose of this study was to develop and assess the nutritional as well as sensory properties of weaning foods that contain powdered beetroot and banana. The goal is to create well-rounded, palatable, as well as reasonably priced formulations that can enhance the health of newborns and elevate the range of nutrient-dense products available on the market.

2. Materials and Methods

2.1.1 Raw materials

Whole wheat flour, banana, beetroot, and milk powder were procured from the local food market of Faisalabad, Pakistan. All the chemicals were of analytical grade.

2.1.2 Processing of raw material

Bananas at the third stage of ripeness and fresh beetroot were thoroughly washed, peeled, as well as sliced to an even thickness of 5 mm using a stainless-steel knife. To prevent enzymatic browning, the slices were first immersed in a 0.2% sodium metabisulfite solution. Like Bassey et al. (2013), bananas were dried in a hybrid oven set at 60°C for five hours. In line with Shilpa et al. (2023), beetroot slices were then dried utilizing a hot air oven set to 60–70°C for 7–10 hours. To guarantee consistent particle size, dried banana as well as beetroot were ground into fine powders separately and sieved over a 60–65 mesh screen. After manually cleaning the whole wheat grains to get rid of any foreign objects, they were rinsed under running water. Then soak for an 8-hour soak in water, the cleaned grains were then dried for 24 hours at 60°C using a hot air oven. In the next step, a grinder was used to ground the dry grains into fine flour according to Bekele and Shiferaw's (2020) methodology.

2.1.3 Product formulation

Six different concentrations of beetroot powder (BRP), banana powder (BP), and whole wheat flour (WWF) food premixes were developed. Chickpea flour served as a base ingredient in each formulation as shown in table 1. Furthermore, milk powder was added to each batch, then

Table 1 Product Formulation

Treatment	Whole wheat flour (%)	Banana powder (%)	Beetroot powder (%)
T1	90	10	-
T2	90	-	10
T3	80	20	-
T4	80	-	20
T5	80	10	10
T6	60	20	20

boiled until it was uniform, and then dried.

2.2. Chemical And Sensory Analysis

2.2.1 Proximate analysis

Utilizing standard methods established by the Association of Official Analytical Chemists (AOAC, 2016), the moisture, crude protein, crude fat, dietary fiber, as well as ash content of the weaning food premixes were evaluated.

2.2.2. Phytochemical analysis

A) Total phenolic content

Calculated as milligrams of gallic acid equivalents (GAE) per 100 grams employing the Folin–Ciocalteu technique as outlined by the American Academy of Nutrition and Acculturation (AOAC, 2016).

B) Total flavonoid content

Assessed in milligrams of quercetin equivalents (QE) per 100 grams and evaluated utilizing the aluminum chloride colorimetric approach in accordance with AOAC (2016) recommendations.

2.2.3. Sensory evaluation

Each weaning meal sample's sensory qualities (color, texture, taste, as well as general acceptability) were assessed by a trained panel of ten judges adopting a 9-point hedonic scale, where 9 represents extremely like and 1 represents extremely dislike. To prevent bias, samples were served in a randomized order under closely controlled settings.

2.2.4. Statistical analysis

Each investigation was performed three times. The mean ± standard deviation was utilized to express the data. A completely randomized design (CRD) was employed to apply one-way analysis of variance (ANOVA), and Tukey's test was applied to compare treatment means at a significance level of $p \leq 0.05$.

3. Results and Discussion

3.1. Proximate analysis

The proximate composition of the weaning food premixes is given in Table 2 and Figure 1. In T1, the moisture level was $7.38 \pm 0.04\%$, while in T6, it was $6.54 \pm 0.03\%$. As the concentration of both banana and beetroot powder increased, the moisture content decreased gradually, and the amount of whole wheat flour also declined in parallel. These results are related to an investigation by Martinez et al. (2015) that found that the fortification of more unripe banana flour to pasta recipes led to a decrease in moisture level of moisture. In a comparable manner, Pandey and Singh (2019) noted reduced moisture in weaning diets augmented with nuts as well as bananas. In T6, the crude protein level was $11.39 \pm 0.06\%$, down from $13.48 \pm 0.07\%$ in T1. These concentrations of beetroot and banana flour showed lower protein contents than whole wheat flour. Between T1 and T6, the premixes' fat levels varied from $3.97 \pm 0.02\%$ to $3.29 \pm 0.01\%$. %. In the paper of Khatun et al. (2013), where the fat contents were found to decrease, and weaning foods are produced using the germinated wheat and lentil flour, the fat level slightly decreases with the increase in the level of banana, as well as beetroot

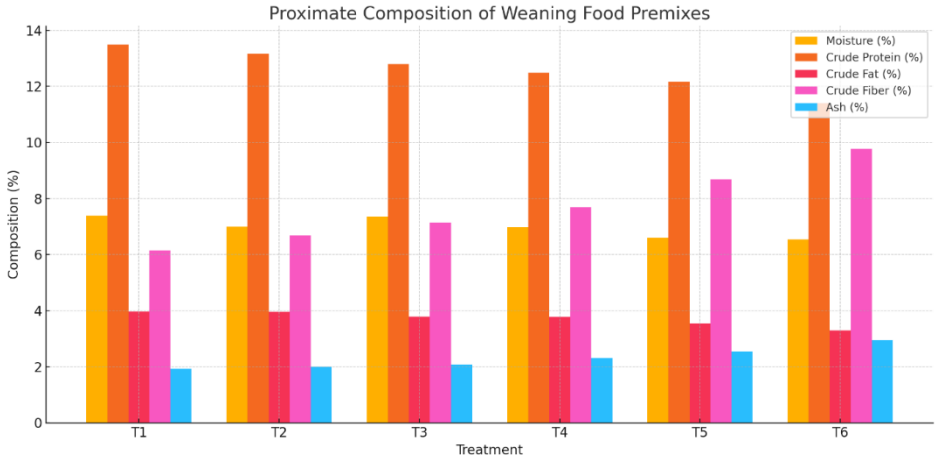

Figure 1 Proximate composition (%) of weaning food premix

powder. In the same case, addition of banana and pineapple pomace to legume-based weaning formulas was found to reduce the amount of fat (Mishra et al., 2014). Between T1 and T6, the crude fiber level rose substantially from 6.14 ± 0.03% to

9.77 ± 0.05%. By the addition of these two flours fiber content increased, but these findings observed less than the outcomes of Borbi et al. (2020), and found that the fiber level varied from 10.35% to 11.21%. Furthermore, the ash content also increased by 1.92 ± 0.01% (T1) to 2.96 ± 0.01% (T6), as observed that greater concentrations of powders, greater the mineral contents. Jahan et al. (2021) noticed that weaning diets made with mung bean and wheat flours had comparable ash levels. Overall, the addition of banana along with beetroot powders affected on the nutrients of formulations, with T1 had greater fat and protein ratios and T6 indicating greater fiber and mineral contents.

Table 2 Proximate analysis (%) of weaning premix

Treatment	Moisture (%)	Crude protein (%)	Crude fat (%)	Crude fiber (%)	Ash (%)
T-1	7.38±0.04^{a}	13.48±0.07^{b}	3.97±0.02^{b}	6.14±0.03^{b}	1.92±0.01^{b}
T-2	6.99±0.04^{a}	13.16±0.07^{c}	3.95±0.02^{b}	6.68±0.03^{c}	1.99±0.01^{c}
T-3	7.36±0.03^{b}	12.80±0.07^{d}	3.79±0.02^{c}	7.14±0.04^{d}	2.08±0.01^{d}
T-4	6.97±0.04^{b}	12.48±0.07^{e}	3.77±0.02^{c}	7.68±0.04^{e}	2.31±0.01^{e}
T-5	6.59±0.03^{c}	12.16±0.07^{f}	3.55±0.02^{d}	8.68±0.05^{f}	2.55±0.01^{f}
T-6	6.54±0.03^{c}	11.39±0.06^{g}	3.29±0.01^{e}	9.77±0.05^{g}	2.96±0.01^{g}

Means that carrying different letters is significantly different from each other
(Tuckey's test, $p \leq 0.05$)
T_1=90%WWF+10%BP
T_2=90%WWF+10%BRP
T_3=80%WWF+20%BP
T_4=80%WWF+20%BRP
T_5=80%WWF+10%BP+10%BRP
T_6=60%WWF+20%BP+20%BRP

Table 3 Phytochemical composition of weaning food premix

Treatments	TPC (GAE mg/100g)	TFC (QE mg/100g)
T-1	9.78±0.05[a]	5.21±0.03[f]
T-2	11.24±0.06[b]	5.65± 0.03[d]
T-3	12.94±0.07[c]	5.84±0.03[e]
T-4	14.5± 0.08[d]	6.46±0.03[c]
T-5	15.3±0.08[e]	6.66±0.03[b]
T-6	16.7±0.09[f]	6.86±0.03[a]

Means that carrying different letters are significantly different from each other (Tuckey's test, $p \leq 0.05$)
T_1=90%WWF+10%BP
T_2=90%WWF+10%BRP
T_3=80%WWF+20%BP
T_4=80%WWF+20%BRP
T_5=80%WWF+10%BP+10%BRP
T_6=60%WWF+20%BP+20%BRP

3.2. Phytochemical analysis

The total amount of phenolic contents (TPC) and the total amount of flavonoid (TFC) of the weaning food formulations are below in Table 3. As the concentration rose gradually, a noticeable rise in TPC was shown. In T1, the TPC values were 9.78 ± 0.05 mg GAE/100g, while in T6, they were 16.7 ± 0.09 mg GAE/100g. The primary motivation of such an enhancement is an increased consumption of beetroot powder, which is a recognized provider of phenolic compounds with considerable antioxidant effects. These findings were consistent with the findings of Farhan et al. (2024), who observed that the level of phenolic compounds in sweets supplemented with beetroot powder was significantly higher. The total level of flavonoid also increased with every treatment, as it increased to 5.21mg QE/100g in T1 to 6.86mg QE/100g in T6. This trend has been contributed to by the inclusion of both beetroot and banana powders that contain natural flavonoids such as quercetin and catechins. The steady increase in TFC is attributed to the combined effects of the two fruit powders that enhanced the total functional properties, as well as to the antioxidant properties of the formulations. Chang et al. (2022) and Bana and Gupta (2015) have reported significant increases in TFC when using fruit powder in flour-based products based on the research using banana variants. In general, the phytochemical

Table 4 Sensory scores of weaning food premix

Treatment	Color	Texture	Taste	Overall acceptability
T-1	7.4±0.04[b]	7.1±0.03[b]	8.2±0.03[b]	8.0±0.04[cd]
T-2	7.6±0.04[c]	7.3±0.04[c]	7.9±0.04[c]	7.8±0.04[e]
T-3	8.0±0.04[d]	7.5±0.04[d]	7.8±0.04[c]	8.2±0.04[ab]
T-4	8.4±0.04[e]	7.7±0.04[e]	7.6±0.04[d]	7.9±0.04[de]
T-5	8.6±0.04[f]	8.1±0.04[f]	7.4±0.04[e]	8.3±0.04[a]
T-6	8.8±0.05[g]	8.3±0.04[g]	7.5±0.04[de]	8.1±0.04[bc]

Means that carrying different letters are significantly different from each other (Tuckey's test, $p \leq 0.05$)
T_1=90%WWF+10%BP
T_2=90%WWF+10%BRP
T_3=80%WWF+20%BP
T_4=80%WWF+20%BRP
T_5=80%WWF+10%BP+10%BRP
T_6=60%WWF+20%BP+20%BRP

analysis indicates that increasing concentrations of both banana and beetroot powders in the weaning food blends increase the overall antioxidant potential of these food products significantly, thereby increasing their health-promoting properties.

3.3. Sensory evaluation

The sensory assessment outcomes for color, texture, taste, as well as overall acceptability of the weaning food mixes are summarized in Table 4 and Figure 2. Under the 9-point hedonic scale, all samples scored within the appropriate sensory range, indicating broad consumer compatibility. From 7.4 ± 0.04 (T1) to 8.8 ± 0.05 (T6), the color scores varied. The score of T6 was much higher (p 0.05), possibly because the beetroot was deeper pigmented and gave it a desirable crimson color. These results are aligned with those of Chuwa et al. (2022), who concluded that the use of colored vegetables added to quick weaning mixtures increased the score on color. The texture score varied between $7.1^{-} 0.03$ (T1) and 8.3 ± 0.04 (T6). The larger percentage of beetroot and banana most likely resulted in a less grainy and coherent texture, which enhanced the mouthfeel. Chuwa et al. (2022) proposed the same improvements to the texture of weaning products based on wheat, banana, and potatoes. The minimum and maximum of the scores on the taste scale were 7.4±0.04 (T5) and 8.4±0.04 (T1). Treatments of a bigger banana composition (T1 and T3) would frequently score more on taste tests since banana powder is naturally sweet. Conversely, the low taste rating of T6 could have been due to the earthy taste of the beetroot, which was not potent enough. T5 had the greatest overall acceptance score (8.3 ± 0.04), preceded by T3 and T6. T5's positive sensory perception in all of the assessed metrics might have been influenced by the appropriate incorporation of beetroot and banana (10% each). Chuwa et al. (2022), who found that composite weaning mixes with vegetable and fruit components had noticeably higher acceptability levels, corroborate their findings. In summary, all formulations were widely recognized among the sensory panel, with T5 indicating the most ideal blend of sensory attributes, rendering it an intriguing option for industrial weaning food development.

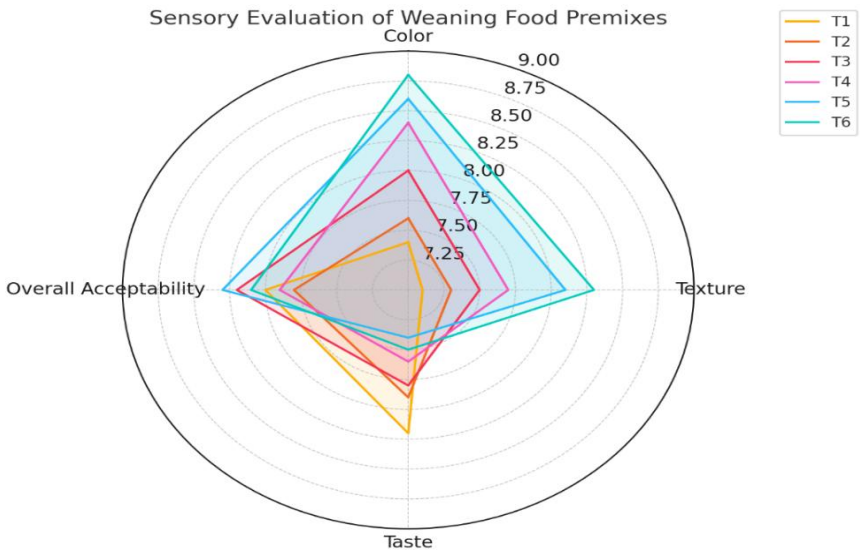

Figure 2 Graphical Representation of Sensory Evaluation

4. Conclusion

In order to enhance nutritional as well as sensory qualities, this study effectively developed and evaluated weaning meal premixes that included whole wheat flour, banana powder, along beetroot powder. The findings indicated that incorporating more banana and beetroot substantially raised the amount of dietary fiber, phenolic, as well as flavonoid content while lowering protein and fat levels very little. With equal amounts of beetroot and banana powders, T5 had the best overall sensory acceptance of any treatment, indicating that it has considerable potential for popularity among consumers. These results indicate the viability of using underused, locally accessible vegetable and fruit sources in the formulation of weaning foods to address baby nutritional shortcomings. In addition to adding functional value, the use of organic substances with antioxidant qualities complies with international guidelines for nutrient-dense, clean-label baby food. These formulations should be studied in the future to determine their therapeutic effects, shelf stability, and storage stability. A sustainable approach to addressing early childhood malnutrition may also be provided by including such goods in maternal-child health policy and community-level nutrition programs.

References

AOAC. (2016). *Official methods of analysis of the Association of Analytical Chemists* (20th ed.). American Association of Analytical Chemists.

Bana, M., & Gupta, R. K. (2015). Formulation, nutritional and phytochemical analysis of ready-to-mix infant food using Gorgon nut, Samak rice and banana powder. *Journal of Pharmacognosy and Phytochemistry*, *4*, 76–81.

Bassey, F. I., McWatters, K. H., Edem, C. A., & Iwegbue, C. M. (2013). Formulation and nutritional evaluation of weaning food processed from cooking banana supplemented with cowpea and peanut. *Food Science & Nutrition, 1*, 384–391. https://doi.org/10.1002/fsn3.50

Bekele, R., & Shiferaw, L. (2020). Development and nutritional evaluation of instant complementary food formulated from vitamin A, iron and zinc rich crops. *Journal of Food Processing & Technology, 11*, 854.

Bhutta, Z. A., Das, J. K., Rizvi, A., Gaffey, M. F., Walker, N., Horton, S., Webb, P., Lartey, A., & Black, R. E. (2013). Evidence-based interventions for improvement of maternal and child nutrition: What can be done and at what cost? *The Lancet, 382*, 452–477. https://doi.org/10.1016/S0140-6736(13)60996-4

Borbi, M. A., Dolan, K. D., Siddiq, M., Hooper, S., & Sami, A. (2020). Development and quality evaluation of banana-rice-bean porridge as weaning food for older infants and young children. *Legume Science, 2*, e41. https://doi.org/10.1002/leg3.41

Chang, L., Yang, M., Zhao, N., Xie, F., Zheng, P., Simbo, J., Yu, X., & Du, S. K. (2022). Structural, physicochemical, antioxidant and in vitro digestibility properties of banana flours from different banana varieties (*Musa spp.*). *Food Bioscience, 47*, 101624. https://doi.org/10.1016/j.fbio.2022.101624

Chhikara, N., Kushwaha, K., Sharma, P., Gat, Y., & Panghal, A. (2019). Bioactive compounds of beetroot and utilization in food processing industry: A critical review. *Food Chemistry, 272*, 192–200. https://doi.org/10.1016/j.foodchem.2018.08.068

Chuwa, C., Saidia, P., & Dhiman, A. K. (2022). Formulation, nutritional and sensory evaluation of ready-to-reconstitute instant weaning mix. *Annals of Phytomedicine, 11*, 1–10.

D'Auria, E., Bergamini, M., Staiano, A., Banderali, G., Pendezza, E., Penagini, F., Zuccotti, G. V., Peroni, D. G., & Italian Society of Pediatrics. (2018). Baby-led weaning: What a systematic review of the literature adds on. *Italian Journal of Pediatrics, 44*, 1–11. https://doi.org/10.1186/s13052-018-0587-8

Farhan, M., Ahmad, Z., Waseem, M., Mehmood, T., Javed, M. R., Ali, M., Manzoor, M. F., & Goksen, G. (2024). Assessment of beetroot powder as nutritional, antioxidant, and sensory evaluation in candies. *Journal of Agriculture and Food Research, 15*, 101023. https://doi.org/10.1016/j.jafr.2024.101023

Grimm, K. A., Kim, S. A., Yaroch, A. L., & Scanlon, K. S. (2014). Fruit and vegetable intake during infancy and early childhood. *Pediatrics, 134*(Supplement 1), S63–S69. https://doi.org/10.1542/peds.2014-0646K

Harris, G., & Coulthard, H. (2016). Early eating behaviours and food acceptance revisited: Breastfeeding and introduction of complementary foods as predictive of food acceptance. *Current Obesity Reports, 5*, 113–120. https://doi.org/10.1007/s13679-016-0202-2

Jahan, S., Bisrat, F., Faruque, M. O., Ferdaus, M. J., Khan, S. S., & Farzana, T. (2021). Formulation of nutrient enriched germinated wheat and mung-bean based weaning food compared to locally available similar products in Bangladesh. *Heliyon, 7*(5), e06929. https://doi.org/10.1016/j.heliyon.2021.e06929

Kabeer, S., Govindarajan, N., Radhakrishnan, P., Alharbi, H. F., Essa, M. M., & Qoronfleh, M. W. (2023). Formulation of fortified instant weaning food from *Musa paradisiaca* (banana) and *Eleusine coracana*. *Frontiers in Nutrition, 10*, 1203955. https://doi.org/10.3389/fnut.2023.1203955

Khatun, H., Haque, M. R., Hosain, M. M., & Amin, M. H. A. (2013). Evaluation of weaning foods formulated from germinated wheat and lentil flour from Bangladesh. *Bangladesh Research Publications Journal, 8*, 152–158.

Liu, R. H. (2013). Health-promoting components of fruits and vegetables in the diet. *Advances in Nutrition, 4*, 384S–392S. https://doi.org/10.3945/an.112.003517

Mishra, G., Mishra, A. A., & Shukla, R. N. (2014). Development of pulse, banana and pineapple pomace based weaning food and its quality evaluation during storage. *International Journal of Development Research, 4*, 1257–1262.

Morison, B. J., Taylor, R. W., Haszard, J. J., Schramm, C. J., Erickson, L. W., Fangupo, L. J., Fleming, E. A., Luciano, A., & Heath, A. L. M. (2016). How different are baby-led weaning and conventional complementary feeding? A cross-sectional study of infants aged 6–8 months. *BMJ Open, 6*, e010665. https://doi.org/10.1136/bmjopen-2015-010665

Ovando-Martinez, M., Sáyago-Ayerdi, S., Agama-Acevedo, E., Goñi, I., & Bello-Pérez, L. A. (2009). Unripe banana flour as an ingredient to increase the undigestible carbohydrates of pasta. *Food Chemistry, 113*, 121–126. https://doi.org/10.1016/j.foodchem.2008.07.082

Pandey, L., & Singh, V. (2019). Development and nutritional evaluation of weaning foods to prevent protein-energy malnutrition in infants. *International Journal of Chemical Studies, 7*, 5–9.

Qasem, W., Fenton, T., & Friel, J. (2015). Age of introduction of first complementary feeding for infants: A systematic review. *BMC Pediatrics, 15*,

107. https://doi.org/10.1186/s12887-015-0409-5

Shilpa, H. S., Sadananda, G. K., GJ, S., Shivapriya Manchali, D., Kumar, S. M., Darshan, M. B., & Hongal, S. (2023). Development of ready-to-eat extruded snack fortified with dehydrated beetroot powder and Chekurmanis leaf powder. *The Pharma Innovation Journal, 2*, 13–18.

Shitemi, C., Kyallo, F., & Kombe, Y. (2018). Complementary feeding practices and nutritional status of children 6 to 24 months: A cross-sectional descriptive study. *African Journal of Health Sciences, 31*, 49–50.

Slavin, J. L., & Lloyd, B. (2012). Health benefits of fruits and vegetables. *Advances in Nutrition, 3*, 506–516. https://doi.org/10.3945/an.112.002154

UCP Journal of Science and Technology
Vol. 3, Issue 1 (July - December 2025)
Journal website: http://ojs.ucp.edu.pk/index.php/ucpjst/index

Prevalence of Head Lice among School Children in Tehsil Shakargarh, Pakistan

Sabila Afzal[1], Wizra Faiz[1], Syed Shakeel Shah[1 *], Afifa Amjad[1], Aneeqa Majeed[1]

Abstract

The purpose of this study was to assess the prevalence of *Pediculosis* infection among school children in relation to their families' economic situation. The research included 439 students from seven government and private schools in Shakargarh. They were checked for lice, and a questionnaire was used to record data on each student's demographic characteristics and other relevant information. A chi-square test was performed to compare the data by using SPSS software; a P-value less than 0.05 was considered as significant. The overall prevalence of head lice infestation was 17.5% (95% CI: 14.1–21.5). Lice infestation was relatively higher among girls (21.8%) than boys (10.0%, $\chi^2 = 9.45$, $p = 0.002$). Government school students showed a higher infestation rate (31.0%) than private school students (6.3%, $\chi^2 = 46.2$, $p < 0.001$). Infestation was significantly associated with larger family size ($\chi^2 = 8.7$, $p = 0.003$), sharing personal items such as combs and scarves ($\chi^2 = 12.1$, $p < 0.001$), and lower socioeconomic status ($\chi^2 = 10.3$, $p = 0.001$). The prevalence of significantly higher among girls who share stuff and have a lower socioeconomic status.

Keywords: Pediculosis, Head lice, Infestation, Risk factor

1. Introduction

Lice are persistent ecto-parasites that must spend their whole life cycle on the host (Saddozai & Kakarsulemankhel, 2008; Majid et al., 2020). It represents a significant public health and social issue rather than a direct medical threat, as the infestation causes irritation, secondary bacterial infections, insomnia, and embarrassment, leading to psychological distress and absenteeism from school. Head lice infestation (HLI) is a worldwide public health issue caused by *Pediculuc humanus capitis* (Gharsan et al., 2016). Globally, prevalence rates vary from 1.6 % to 87 % [4](Rassami & Soonwera, 2012). Head lice are wingless parasitic insects that are between 1/6 to 1/8 inch in length (Frankowski et al., 2002). Human heads are infested with Pediculosis, which lives and deposits its eggs on the hair of the head (Leo et al., 2005). There are three stages of Pediculosis, i.e., (a) egg, (b) nymph, and (c) adult. Throughout their lifetimes, female *P. capitis* can produce up to 100 eggs (nits). Nit sheath is a protective egg sheath produced by lice to help attach freshly laid eggs to hair. This sheath-forming material, also known as louse glue, is secreted from a pair of female accessory glands (Kim et al., 2021). The female may survive for 3-4 weeks and can lay up to 10 eggs each day when fully mature. Because of their tiny size and ability to blend in, lice can be difficult to spot (Devore et al., 2015). Lice may eat and mate every 4 hours, and they can do both at the same time (Hansen, 2004).

1Department of Zoology, University of Narowal, Pakistan
*Corresponding author's E-mail: shakeel.shah@uon.edu.pk
Received: 11 April 2025; Received in revised form: 07 July 2025; Accepted: 17 November 2025.
Available online: 23 December 2025.

DOI: https://doi.org/10.24312/ucp-jst.03.01.505

Head lice are seldom able to survive outside of their host for longer than 36 hours without feeding on blood. Light repels them; therefore, they prefer gloomy places (Madke & Khopkar, 2012). Fomite transmission and direct head-to-head contact are the two main ways that head lice spread. A fomite is anything that could potentially spread a pathogenic organism to other people. Inanimate objects that could have lice include hair brushes, combs, hair accessories, blow-dryers, bedding, helmets, headgears, etc. (Burkhart & Burkhart, 2007).

Age, sex, family size, clothing sharing, and socioeconomic position all impact the course and spread of head lice in a group of people (Weems & Fasulo, 1999). Infestation of head lice is frequently seen in children between the ages of 6 and 12; however, females are at a 2-4-times higher risk than males (Bloomfield, 2002; Saraswat et al., 2020). Lice lay more eggs and are typically more active at warmer temperatures or conditions than in colder temperatures or environments (Hansen, 2004). Sleep loss, irritation, pruritus, pain, and secondary bacterial infections are among the symptoms of *P. capitis*. It's unappealing, and it's a social embarrassment. To hatch, nits require a temperature comparable to that found near the human scalp (Gharsan et al., 2016). A head lice infestation can cause irritation, pruritus, insomnia, and (in severe cases) anaemia. The main symptom of head lice

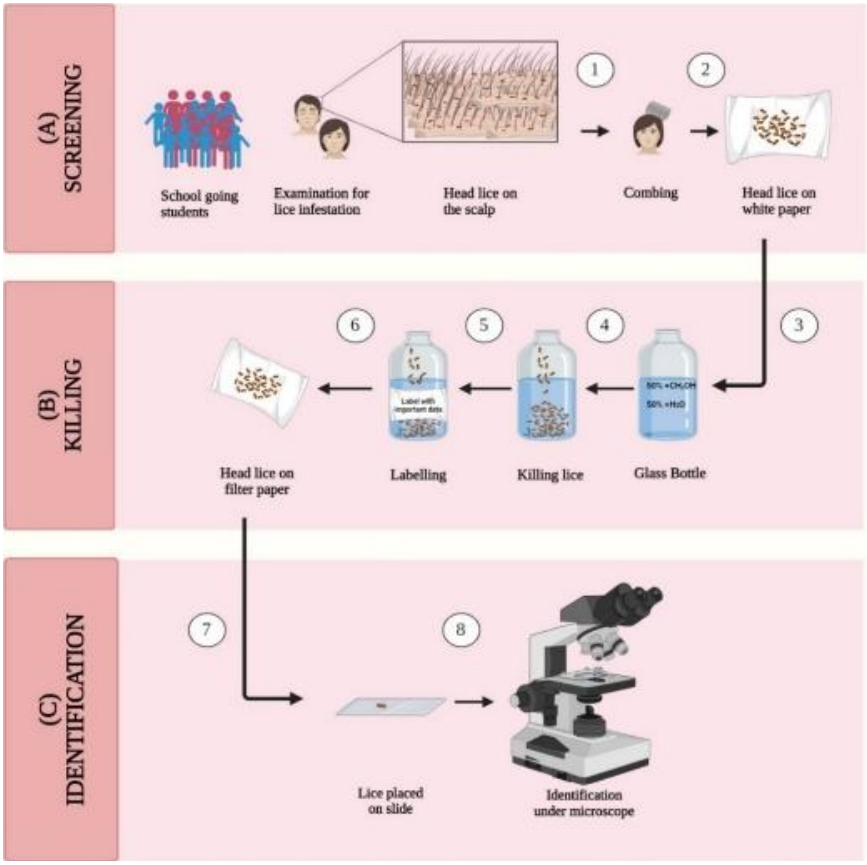

Figure 1 Screening and identification of Pediculus humans capitis.
(A) Visual inspection of scalp and hair; (B) Collection of lice using a fine-tooth comb over white paper; (C) Microscopic identification at 100× magnification

Table 1 Questionnaire filled for each student participating in the current study

Variable	Categories	Description
Gender	Male / Female	Biological sex
Age group	3–6 / 7–10 / 11–13 years	Child's age
School type	Government / Private	Institutional classification
Family size	2–5 / 6–9 members	Household size
Father's occupation	Employed / Unemployed / Business	Socioeconomic proxy
Sharing personal items	Yes / No	Habitual sharing of combs, scarves, or bedding
Transport use	Yes / No	Use of private transport
Family type	Nuclear / Joint	Living arrangement

patients is scalp pruritus. Hypersensitivity to the lice's saliva injection during blood feeding may cause itchy papules to appear. Other types of head lice infestation include irritability and a tickling sensation; secondary bacterial infections can also arise from scratching scores on the scalp (Alberfkani & Mero, 2020). The objective of this study was to collect data on the prevalence of head lice infestations among school-aged children, so that effective measures can be taken to alleviate the problem and enhance these children's quality of life.

2. Materials and Methods

District Narowal is located on the western bank of the river Ravi in the northeast of the province of Punjab. It is divided into three Tehsils, i.e., Tehsil Narowal, Tehsil Shakargarh, and Tehsil Zafarwal. The study was conducted in Tehsil Shakargarh, District Narowal, Punjab, Pakistan, located between 32.25°N and 74.90°E. This was a descriptive cross-sectional survey carried out between September and November 2022. A total of 439 students aged 3–13 years were selected from seven schools (four private and three government). To maintain confidentiality, school names were anonymized as Private Schools A–D and Government Schools E–G. Schools were selected using stratified random sampling, ensuring representation from both public and private sectors. Within each school, systematic random sampling was used to choose participants proportionate to class size. The screening was conducted through visual inspection of the students' hair and scalp. Students aged 3–13 years, enrolled during the study period, with parental consent. Students were excluded from this study with scalp disorders other than lice infestation or those unwilling to participate.

A structured questionnaire recorded demographic and socioeconomic details (age, sex, grade, family size, father's occupation), and behavioral factors (sharing of combs, scarves, bedding, and transport use). "Sharing personal items" was defined as habitual sharing of combs, scarves, hats, or bedding at least twice a week, and Father's occupation was categorized (El-Sayed et al., 2017) (Table 1).

Each student was thoroughly examined for approximately 2-4 minutes under illuminated conditions. The students were

examined while sitting on a chair in a well-lit room, which greatly aided in the detection of lice. Students suspected of having lice were combed with a fine-toothed comb for about 5 minutes over a 60×75 cm (about 2.46 ft) white paper. A child was classified as positive if visible evidence of parasites was found. The comb was cleaned with a tissue and water, and carefully checked to detect any live head lice.

Lice were counted after they were transferred to a bottle containing a 50% methyl alcohol and 50% water solution, which killed them (Suleman & Jabeen, 1989). The bottle was labelled with the necessary data for further processing. Specimens were transferred to the laboratory of the Department of Zoology, University of Narowal, for identification. Lice were taken from the bottle and were placed on filter paper for the removal of excess methanol. They were mounted on the microscope slide and were identified under microscope at 100X magnification (Dehghani et al., 2012) (Fig. 1).

Ethical Considerations

Ethical approval was obtained from the Departmental Ethics Committee, University of Narowal (Ref. No. UON-ZOO/2022/19). Written informed consent was obtained from parents or guardians, and verbal consent was obtained from each child. School administrators provided formal permission prior to data collection.

Statistical Analysis

SPPSS version 25 was used to analyze the data. Descriptive statistics were used to calculate prevalence. Association between categorical variables were tested using chi-square (χ^2). Odds ratios (OR) and 95% confidence intervals (CI) were computed. A p-value < 0.05 was taken as statistically significant.

Table 2 Prevalence of head lice infestation by demographic and socioeconomic factors

Variable	Category	Total	Infested	Prevalence (%)	χ^2	p-value
Gender	Male	159	16	10.0	9.45	0.002
	Female	280	61	21.8		
School type	Private	239	15	6.3	46.2	<0.001
	Government	200	62	31.0		
Age group	3–6	180	17	9.4	7.8	0.01
	7–10	175	38	21.7		
	11–13	84	22	26.1		
Father's occupation	Employed	47	4	8.5	10.3	0.001
	Unemployed	287	64	22.2		
	Business	105	9	8.6		
Family size	2–5	300	38	12.7	8.7	0.003
	6–9	139	39	28.0		
Sharing items	No	220	18	10.7	12.1	<0.001
	Yes	219	44	25.8		
Transport use	Yes	75	6	8.0	2.3	0.13
	No	364	71	19.5		

3. Results

Out of 439 students examined, 77 (17.5%) were infested with head lice (95% CI: 14.1–21.5). As shown in Table 2, infestation was significantly higher among government school students (31.0%) than private school students (6.3%) ($\chi^2 = 46.2$, $p < 0.001$). Children enrolled in government schools were approximately 6.5 times more likely to be infested than their counterparts in private schools (OR = 6.54; 95% CI: 3.51–12.18). This disparity is depicted in Table 2, which shows a steep contrast between the two school types. The difference likely reflects variations in socioeconomic background, classroom density, hygiene infrastructure, and health education emphasis between public and private institutions.

Out of 159 boys examined, 16 (10.0%) were infested, compared to 61 (21.8%) of 280 girls. This gender difference was statistically significant ($\chi^2 = 9.45$, df = 1, $p = 0.002$). The odds of infestation among girls were 2.5 times higher than in boys (OR = 2.49; 95% CI: 1.33–4.67). This trend is shown in Table 2, where female students consistently show higher rates across both government and private schools. The infestation rate among girls in government schools (37.3%) was nearly double that among boys in government schools (19.7%), suggesting a gendered pattern of vulnerability likely influenced

by hair length, grooming practices, and sociocultural norms related to physical contact.

Father's occupation was used as a proxy for socioeconomic status (SES). Among 287 children with unemployed fathers, 64 (22.2%) were infested, whereas only 4 (8.5%) and 9 (8.6%) were infested in the employed and business categories, respectively. The difference was highly significant ($\chi^2 = 10.3$, df = 2, $p = 0.001$). Children of unemployed fathers were 3.1 times more likely to be infested than those of employed fathers (OR = 3.13; 95% CI: 1.42–6.90). The prevalence of head lice infestation was higher in students who were aged from 11-13 years, 26.14% (22/84), and a lower infestation rate of head lice was in 7-10 year 21.7 % (38/175), followed by 3-6 year i.e., 9.44% (17/180). There was a significant relationship between the age statistics ($P < 0.01$) (Table 2).

Infestation was more frequent among children from larger families (6–9 members), with 39 of 139 (28.0%) affected, compared to 38 of 300 (12.7%) in smaller families (2–5 members). This association was statistically significant ($\chi^2 = 8.7$, df = 1, $p = 0.003$; OR = 2.65; 95% CI: 1.40–5.00). In contrast, family structure (joint vs. nuclear) did not significantly affect infestation rates ($\chi^2 = 0.32$, $p = 0.57$). Joint families exhibited 16.3% prevalence versus 17.8% in nuclear families. These results indicate that family size—not structure—is the stronger determinant of transmission risk.

The habit of sharing personal items such as combs, scarves, or bedding was a major predictor of infestation. Among children who shared items, 44 of 219 (25.8%) were infested compared to 18 of 220 (10.7%) who did not share. This difference was highly significant ($\chi^2 = 12.1$, df = 1, $p < 0.001$; OR = 2.89; 95% CI: 1.58–5.27). These findings confirm that indirect transmission via fomites plays a substantial role in sustaining infestation within schools and households. Transport use (shared vs. personal) showed no significant relationship with infestation ($\chi^2 = 2.3$, $p = 0.13$), possibly because lice transmission is limited to close physical contact, not brief proximity during travel.

4. Discussion

This study was conducted to determine the head lice and infestation in the primary school students in Shakargarh city. A total of 439 students were studied, including 281 (64.0%) girls and 158 (36%) boys. Out of 439 school children, 239 are private school students and 200 are government.

school students. Current research shows that head lice is most common in students aged 10-13, followed by the 7-10 year age group, and lowest level in the age of 3-7. The reason for this is likely due to the fact that these younger children are still under their parents' constant attention. They were washed and combed daily by their parents. These results were similar to those of Sadegh Mohammadi-Azni (2014), as he also stated that the prevalence of the infection increases with age and found most cases among fifth-grade students (Azni, 2014). Contrary to the findings of Majidi *et al.* (2017), who focused on the first six grades and observed the highest prevalence among third-grade students (Majidi et al., 2017). According to Archna et al. (2009), Girls are more likely to be infested than boys, i.e., 2.54% and 0.29% ($P < 0.05$), respectively (Rashmi et al., 2009). Similarly, Ibrahim and Mohamed (2020) showed the relationship between the prevalence of infection and gender, where the overall prevalence of Pediculosis was 38.6% (375/971), and the infestation rate was higher in girls (55.0%) than in boys (27.1%) ($P < 0.0001$) (Ibrahim & Mohamed, 2020). Similar studies were reported by Lashari et al. (2015) with significance ($P < 0.001$) and Chaudhry *et al.* (2012), where they found Pediculosis was more prevalent in girls (85.45%) as compared to boys (52.45%) (Lashari et al., 2015; Chaudhry et al., 2012). The present study also demonstrates that the prevalence of head lice was more prevalent in girls (21.78%) than in boys (10.0 %), which indicates that our result correlates well with the findings of previous studies.

Ibrahim and Mohamed (2020) observed that the rate of lice infestation has a significant relation with shared items like head cover/scarf, 53.0% among children who shared, than 29.8% in those who did not share ($P < 0.0001$) (Ibrahim & Mohamed, 2020). The rate of Pediculosis prevalence had a significant relationship with the variable, such as using personal devices ($P < 0.05$) (Jahandideh et al., 2017). In our investigation, we found that the rate of infestation was strongly correlated with the number of shared goods, a finding that is consistent with the results of other studies. The highest percentage of Pediculosis was found among the students whose fathers had the profession of laborers (83.3%) by Afsar and his co-workers (Omidi et al., 2013). Sadia Chaudhry and her colleagues (2012) found that the prevalence of Pediculosis was higher in people having low socioeconomic status than in middle and high socioeconomic status. They also studied the Pediculosis incidence in low, middle, and high socio-economic groups were also studied which were 61.40%, 50.00% and 29.41% in boys, whereas 95.48%, 81.90% and 60.31% in girls, respectively (Chaudhry et al., 2012). Similarly, in another study by Jahandideh et.al. (2017) indicated that the relation between the infection and fathers' profession shows the highest percentage of infection (6.49%) in children with a businessman father and the lowest (6.48%) with a government-employed father, which is a statistically significant difference ($P>0.05$) (Jahandideh et al., 2017). As crowded conditions in the house are a common effect of financial hardship, it was hypothesized that this factor might contribute to head lice infection (Ali & Ramzan, 2004). Our findings were consistent with the results of these studies. In the present study, the prevalence of Pediculosis among children of unemployed parents was almost two times higher than children's of employed parents, and one time higher than children's of businessman.

In a study performed by Dehghani and his coworkers in 2009, they found that the infestation rate among larger families (5+ members) was 1.98%, while it was 0.4% among families having 3-4 members. There was a correlation between the

infestation rate and the family size ($P < 0.031$). The likelihood of infestation among children with five or more family members was 5.02 times more than those having 3-4 family members (Dehghani et al., 2012). Similarly, in another study, it was noted that there was an increase in infested proportion (48.8%) among students if the student had five or more siblings with infection (Al-Zanbaqi & Al-Hashdi, 2025)**.** There is a significant association between head lice intensity and number of siblings ($P = 0.008$), and Pediculosis infestation increases when the number of siblings increases ($r = 0.153$). Our findings indicate that the infestation rate increases with the number of children in the family. Consistent with prior research, these results show that children in large families are more likely to pick up head lice from one another, maybe because parents in those households find less time for their children's hair maintenance. The higher rate of prevalence belonged to the public schools (1.2%) as compared to the private schools (0.3%) reported by Afsar and his colleagues (2013). The results showed a significant relationship between the school type and the prevalence rate ($P = 0.003$) (Omidi et al., 2013). Our study also corroborated their findings, which indicated a higher prevalence of Pediculosis among students attending public schools.

5. Conclusion

Pediculosis is a common public health problem mostly affecting school-going children. The prevalence of lice was found to be significantly higher in girls, families with lower economic status, among the young age group (10-13 years), sharing of different items, and more number of family members. Therefore, the awareness programs should have focused on the school-going children to educate them about the importance of sanitation and personal hygiene.

Acknowledgements

All authors would like to express our gratitude to the University of Narowal which provided support to complete this research work.

Funding

This research was supported by no external funding sources.

Reference

Abd Majid, M., Khoo, J. J., Lim, F. S., et al. (2020). Prevalence, distribution and associated risk factors of head lice (Pediculus humanus capitis) infestation among primary school children in Malaysia. Parasites & Vectors, 13, Article 561. https://doi.org/10.1186/s13071-020-04420-1

Alberfkani, M. I., & Mero, W. M. (2020). The incidence of scabies and head lice and their associated risk factors among displaced people in Cham Mishko Camp, Zakho City, Duhok Province, Iraq. *Polish Journal of Microbiology, 69*, 463–469.

Ali, N., & Ramzan, F. (2004). Head lice infestation in school children at Dera Ismail Khan. *Pakistan Journal of Zoology, 36*, 273–280.

Al-Zanbagi, N., & Al-Hashdi, D. (2025). Prevalence of head lice in Jeddah City, Saudi Arabia according to crowding criteria. *Journal of Basic and Applied Research in Biomedicine, 2*, 22–26.

Azni, S. M. (2014). Prevalence of head lice at the primary schools in Damghan. *Zahedan Journal of Research in Medical Sciences, 16*, 47–49.

Bloomfield, D. (2002). Head lice. *Pediatrics in Review, 23*, 34–35.

Burkhart, C. N., & Burkhart, C. G. (2007). Fomite transmission in head lice. *Journal of the American Academy of Dermatology, 56*, 1044–1047.

Chaudhry, S., et al. (2012). The importance of socio-economic status and sex on the prevalence of human

pediculosis in government school children in Lahore, Pakistan. *Pakistan Journal of Medical Sciences, 28*(5), 952–955.

Dehghani, R., et al. (2012). Prevalence of head lice infestation among 3–6-year-old nursery children in Kashan (2009). *Journal of Occupational Health and Epidemiology, 1*, 81–86.

Devore, C. D., et al. (2015). Head lice. *Pediatrics, 135*, e1355–e1365.

El-Sayed, M. M., Toama, M. A., Abdelshafy, A. S., Esawy, A. M., & El-Naggar, S. A. (2017). Prevalence of pediculosis capitis among primary school students at Sharkia Governorate by using dermoscopy. *Egyptian Journal of Dermatology and Venerology, 37*, 33.

Frankowski, B. L., Weiner, L. B., Committee on School Health, & Committee on Infectious Diseases. (2002). Head lice. *Pediatrics, 110*, 638–643.

Gharsan, F. N., Abdelhamed, N. F., Elhassan, S. A. M., & Gubara, N. G. A. (2016). The prevalence of infection with head lice *Pediculus humanus capitis* among elementary girl students in Albaha Region, Kingdom of Saudi Arabia. *International Journal of Research in Dermatology, 12*, 12–17.

Hansen, R. C. (2004). Overview: The state of head lice management and control. *American Journal of Managed Care, 10*, S260–S263.

Ibrahim, H. M. S., & Mohamed, H. O. A. (2020). Prevalence and associated factors of *Pediculus humanus capitis* infestation among primary schoolchildren in Sebha, Libya. *Journal of Pure and Applied Sciences, 19*, 132–138.

Jahandideh, S., Eslamifar, M., Barimani, K., & Motevalli-Haghi, S. F. (2017). Epidemiologic study of pediculosis and the effective factors in the Sari Township kindergartens in 2014. *Journal of Entomology and Zoology Studies, 5*, 87–90.

Kim, J. H., Lee, D. E., Park, S., Clark, J. M., & Lee, S. H. (2021). Characterization of nit sheath protein functions and transglutaminase-mediated cross-linking in the human head louse, *Pediculus humanus capitis*. *Parasites & Vectors, 14*, 425.

Lashari, M. H., et al. (2015). Prevalence of head lice among school children. *Gomal Journal of Medical Sciences, 13*.

Leo, N., et al. (2005). The head and body lice of humans are genetically distinct (Insecta: Phthiraptera, Pediculidae): Evidence from double infestations. *Heredity, 95*, 34–40.

Madke, B., & Khopkar, U. (2012). Pediculosis capitis: An update. *Indian Journal of Dermatology, Venereology and Leprology, 78*, 429.

Majidi, S., Farahmandfard, M. A., Solhjoo, K., Mosallanezhad, H., & Arjomand, M. (2017). The prevalence of pediculosis capitis and its associated risk factors in primary school students in Jahrom, 2016. *Journal of Jahrom University of Medical Sciences, 15*, 50–56.

Omidi, A., Khodaveisi, M., Moghimi, B. A., Mohammadi, N., & Amini, R. (2013). Pediculosis capitis and relevant factors in secondary school students of Hamadan, West of Iran. *Journal of Research in Health Sciences, 13*(2), 176–180.

Rashmi, A., Bansal, N., Arya, G., & Ahmad, A. (2009). Prevalence of *Pediculus humanus capitis* in a school of low socio-economic area in Rampur (UP), India. *Journal of Applied and Natural Science, 1*, 284–285.

Rassami, W., & Soonwera, M. (2012). Epidemiology of pediculosis capitis among schoolchildren in the eastern area of Bangkok, Thailand. *Asian Pacific Journal of Tropical Biomedicine, 2*, 901–904.

Saddozai, S., & Kakarsulemankhel, J. K. (2008). Infestation of head lice, *Pediculus humanus capitis*, in school

children at Quetta city and its suburban areas, Pakistan. *Pakistan Journal of Zoology, 40*, 45.

Saraswat, N., Shankar, P., Chopra, A., Mitra, B., & Kumar, S. (2020). Risk factors associated with head lice infestation in rural pediatric patients. *Indian Dermatology Online Journal, 11*, 25.

Suleman, M., & Jabeen, N. (1989). Head lice infestation in some urban localities of NWFP, Pakistan. *Annals of Tropical Medicine & Parasitology, 83*, 539–547.

Weems, H. V., Jr., & Fasulo, T. R. (1999). *Crab louse, Pthirus pubis (Linnaeus) (Insecta: Phthiraptera: Pediculidae)*. University of Florida IFAS Extension.

Manuscript Submission Guidelines

Manuscript Submission
Submission of a manuscript implies: that the work described has not been published before; that it is not under consideration for publication anywhere else; that its publication has been approved by all co-authors, if any, as well as by the responsible authorities – tacitly or explicitly – at the institute where the work has been carried out. The publisher will not be held legally responsible should there be any claims for compensation.

Permissions
Authors wishing to include figures, tables, or text passages that have already been published elsewhere are required to obtain permission from the copyright owner(s) for both the print and online format and to include evidence that such permission has been granted when submitting their papers. Any material received without such evidence will be assumed to originate from the authors.

Online Submission
Please follow the hyperlink "Submit manuscript" and upload all of your manuscript files following the instructions given on the screen.

Source Files
Please ensure you provide all relevant editable source files at every submission and revision. Failing to submit a complete set of editable source files will result in your article not being considered for review. For your manuscript text please always submit in common word processing formats such as .docx or LaTeX.

Title Page
The title page should include:

- The name(s) of the author(s)
- A concise and informative title
    - Please avoid acronyms in the title of your article
    - For local studies, please indicate the name of the region and country in the title.
- The affiliation(s) and address(es) of the author(s)
- The e-mail address, telephone and fax numbers of the corresponding author

Abstract
Please provide an abstract of about 200 words for review and research article and 100 words for a case study. The abstract should begin with a brief but precise statement of the problem or issue, followed by a description of the research method and design, the major findings, and the conclusions reached.

Keywords
Please provide 3 to 5 keywords which can be used for indexing purposes.

Text Formatting

- Manuscripts should be submitted in Word.

- Use a normal, plain font (e.g., 10-point Times Roman) for text with 1 line spacing.
- Use the automatic page numbering function to number the pages.
- Do not use field functions.
- Use tab stops or other commands for indents, not the space bar.
- Use the table function, not spreadsheets, to make tables.
- Use the equation editor or MathType for equations.

Tables

- All tables are to be numbered using Arabic numerals such as **Table 1**
- Tables should always be placed and cited in text in consecutive numerical order.
- For each table, please supply a table caption (title) explaining the components of the table.
- Table captions begin with the term Figure. in bold type, followed by the figure number, also in bold type.
- Identify any previously published material by giving the original source in the form of a reference at the end of the table caption.
- Footnotes to tables should be indicated by superscript lower-case letters (or asterisks for significance values and other statistical data) and included beneath the table body.

Figure Lettering

- To add lettering, it is best to use Helvetica or Arial (sans serif fonts).
- Keep lettering consistently sized throughout your final-sized artwork, usually about 2–3 mm (8 pt).
- Avoid effects such as shading, outline letters, etc.
- Do not include titles or captions within your illustrations.

Figure Numbering

- All figures are to be numbered using Arabic numerals such as **Figure 1**
- Figures should always be cited in text in consecutive numerical order.
- Figure parts should be denoted by lowercase letters (a, b, c, etc.).

Figure Captions

- Each figure should have a concise caption describing accurately what the figure depicts. Include the captions in the text file of the manuscript, not in the figure file.
- Figure captions begin with the term Figure. in bold type, followed by the figure number, also in bold type.
- Identify all elements found in the figure in the figure caption; and use boxes, circles, etc., as coordinate points in graphs.
- Identify previously published material by giving the original source in the form of a reference citation at the end of the figure caption.
- Figures should be provided in our required file formats, .jpg, .tif. If your figure is not in .jpg, .tif or .pdf, please convert to the accepted file type that allows the highest quality having 900-1200 dpi (resolution).

- Artwork is of high quality (correct resolution, not blurred, stretched or pixelated)

Headings
Please use no more than three levels of displayed headings.
Main heading should be bold with the font size 12-point Times Roman and sub headings should be 10-ponit Times New Roman and Bold.

Abbreviations
Abbreviations should be defined at first mention and used consistently thereafter.

Footnotes
Footnotes can be used to give additional information, which may include the citation of a reference included in the reference list. They should not consist solely of a reference citation, and they should never include the bibliographic details of a reference. They should also not contain any figures or tables.
Footnotes to the text are numbered consecutively; those to tables should be indicated by superscript lower-case letters (or asterisks for significance values and other statistical data). Footnotes to the title or the authors of the article are not given reference symbols.
Always use footnotes instead of endnotes.

Acknowledgments
Acknowledgments of people, grants, funds, etc. should be placed in a separate section on the title page. The names of funding organizations should be written in full.

Additional Information Text Formatting
All manuscripts should be formatted containing continuous line numbering. Use the page and line numbering function to number the pages.

References
APA Citation Style Guide (7th Ed.)

Citation
Cite references in the text by name and year in parentheses. Some examples:
Negotiation research spans many disciplines (Thompson, 1990).
This result was later contradicted by Becker and Seligman (1996).
This effect has been widely studied (Derwing, Rossiter, & Munro, 2002; Krech Thomas, 2004)

Reference list
The list of references should only include works that are cited in the text and that have been published or accepted for publication. Personal communications and unpublished works should only be mentioned in the text.
If available, please always include DOIs as full DOI links in your reference list (e.g. “https://doi.org/abc”).

- **Journal article**

Derwing, T. M., Rossiter, M. J., & Munro, M. J. (2002). Teaching native speakers to listen to foreign-accented speech. *Journal of Multilingual and Multicultural Development,* 23(4), 245-259.

- **Article by DOI**
  David, H., & Juyuan, J. (2013). A study of smog issues and PM 2.5 pollutant control strategies in China. *Journal of Environmental Protection*, 21(3), 16-21 DOI:10.4236/jep.2013.47086
- **Book**
  Referring a book should follow format: Author, Initial. (Year). Book title. City of publication, Country/State: Publisher.
  Gazda, G. M., Balzer, F. J., Childers, W. C., Nealy, A. U., Phelps, R. E., & Walters, R. P. (2005). *Human relations development: A manual for educators* (7th ed.). Boston, MA: Pearson Educational
- **Book chapter**
  Easton, B. (2008). Does poverty affect health? In K. Dew & A. Matheson (Eds.), *Understanding health inequalities in Aotearoa New Zealand* (pp. 97–106). Dunedin, New Zealand: Otago University Press.
- **Dissertation**
  Krech Thomas, H. (2004). Training strategies for improving listeners' comprehension of foreign-accented speech (Doctoral dissertation). University of Colorado, Boulder.

Statements & Declarations

The following statements must be included in your submitted manuscript under the heading 'Statements and Declarations'. This should be placed after the References section. Please note that submissions that do not include required statements will be returned as incomplete.

Funding

Please describe any sources of funding that have supported the work. The statement should include details of any grants received (please give the name of the funding agency and grant number).
Example statements:
"This work was supported by […] (Grant numbers […] and […]). Author A.B. has received research support from Company A."
"The authors declare that no funds, grants, or other support were received during the preparation of this manuscript."

Competing Interests

Authors are required to disclose financial or non-financial interests that are directly or indirectly related to the work submitted for publication. Interests within the last 3 years of beginning the work (conducting the research and preparing the work for submission) should be reported. Interests outside the 3-year time frame must be disclosed if they could reasonably be perceived as influencing the submitted work.
Example statements:
"Financial interests: Author A and B declare they have no financial interests. Author C has received speaker and consultant honoraria from Company M. Dr. C has received speaker honorarium and research funding from Company M and Company N. Author D

has received travel support from Company O. Non-financial interests: Author D has served on advisory boards for Company M and Company N."
"The authors have no relevant financial or non-financial interests to disclose."
Please refer to the "Competing Interests" section below for more information on how to complete these sections.